Project THEMIS
Technical Report No. 29

VORTEX-CONTAINING WAKES OF
SURFACE OBSTACLES

by

A. Craig Hansen
and
J. E. Cermak

FLUID MECHANICS PROGRAM
ENGINEERING RESEARCH CENTER
COLLEGE OF ENGINEERING

COLORADO STATE UNIVERSITY
FORT COLLINS, COLORADO

Project THEMIS
Technical Report No. 29

VORTEX-CONTAINING WAKES OF
SURFACE OBSTACLES

by

A. Craig Hansen
and
J. E. Cermak

Fluid Dynamics and Diffusion Laboratory
College of Engineering
Colorado State University
Fort Collins, Colorado

U18401 0074328

December 1975   CER75-76ACH-JEC16

ABSTRACT

VORTEX-CONTAINING WAKES OF
SURFACE OBSTACLES

There are many examples in nature of the occurrence of longitudinal

trailing vortices in the lee of surface-mounted obstacles in a turbulent

boundary layer. The vortices may be either horseshoe vortices or the

well-known roof-corner vortices. This dissertation reports an experi-

mental and theoretical investigation of surface-obstacle wakes which

contain organized longitudinal vorticity.

A wind-tunnel study of the wakes behind a hemispherical obstacle

and rectangular-block building model with two approach wind directions

was conducted. The obstacles were surface mounted in a thick, simulated

planetary boundary layer. Measurements of mean longitudinal velocity,

mean swirl (or cross-flow) velocity and vortex strengths, longitudinal

velocity fluctuation intensity, spectra, and two-point space correla-

tions, and the hemisphere surface pressure distribution, at Reynolds

numbers between 10^4 and 10^5, were made. In addition, an inviscid model

was developed to predict the strength of the horseshoe vortex generated

by passage of a shear flow around a hemisphere and to determine the

effect of vortex meander on the average strength of the vortex. A

theory of combined vortex and momentum wakes developed by J. C. R. Hunt

is given preliminary evaluation.

It was found that the vortex-containing wake is quite different

from a momentum wake in two important ways. First, the vortex wake is

extremely persistent when compared to its momentum wake counterpart.

Wake extents of 100 model heights were observed in the vortex-containing

wakes, but a momentum wake in the same boundary layer extended only 15

to 20 model heights. Second, the vortex wake contained large regions of mean velocity excess and turbulence intensity deficit. It was found that both the remarkable extent of the wake and its velocity excess character are due to the convective motion induced by the highly persistent vortices.

The theoretical predictions of the horseshoe vortex circulation and the effect of the vortex meander were satisfactory. Meander of the vortex in the turbulent boundary layer resulted in measured (or average) vortex strengths that were only a small fraction of the instantaneous vortex strength. The meander also caused a rapid decay of the average vortex strength while there was very slow decay of the instantaneous vortex strength. Hunt's theory contains the essential feature of the vortex-shear flow interaction to correctly predict the velocity-excess and persistent nature of the wake. Though refinement is needed the theory can be useful in its present state as a research tool.

TABLE OF CONTENTS

LIST OF FIGURES

vii

LIST OF SYMBOLS

Symbol	Definition
A	Hot-film anemometer calibration constant
a	Vortex viscous core radius
a	Constant in vortex decay law of Saffman
A_1, A_2, A_3	Rotating hot-film anemometer calibration constants
A_b	Base area of hemisphere. $A_b = \pi R^2$
B	Hot-film anemometer calibration constant
c	Rotating hot-film anemometer calibration constant
C_2, C_3	Overturning couple on two- and three-dimensional obstacles
C_D	Drag coefficient $\quad C_D = \dfrac{\text{Drag}}{\frac{1}{2}\rho U_\infty^2 A_b}$
C_p	Pressure coefficient $\quad C_p = \dfrac{P-P_s}{\frac{1}{2}\rho U^2 (R)}$
E	Mean anemometer bridge voltage
E_{rms}	Root-mean-square anemometer bridge voltage
F_j	Defined in equation (A.6)
H	Height of obstacle or bluff body $\quad$ (H = R for hemisphere)
h	Height of vortex above the ground
K	$K = \kappa^2 n$
M	Defined in equation (2.5)
n	Hot-film anemometer calibration constant
n	Mean-velocity power-law exponent
P	Surface static pressure on hemisphere
P_s	Static pressure in free-stream
$p(\eta,\zeta)$	Probability density of vortex location
R	Hemisphere radius

Symbol	Definition
Re	Reynolds number $Re = \dfrac{U(H)H}{\nu}$
r	Radial distance in cylindrical coordinates $r^2 = y^2 + z^2$
r_∞	Value of r far upwind of obstacle
r_1	Radius of vortex viscous core
t	Age of vortex
U,V,W	Mean velocities in x, y, z directions
u,v,w	Mean velocity perturbations
U_o	Mean velocity in approach flow
U_{rms}	Root-mean-square of longitudinal velocity fluctuations
U(R)	Mean velocity at the height of the hemisphere in the undisturbed approach flow
U(H)	Mean velocity at the height of the obstacle in the undisturbed approach flow
U_s	Mean swirl velocity $U_s^2 = V^2 + W^2$
U_T	Total velocity vector magnitude $U_T^2 = U^2 + V^2 + W^2$
U_∞	Velocity at the top of the boundary layer
ΔU	Mean velocity deficit. $\Delta U = U_o - U$
ΔU_{rms}^2	Excess of mean square velocity fluctuations $\Delta U_{rms}^2 = U_{rms}^2 - U_{o_{rms}}^2$
u_e	Mean velocity at the edge of a wake of a two-dimensional obstacle
v_1	Maximum swirl velocity in a vortex
$\bar{v}$	Average swirl velocity in meandering vortex
v'	Root-mean-square lateral velocity fluctuation
X	Defined in equation (A.8)
x_o	Position of virtual origin of the wake

Symbol	Definition
x, y, z	Space coordinates, x downwind, z vertical
$\bar{y}, \bar{z}$	Lateral coordinates of average vortex position

Greek Symbols

Symbol	Definition
α	Approach wind direction
β	Horizontal angle between the x-z plane and the velocity vector. Depicted in Figure 14.
Γ, Γ_o	Instantaneous circulation about a large circuit around the vortex
$\bar{\Gamma}$	Average circulation about a large circuit around the vortex
δ	Boundary layer thickness at the location of the model in the absence of the model
δ_g	Thickness of the vortex-induced boundary layer
δ_v	Radius of the region (V_+) in Hunt's theory
ϵ	Normalized thickness of the boundary layer on the hemisphere
θ	Angle between the velocity vector and the hot-film sensor
κ	von Karman's constant, $\kappa = 0.4$
Λ_y	Lateral turbulent integral scale
ν_T	Perturbation eddy viscosity
ν_z, ν_y	Perturbation eddy viscosities
$\tilde{\nu}$	Dimensionless perturbation eddy viscosity. $\tilde{\nu} = 2\kappa^2 nh$
ρ	Air mass-density
σ	Vortex meander amplitude standard deviation
σ_β	Standard deviation of angle β in undisturbed boundary layer measurements
σ_ϕ	Standard deviation of angle ϕ in undisturbed boundary layer measurements
τ_{xy}, τ_{xz}	Perturbation Reynolds stresses

Symbol	Definition
ϕ	Vertical angle between the x-axis and the mean velocity vector. Depicted in Figure 14.
ψ	Angle defined in Figure 14
ω_s	Streamwise component of mean vorticity

Chapter I

INTRODUCTION

Several examples can be found in nature where passage of a shear

flow around a surface obstacle creates a system of longitudinal vortices

in the wake of the obstacle. Horseshoe vortex flow patterns have been

observed in the wakes of isolated surface protuberances in laminar

boundary-layer flow by Gregory and Walker (1951) and Mochizuki (1961),

to name only a few. Greeley et al. (1974) have reported that sand

deposition patterns in the lee of rim craters on Mars are due to the

scouring and swirl of the horseshoe vortex generated at the base of the

crater. The same pattern has been observed behind craters of sizes

0.20 m (in wind-tunnel tests), 6 m (a man-made crater), and 1200 m

(Martian and Australian craters). Styles and McCallum (1972) observed

lines of snow deposited behind barbed-wire fence posts in a flat, open

field. The snow lines extended in the direction of the wind about 37 m

beyond each fence post before becoming lost in the snow cover on the

ground. The persistence of the fence post wakes to such a remarkable

downwind distance is perhaps indicative of the formation of a horseshoe

vortex at the base of each post. Ostrowski, Marshall and Cermak (1967)

have reported the generation of vortices at the leading roof corner of

a building which is at an angle of incidence to the approach flow.

These vortices, which are responsible for the low pressures observed

on leading roof corners, must persist into the wake of the building.

To persons involved in wind engineering the need for understanding

of wakes behind obstacles in a shear flow requires little elaboration.

Wakes of isolated buildings or hills in the planetary boundary layer

affect, at one time or another, almost every aspect of wind engineering. See, for example, Wise (1971). With the advent of STOL (Short Take-Off and Landing) airports in and near urban areas the question of safety of aircraft operating in the vicinity of buildings becomes very real indeed, Cass, Scoggins, and Chevalier (1973). The increased turbulence levels and strong wind shears in a building wake could pose a significant hazard to aircraft. The added possibility of encountering strong organized vorticity and the associated pitch or roll moments on the aircraft in a vorticity augmented wake (or "vortex wake") only increases the cause for concern and need for wake investigation.

It is well-known that diffusion of passive contaminants is altered by the presence of buildings or other structures in the flow, Munn and Cole (1967). But the effect of the building on diffusion rates may be quite different depending on whether the building has a normal wake or a wake containing organized vorticity. Until the flow in the vortex wake is understood it will not be possible to interpret the effect of the building on diffusion.

Another problem of concern to wind engineers is wind forces on structures. If one building is in the wake of another, the wind forces on that building will be determined in large part by the characteristics of the wake of the upwind structure. If the turbulence intensity in the wake is increased above that which would be encountered in the absence of the upwind building, then the fluctuating forces on the building in the wake will be increased (Mair and Maull (1971)).

But there are applications of the study of wakes containing organized longitudinal vorticity to problems other than wind-engineering problems. Protrusions on ship hulls or aircraft may alter the wake

signature or persistence, or the noise generation by the body. This possibility is particularly evident if the protuberances generate a vortex wake. Another type of vortex wake that is quite familiar is the trailing vortex wake behind an aircraft. Though the present study does not examine this type of vortex wake, the measurement techniques, and perhaps some of the results, will be applicable to the aircraft problem. In spite of the vast amount of research that has been devoted to the trailing vortex it has only been very recently that the situation of the aircraft flying through the planetary boundary layer has been examined. A great deal more knowledge is needed about the interaction between a line vortex and a turbulent shear layer. In this sense, then, the building vortex wake and the aircraft trailing vortex wake problems are related. As a final example of the relevance of this work the contribution of this dissertation to the basic three-dimensional boundary layer research data base cannot be ignored.

Though the existence of vortex wakes has been well-known for many years there has never been an attempt made to understand the nature and physical processes of the wakes. This dissertation reports a study of vortex-containing wakes behind surface-mounted bluff bodies deeply submerged in a turbulent boundary layer. The study was undertaken to determine the nature of the wakes and to generate a basic physical model of the processes and events observed in the wakes.

The study consisted of two major parts. Insofar as was possible the two phases of the study were carried out simultaneously so as to complement one another. Wind-tunnel experiments in wakes of two differently shaped obstacles comprised the major phase of the work. Hemispheres of various sizes and a simple rectangular block were the models

used. The models were placed on the wall in a turbulent boundary layer much thicker than the model heights. A schematic of the experimental arrangement with definitions of some symbols and the coordinate system is shown in Figure 1. The choice was made to look at many features of only a few different wakes rather than looking at one or two features in greater detail. It was decided that there was a basic need for understanding the physical mechanisms in the wakes and that this need would be best met by learning about the interactions and processes in a limited number of different flows. Measurements of mean and fluctuating longitudinal velocities, vortex swirl velocities and vortex circulations, space correlations, and one-dimensional energy spectra were all made with the goal of improving understanding of the fluid mechanics of the wakes. At the beginning of this study no work had previously sought to determine the nature of the vortex wake behind a building, though there was some theoretical basis available for interpretation of observations and prediction of gross features of the flow. The second phase of the study was directed toward developing the existing theories in such a way as to be useful to the prediction and understanding of vortex wakes, and to modifying or developing new theoretical considerations to apply to the vortex wake problem. Very recently (since the completion of these experiments) a theory of vortex wakes has been put forth by J. C. R. Hunt. This theory will be discussed and tested against the observations of the present experiments.

No attempt has been made in this work to obtain an empirical description of the vortex wake by systematically varying flow parameters. Rather, the purpose has been to gain understanding of the nature and mechanisms of the wakes. This understanding will permit design of

future experiments addressing specific issues--such as the effect of the various approach flow parameters on the wake characteristics. The lack of a data base or understanding of even the simplest characteristics (such as downwind extent) of the wakes at the beginning of the present experiments prohibited their design beyond the most fundamental level. With the completion of this first series of tests, it is hoped future investigators will have the necessary guidelines required to plan further study. The theoretical background sought in this work should be of great interest to future investigations.

Since a major application of this work is to wind engineering problems it is appropriate to discuss briefly the use of wind-tunnel modeling in wind engineering applications. A great deal has been published concerning the use of wind tunnels in simulating planetary boundary-layer flows. Hence there is no need to discuss this matter further except to direct the reader to the review paper by Cermak (1975). This paper discusses the many applications of wind tunnels to wind engineering problems and deals extensively with the verifications between model and full-scale experiments that have been performed.

The advantages of wind-tunnel modeling over full-scale measurements are many. There is a vast difference between the amounts of time and money required to do a laboratory simulation and the amounts required to do an adequate field study. In addition, the wind tunnel allows the experimenter to avoid the many caprices of nature and control his experiment to his satisfaction. A higher degree of accuracy and resolution are attainable with fine laboratory instruments. Perhaps most important, the ease of parameter variation and "quick looks" at situations that may be of interest so essential to research in new areas is unsurpassed in the laboratory situation.

The remaining chapters are organized in the following manner: In Chapter II the many diversified areas of fluid mechanics that have made contributions to understanding of the vortex wake are discussed according to their common ties. In Chapter III extensions of current theories are made, where applicable, to improve the agreement between theory and observations. Chapter IV describes the techniques used in obtaining and analyzing the experimental data. Chapter V presents the experiment results and their interpretation. The observations are combined and compared with the theories to derive a simplified physical picture of the flow in the vortex wake. In Chapter VI there is a recapitulation of the major conclusions of the study in addition to brief speculation about worthwhile areas of further investigation.

Chapter II

LITERATURE SURVEY

Introduction

All analyses of turbulent flows share a common problem--closure of the equations governing the flow. Inevitably, all theories of turbulent flows must rely on some degree of empiricism to "close" the theoretical problem before solutions can be found. The problem of a three-dimensional bluff body immersed in a turbulent boundary layer is complex indeed. Its "solution" will depend largely on experimental observations and empiricism. At this time it appears that many of the elements of this problem must be treated separately as much as is possible with a merger or blending of the various elements occurring only in the final stages of development of the theory.

A considerable amount of effort has been devoted to many of the different elements of this problem. The intent of this chapter is to survey and draw together these major areas of research as they apply to the vortex wake problem. The result cannot be a unified mathematical model of the entire wake, but instead a physical model which describes the essential features observed in a vortex wake.

Wakes Behind Buildings

Both theoretical and experimental research to determine the nature of wakes behind buildings or other obstacles in the planetary boundary layer have been conducted for many years. Efforts have been directed both at obtaining experimental measurements and at developing theoretical models of the wakes. Wind-tunnel experiments have been conducted by Counihan (1971), Lemburg (1973) and Castro and Robins (1975).

8

Colmer (1971) has made the only measurements in the wake of a full-scale
building reported to date in the literature. However, a measurement
program is underway at a field site at the NASA George C. Marshall
Space Flight Center in Huntsville, Alabama. Reports of these measure-
ments should be forthcoming soon (Frost et al., 1975). Hansen, Peterka,
and Cermak (1975) conducted a wind-tunnel model study of the NASA
Huntsville field-site building wake. They reported some of the results
contained in this dissertation. J. C. R. Hunt (1974) has developed a
theoretical model of wakes behind two- and three-dimensional obstacles.
The remainder of this section is devoted to discussion of some of the
pertinent details and findings of these studies.

The first detailed wind-tunnel experiments in building wakes known
to this author were reported by Counihan (1971). Using a short test-
section wind tunnel with an artificially stimulated, thick turbulent
boundary layer, Counihan made measurements in the wake of a two-
dimensional block and a cube. The block was 0.02 m high and 0.02 m
deep and the cube measured 0.02 m on a side. The ratio of model height
to boundary-layer thickness was 1:8, and the boundary-layer power-law
exponent was 0.15. Quantities measured included mean longitudinal
velocity, the three root-mean-square (rms) fluctuating velocities,
Reynolds stresses, space correlations of longitudinal velocity fluc-
tuations along lines parallel to the three coordinate axes, and spectra
of longitudinal, lateral, and vertical velocity fluctuations. Measure-
ments were made over a grid covering the wake from a distance 4H to 18H
downwind of the model.

Interesting results include the finding that wakes of three-
dimensional bodies decay more rapidly than the wakes of two-dimensional

bodies in the same approach flow. The wake of the cube had disappeared within 12 building heights downstream of the obstacle, but the wake of the two-dimensional obstacle was still strong at x = 18H. He also observed that turbulent integral length scales are reduced in the wake from the value they would have at the same height in the undisturbed boundary layer. The only exception to this observation is that lateral scales in the wake of the two-dimensional body are slightly increased. The primary purpose of the research was to generate a data base for development of theoretical models. Much of the data is presented for use of other researchers with little attempt to explain the observations or develop a model of the flow.

There is one major uncertainty in Counihan's work. Due to the nature of the experimental facility it was more convenient to move the building model rather than the instrument probe to examine the various regions of the wakes. This creates the problem that for each measurement position the model was in a slightly different approach flow. Interpretation of the data is difficult under these circumstances.

Measurements in model building wakes were also made by Lemburg (1973) at the University of Western Ontario. Lemburg reported measurements of mean and fluctuating longitudinal velocities in the wakes of six obstacles. He also used a force balance to measure the overturning moment on each model. The models included a 0.10 m cube and a square cylinder with a height of 0.15 m and a base of 0.10 m. These models were oriented with the flow both normal to the face and along the diagonal of the top face. Circular cylinders of heights 0.10 and 0.15 m with a base diameter of 0.10 m were also used as building models. The models were placed in a naturally developed turbulent boundary layer

with a power-law exponent of 0.15 and a thickness of 0.61 m. Measurements were made to a distance of 18.2 obstacle heights behind the models.

Lemburg's data indicate that the mean velocity building wakes extend to only 12 building heights but the building affects the turbulence of the flow to 50H for the sharp-edged models and to 80H for the circular cylinders. (These turbulence excess extents were extrapolated from data points upwind of the point x/H = 18.2.)

In addition to his wind-tunnel measurements, Lemburg performed some interesting flow visualization experiments in a water channel. He observed systems of horseshoe vortices generated at the bases of all his models. The vortex pair at the base of the circular cylinders appeared to be the strongest, best-defined pair. Lemburg made note of the effects these longitudinal vortices may have on the wakes but he failed to mention the possibility that greater persistence of the wake of the cylinders may be caused by the vortex pair. The grid of lateral measurement locations (the point spacing was 0.5H) was too coarse to show if the vortices have an effect on the lateral profiles of mean velocity or turbulence intensity.

A major part of Lemburg's dissertation was devoted to the comparison of his measurements with the theory of Hunt (in part as extended by Lemburg). This work will be discussed in a later section.

The most recent measurements in the wake of a model building were performed by Castro and Robins (1975). They placed a cube measuring 0.20 m on a side in a simulated planetary boundary layer. The cube was placed at two orientations: with the flow normal to a face and at an angle of 45 degrees to the face. The boundary layer had a thickness

of 2 m and a power-law exponent, n = 0.24. The turbulence intensity in the approach flow at the height of the cube was 26 percent. This boundary layer simulated flow over terrain more rough than that simulated by Counihan or Lemburg.

Castro and Robins used a pulsed wire anemometer for most of the velocity measurements. This made it possible to measure accurately the longitudinal mean velocity and turbulence intensity very near the model. Surface pressure measurements are also presented in the report.

The wake of the cube extended only a short distance downwind. At x/H = 4.5 the velocity deficits were only "a few percent" and at x/H = 8.5 the wake was too weak to be observed. This short wake extent is consistent with trends pointed out by Lemburg (1973) and Hansen, Peterka and Cermak (1975). Increased turbulence intensity and shear in the approach flow have resulted in decreased wake extent in all wind-tunnel investigations reported to date.

Castro and Robins (1975) obtained interesting comparisons by placing the cube in a uniform flow. When the approach flow was along the diagonal of the top of the cube a strong roof-corner vortex system was observed. The effect of the vortices on the longitudinal velocities was quite pronounced in the near wake of the cube. The velocity profile along a lateral traverse showed the minimum velocity off the centerline and nearly a return to the undisturbed velocity on the wake centerline. Castro and Robins (1975) state that the vortex cores are located at the minimum points on the lateral velocity profile. It is more likely, however, that the vortex cores were located between the minimum points and the centerline. Inboard of the vortices the motion induced by the vortices was downward. This resulted in a transport of momentum

downwards and an increased velocity on the centerline of the wake. But outboard of the vortices the motion was upward. Thus there was a loss of momentum and a decrease in the longitudinal velocity outboard of each vortex.

The wake of the cube with the same orientation in the boundary-layer approach flow showed very little effect of the vortices on the longitudinal velocities. The authors attribute the decreased influence of the vortices to the increased turbulence of the approach flow. They note the need for further understanding of the influence of longitudinal vortices on the wake characteristics.

As mentioned earlier, the only field measurements made behind a full-scale building reported to date are those of Colmer (1971). Colmer made his measurements behind a 10 m high hangar at RAE Bedford. The planetary boundary-layer profile had an exponent of 0.18 and a thickness of 600 m. Instrumented towers 5H, 14H and 23H downwind of the hangar were used to measure all three components of mean and fluctuating velocities in the wake. From these data turbulence intensities, auto-correlations, spectra and mean velocities were calculated.

Only one test was recorded and analyzed by Colmer (1971). During this test there was an oscillation in the approach flow (possibly due to upwind buildings) that also created an oscillation of the same frequency in the wake flow. The limited number of data points do not allow determination of the wake extent with satisfactory resolution. Colmer's data are discussed and compared with theories and wind-tunnel measurements in Hunt (1974), Lemburg (1973), Hansen, Peterka and Cermak (1975), and Peterka (1975).

The wake extent measured by Counihan and Lemburg is much greater than it appears to be from Colmer's limited data. Lemburg states, and this author agrees, that this is due primarily to the large difference in the H/δ ratios in the full-scale tests and in the model tests (or the difference in approach turbulence intensity). Hansen, Peterka and Cermak report measurements behind a small block model $(H/\delta = 0.05)$ that agree more nearly with Colmer's data.

It should be clear from this brief description that more full-scale measurements are needed, particularly for verification of wind-tunnel simulation techniques.

The theory of normal wakes developed by Hunt (1970) is based on the assumption that the obstacle produces only a small perturbation of the boundary-layer flow in which it is immersed. This assumption imposes two basic restrictions on the application of the theory. First, the height of the obstacle must be much less than the thickness of the boundary layer in which it is submerged: $(H/\delta \ll 1)$. Second, the theory can only be expected to apply in the far wake of the body where the velocity perturbations due to the body are small. The zone of separated flow behind the body obviously does not meet this second criterion and therefore the flow in this region cannot be predicted by the theory. It is also assumed that the approach flow mean velocity profile obeys a power law $U_o(z) = U_o(H)\left(\frac{z}{H}\right)^n$ where the exponent n is small $(n \ll 1)$. (Typically n lies in a range between 1/7 and 1/3.) The mean velocities in the wake are expressed as perturbations on the approach wind velocity. Thus, $U = U_o(z) + u(x,y,z)$, $V = v(x,y,z)$, $W = w(x,y,z)$ where the perturbations are assumed small compared to

$U_o(z)$ and vanish as $x \to \infty$. The closure hypothesis chosen by Hunt is the simplest possible. An eddy viscosity, which is constant over most of the wake (not very near the ground), is selected to relate the perturbation shear stress to the local mean velocity gradient. Thus, $\tau_{xz} = \nu_T \frac{\partial u}{\partial z}$ and $\tau_{xy} = \nu_T \frac{\partial u}{\partial y}$, where ν_T is given by $\nu_T = \gamma \kappa^2 nHU(H)$. κ is the von Kármán constant ($\kappa = 0.4$), and γ is a constant which is equal to 1.0 in a two-dimensional wake and of order 1 in a three-dimensional wake. This closure hypothesis is admittedly an over-simplification, but Hunt notes that the usefulness of the assumption is borne out in agreement between observations and the theory.

With the foregoing assumptions and the additional assumption that the velocity deficit profile is self-preserving the equations of motion can be solved for the first order solution. Expressions are obtained by Hunt for the mean velocity deficit, turbulence intensity excess, and perturbation Reynolds stress.

An important result of the theory is that it gives a form for plotting experimental data. In a two-dimensional wake, profiles of mean velocity deficit at various positions along the wake can be made to lie on a single curve by plotting $u/U_o(H) \cdot x/H$ vs $(z/H)/[K(x/H)]^{(1/n+2)}$. K is given by $K = \kappa^2 n$. A similar result can be obtained in a three-dimensional wake by plotting $u/U_o(H) \left(\frac{x-x_o}{H}\right)^{\frac{3+n}{2+n}}$ vs $(z/H) \left(\frac{x-x_o}{H}\right)^{\frac{1}{n+2}}$. x_o is the origin of the wake determined by plotting $(u/U_o(H))^{-2/3}$ vs x/H and extrapolating to the x-axis. Hunt shows that, since n is small, the velocity deficit decays approximately as $u/U_o(H) \propto x^{-1}$ in a two-dimensional wake and as $u/U_o(H) \propto x^{-3/2}$ in a three-dimensional wake.

The momentum deficit in a wake of a body in a uniform flow is directly related to the total drag force on the body. An analogous expression is obtained by Hunt which relates the total moment acting on the body to the moment of momentum deficit in the wake. The expressions are only approximate and are discussed in detail in Hunt (1971b). In a two dimensional wake the wake constant (or couple) is $C_2 =$ $-\rho \int_0^\infty z(u-u_e)U_0(z)dz$. u_e is the velocity at the edge of the wake. In a three-dimensional wake a double integral is obtained for the similar expression: $C_3 = -\rho \int_0^\infty \int_{-\infty}^\infty zuU_0(z)dydz$.

Relations are also given for the perturbation fluctuating velocity in the wake. Briefly, the mean-square longitudinal fluctuating velocity has approximately a power law behavior: $\Delta U^2_{rms_{max}}/U_0^2(H) \simeq \dfrac{10\ K^{1/2}}{(x/H)^{3/2}}$ in a two-dimensional wake and $\Delta U^2_{rms}/U_0^2(H) \simeq \dfrac{1.0}{(x/H)^2}$ in a three-dimensional wake with $n = 0.15$.

When compared with results of wind-tunnel tests many of the predictions of Hunt agree satisfactorily with the observations. The universal form for plotting vertical profiles of velocity deficit does collapse the data onto a single curve. Even in the wake observed by Castro and Robins the theory worked quite well, in spite of the fact that the perturbations were not small. The power-laws of velocity deficit decay match very closely with the observations in the limited data published. The wake constants agreed rather well (within 10 percent) with the measurements of the moment on the body by Lemburg. There is considerable error in the prediction of the lateral profiles of mean velocity deficit. Predictions of the perturbation Reynolds

stress and fluctuating velocities are in need of improvement. The poor
Reynolds stress prediction is almost certainly due to the oversimplifi-
cation in the closure hypothesis. The points of agreement between the
theory and observations do not necessarily establish the validity of
the constant eddy viscosity. Rather, they merely indicate a certain
amount of insensitivity to the closure hypothesis selected. The poor
prediction of the Reynolds stresses demonstrates the inadequacy of the
constant eddy viscosity concept.

The theoretical work of Hunt has been published in several reports
and papers. It may be helpful to give a brief account of the many
publications in addition to this description of the theory. Hunt and
Smith (1969) first proposed the theory in 1969. This work has since
been extended and slightly corrected by Hunt. Laminar two-dimensional
wakes are discussed in a 1971 paper (Hunt, 1971b). In this paper the
important relationship between the couple exerted on the body and the
moment of momentum deficit in the wake is derived in detail. Two
articles give useful, descriptive, somewhat tutorial accounts of the
theories available to describe wakes (1971a, 1972). These papers are
excellent introductions and summaries of the work that has been done.
Details and a summary of the current state of development of Hunt's
theories are given in three additional papers (Counihan, Hunt, and
Jackson, 1974; Hunt, 1970; Hunt, 1974).

Lemburg, in addition to his wind-tunnel experiments, also examined
building wakes theoretically. His work was an extension of the theory
of Hunt. The major alteration to Hunt's work was the use of a variable
eddy viscosity to close the equations of motion. Lemburg's theory

assumes the eddy viscosity is of the form $\nu_z = Kz^aHU_o(H)$ where K and a are arbitrary constants to be determined by matching with experimental observations. The eddy viscosity for shear in the y-direction was assumed proportional to ν_z with the constant of proportionality given by the ratio of the building frontal width to the building height. Thus, $\nu_y = \nu_z(W/H)^2$. In contrast, Hunt assumed the viscosity is constant in the wake. And though provision was made in Hunt's theory for a lateral viscosity proportional to the vertical eddy viscosity the constant of proportionality was assumed to be unity for calculation of the final results. Lemburg determined from matching his theory to his measurements that the exponent a in the variable eddy viscosity formulation should be equal to the boundary-layer velocity profile exponent n. Thus the formulation he used assumed that the eddy viscosity in the wake is proportional to the mean velocity at the same height in the approach flow.

This extension of Hunt's theory does result in somewhat better agreement between theory and observation but it lends no further insight into the physical processes in the wake. The eddy viscosity approach to the closure problem is questionable indeed and there can only be limited value in finding an eddy viscosity formulation that gives a good fit to a small amount of data. The most simple formulation is probably adequate until an entirely different approach to the closure problem can be developed. Fundamental understanding is most necessary at this time when so little is known about wakes of bluff bodies in a shear flow.

The theories of Lemburg and Hunt both assume a Gaussian distribution of velocity deficit along lateral traverses. Measurements do

not, admittedly, bear out this hypothesis (Peterka, 1975). Improvement
is needed in this area.

As mentioned in the introduction, no extensive studies of a
building wake containing organized longitudinal vorticity were under-
taken prior to the present work. While serving as a visiting professor
in the Fluid Mechanics and Wind Engineering Program at Colorado State
University, J. C. R. Hunt (to be published) developed a small perturba-
tion theory of vortex wakes behind isolated buildings in the planetary
boundary layer.

The theory is an adaptation of the concepts developed in the
momentum wake theory. But it considers the interaction between a
single line vortex and the mean velocity vertical shear. The downwards
convection of longitudinal momentum by the vortex creates a region of
increased velocity in the wake on the inboard side of the vortex. The
vortex can be either the dominant branch of the roof-corner vortex
system or either branch of the horseshoe vortex system. When multiple
vortices are present in the wake the solutions for each vortex must be
superimposed. All of the assumptions of the momentum-wake analysis are
included in the vortex-wake theory. Once again the turbulence is
modeled using a constant-eddy-viscosity hypothesis. The equations of
motion become linear in the perturbation quantities and hence the solu-
tion can be expressed as the superposition of the momentum-wake solu-
tion and the vortex-wake solution.

For the vortex-wake analysis the wake is divided into regions
where different assumptions can be applied--see Figure 2. In the
external region (E) the flow is assumed inviscid. There is a balance

between inertial and pressure-gradient forces. The region (E) is out-side the vortex-core regions (V_+) and (V_-). These are the viscous regions surrounding the vortex (V_+) and its image (V_-) where there is a balance between inertial forces and Reynolds stresses. The vortices induce a lateral motion at the surface. Therefore, there must be a region near the surface (G) where the boundary-layer assumptions apply. At a sufficient distance downstream these regions all merge. The vortex cores grow as $\delta_v \sim \sqrt{\tilde{\nu}x}$ where $\tilde{\nu} = \nu_T/U(h)$ and h is the height of the vortex. The boundary-layer region (G) grows as $\delta_G \sim \sqrt{4\tilde{\nu}x}$. When $x/h \ll h/4\tilde{\nu}$ the regions remain distinct. When $x/h \gg h/4\tilde{\nu}$ the regions merge together beneath the vortex. Typically $\tilde{\nu}/h$ has a value between 0.05 and 0.15 ($\tilde{\nu}/h = 2n\kappa^2$). Thus, $h/4\tilde{\nu}$ has a value between two and five.

Only some asymptotic results of the calculations are available at this time. The exact solutions to the equations involve some triple integrals which have not yet been evaluated. But the asymptotic results are quite interesting and provide some basis for evaluating the validity of Hunt's model. Hunt found the vertical swirl velocity, w, is of the form

$$w \sim \Gamma/\sqrt{4\tilde{\nu}x} \; f_1(y/\sqrt{4\tilde{\nu}x}, \; z/\sqrt{4\tilde{\nu}x}) \quad \text{when} \quad x/h \ll h/4\tilde{\nu}$$

and
$$\tag{2-1}$$

$$w \sim \Gamma h/\tilde{\nu}x \; f_2(y/\sqrt{4\tilde{\nu}x}, \; z/\sqrt{4\tilde{\nu}x}) \quad \text{when} \quad x/h \gg h/4\tilde{\nu}$$

Γ is the circulation about the vortex at $x = 0$. Note that the swirl velocity decreases as $x^{-\frac{1}{2}}$ until the viscous regions merge. Then w

decays as x^{-1}. In the region (E) the longitudinal velocity excess is given by

$$u = \frac{n\Gamma hyx}{\pi} \left(\frac{1}{(y^2 + h^2 + z^2)^2 - 4z^2h^2} \right) \qquad (2-2)$$

when $|y| \gg \sqrt{4\tilde{\nu}x}$, $z \gg \sqrt{4\tilde{\nu}x}$, and $x \gg |y|$, $|z-h|$. y in these equations is measured crosswind from the center of the vortex. The maximum longitudinal perturbation velocity excess increases as $x^{\frac{1}{2}}$ when $x/h \ll h/4\tilde{\nu}$ and decreases as $x^{-\frac{1}{2}}$ for $x/h \gg h/4\tilde{\nu}$.

The asymptotic solution in the region $x/h \gg h/4\tilde{\nu}$ has not been obtained. But Hunt states that it will be of the form

$$u \sim \frac{n\Gamma}{h(x/h)^{\frac{1}{2}} (\tilde{\nu}/h)^{\frac{1}{2}}} f_3 (y/\sqrt{4\tilde{\nu}x}, z/\sqrt{4\tilde{\nu}x}) \qquad (2-3)$$

Again, u decreases in proportion to $x^{-\frac{1}{2}}$.

All of these velocity perturbations are due to the vortex interacting with the mean velocity shear. To determine the velocity perturbations that will be observed in the wake the momentum wake perturbations must be calculated and superimposed on the vortex wake perturbations. The vortex wake perturbations lead to an increase in velocity inboard of the vortex while the momentum wake always results in velocity deficits in the wake. Since the momentum wake decays in proportion to $x^{-3/2}$ and the vortex wake strength decreases much more slowly (as $x^{-\frac{1}{2}}$) it can be expected that at sufficient distance downwind of the obstacle the vortex wake will be dominant and there will be a region of velocity excess.

The theory assumes that the vortex strength and position are known. This, of course, is not always the case, and in fact there are few situations where the vortex strength can be predicted. This drawback will require further attention. The theory, even in its present rather infant state, will be quite useful as a research tool.

Mention has not been made of numerical modeling efforts to develop a description of building wakes. Work is underway in this field at the present time (see, for example, Frost, Maus, and Simpson (1973) and Hirt and Cook (1971)). However, due to the difficult, complex nature of the flow, and, in particular, difficulties in dealing with the separation bubble in the wake, progress has been rather limited. Some problems have been overcome and various techniques tested, but presently there is no numerical model available to describe the flow in the wake of a building in a turbulent boundary layer. Numerical modeling relies heavily on use of experimental observations to assist in developing a model. There is still a need for more observations, and perhaps an empirical model of the wake, to allow testing and revision of numerical schemes. Frost (1973) has presented a survey of the wake models that are being developed.

The Secondary Flow Behind a Hemisphere

An inviscid theory for prediction of secondary circulation was developed by Hawthorne (1951). The theory demonstrates that secondary circulation will result if a fluid with a nonuniform velocity distribution passes around a bend such that the vortex lines are rotated. Hawthorne and Martin (1955) applied this theory to the flow of an

inviscid fluid with vertical velocity and density gradients around a hemisphere attached to a horizontal wall.

For the purposes of this dissertation it is useful to look only at the effect of velocity gradients in the approach flow. In the two-dimensional shear flow approaching the hemisphere the vortex lines are parallel to the wall and normal to the flow direction (lines of x = constant, z = constant). These vortex lines are rotated toward a longitudinal orientation and stretched as they pass by the hemisphere. This results in generation of streamwise vorticity in the wake. The rotation of the vortices is such that there is a downward component of velocity on the centerline of the wake. Those vortex lines approaching the stagnation point will be subject to infinite stretching in the inviscid theory. Hence the theory predicts a line of infinite streamwise vorticity along the stagnation streamline in the wake.

The theory is based upon the assumption that an inviscid fluid approaches the hemisphere. The flow is nearly uniform--having a small vertical shear perturbation velocity imposed on the uniform flow. It is also assumed that there is no separation on the lee of the body and that the ground plane exerts no influence on the flow (through viscous effects or image vortices). With these assumptions an explicit solution for the component of vorticity in the streamwise direction can be obtained from the equations of motion.

The quantitative results of Hawthorne's prediction are as follows: The streamwise vorticity, ω_s, on a streamline far downstream of the obstacle, is given by the relation

$$R\omega_s/U_o(r_\infty) = -2 \cos \alpha \, R \frac{U_o'(r_\infty)}{U_o(r_\infty)} M \, . \tag{2-4}$$

In this expression R is the hemisphere radius, $U_o(r_\infty)$ is the velocity

on the same streamline in the approach flow, and $U_o'(r_\infty)$ is the approach

velocity gradient, also on the same streamline. The angle α is shown

in Figure 3. The quantity M is given by an integral along the

streamline,

$$M(y,z) = \int_{x=-\infty}^{x=\infty} \frac{d\theta}{(r/r_\infty) \, \dfrac{U(x,y,z)^2}{U_o(r_\infty)^2}} \tag{2-5}$$

In this expression r and r_∞ are the radii (in cylindrical coordi-

nates) to the streamline at the point (x,y,z) and to the same streamline

far upstream, respectively. The element $d\theta$ is the angle of rotation

of the tangent to the streamline between successive elements along the

streamline. On the stagnation streamline $(r_\infty = 0)$ the integral

becomes infinite. Results, as given by Hawthorne and Martin (1955),

of calculation of the streamwise vorticity due to flow about a hemi-

sphere are given in Figure 2. Notice the infinite vorticity along the

stagnation streamline.

In their paper Hawthorne and Martin show photographs of smoke flow

visualization behind the hemisphere with a variety of approach flow

conditions. The longitudinal vortices predicted by the theory are

clearly evident in the photographs, though not in the locations

predicted.

The most apparent limitation of the theory, other than the obvious

prediction of a line of infinite vorticity due to the assumption of

inviscid flow, is the neglect of flow separation on the lee of the
hemisphere. The vortex sheet will be shed from the body at the separa-
tion line rather than continuing to bend around the body as the calcu-
lations assume. Thus, the vorticity actually generated by the flow will
be less than that predicted by the theory because the bending of the
flow will be less. Also, the positions of the vortices will not be
those predicted by the theory because the vorticity will be shed near
$r = R$ rather than around $r = 0$. Revision of Hawthorne and Martin's work
to account for flow separation will be discussed in the next chapter.

Trailing Vortices Behind Aircraft

There has been extensive research into the problem of the aircraft
trailing vortex because of the serious hazard such a vortex can present
to another aircraft which encounters it. Loss of control and structural
damage resulting in fatal accidents have been attributed many times to
the trailing vortex wake of large aircraft. The research is far too
extensive to be given adequate treatment here. Only the areas that are
deemed relevant to the building vortex wake study will be described
briefly. Collections of publications are available for persons inter-
ested in more details. Olsen, Goldburg and Rogers edited a collection
of important papers in 1971 (Olson, Goldburg, and Rogers, 1971). An
American Institute of Aeronautics and Astronautics Professional Study
Series collection is also available (Donaldson, 1973). Widnall (1975)
has published a very recent review of the problem with a useful list
of references.

In applying the findings of research into the aircraft trailing
vortex to the problem of the building vortex wake one must keep one

major difference between the two problems in mind. The vortex behind a heavy aircraft is the dominant feature of the wake. The character of the wake is determined almost entirely by the vortex itself and to a much lesser extent by the ambient conditions and turbulence generated by the aircraft. In a building vortex wake in a turbulent boundary layer the ambient turbulence of the boundary layer plus the ambient turbulence generated by the body may be as important in determining the wake characteristics as the vortex. The vortex is not a dominant feature of the wake and its interaction with its surroundings must be considered in any analysis. Of course, the knowledge already available about vortex structure, rollup and decay is still useful to the building-wake problem.

The study of vortex structure is one of the oldest subjects of fluid mechanics. The potential vortex is a conceptually simple but physically unrealizable model of vortex structure. The swirl velocity decreases in inverse proportion to the distance from the vortex center. All of the vorticity of the vortex is concentrated at the center of the vortex (where the swirl velocity becomes infinite). Of course, the infinite velocity and infinite shear at the center of the potential vortex are not possible in a viscous fluid. Hence, the Rankine vortex model was developed to pose a more realistic structure in a still simple model. In the Rankine vortex there is a core of radius $r = a$ in which the motion is that of solid body rotation. Beyond this core of constant vorticity the structure is that of the potential vortex. This model of the vortex is much more realistic though it still has a discontinuity in the swirl velocity distribution at the edge of the vortex core. However, attempts to match observed swirl velocity distributions in trailing vortices with the Rankine vortex model were unsuccessful. The

core of the observed vortex was much smaller than that predicted and there was vorticity present outside the core of the vortex. The most realistic (and also most complex) model of vortex structure was obtained when Donaldson (Donaldson, 1971) applied, in 1971, the ideas Betz put forth in 1932 (Betz, 1932). The Betz model is a distributed vorticity model in which the structure of a vortex is directly related to the body that generated the vortex. To calculate the vorticity distribution behind an aircraft with the Betz model one only needs the vorticity (or lift) distribution on the wing and the simple theorems Betz proposed in his original work. These theorems state that, in addition to the conservation of total vortex circulation, the center of gravity of the vorticity will remain constant as the vorticity rolls up into a line vortex and the polar moment of inertia of the vorticity about its center of gravity will also be conserved. Thus, much can be known about the farfield distribution of vorticity--and hence the swirl velocity--with no knowledge of the rollup process itself. The theorems give no information about the length of time required for the rollup process and assume that the vortex is under the influence of no other vortex (either a real or an image vortex) during the rollup. The alternative to using the Betz rollup model is a detailed calculation of the motion of individual elements of vorticity in the vortex sheet shed from the wing. This method has met with only very limited success in application to the aircraft trailing vortex problem and will not be considered further.

With the structure of the vortex predicted simply in terms of the wing configuration (or vorticity distribution in the vortex sheets that are shed from the body) it remains only to calculate the motion and decay of the vortex line in the far wake of the body. The vortex ceases to be

a problem only when it decays to a harmless strength through viscous action or when it is destroyed by interaction with other vortices. Vortex interaction such as described by Crow (1970) only occurs at very great distances behind the aircraft though it appears to be the primary cause of vortex breakdown. Vortex interaction causes an unstable sinusoidal disturbance in the vortex line that grows in amplitude until the two lines meet. When the vortex lines meet they break apart into a series of vortex rings which pose little hazard to other aircraft. This phenomenon can be observed by watching aircraft contrails on a day when they are observable for a long period of time. Vortex decay is a very slow process requiring several minutes in an aircraft wake if the Crow instability does not destroy the vortex first.

The decay of a turbulent vortex is treated analytically through the use of an eddy viscosity closure hypothesis (Saffman, 1973, and Govindaraju and Saffman, 1971). When a constant eddy viscosity is assumed the solution is of the form of Lamb's solution for the decay of a laminar vortex. The maximum value of the circumferential velocity (or swirl velocity) v_1 decays asymptotically like $v_1 = (0.053/a^{\frac{1}{2}})(\Gamma_0/t)^{\frac{1}{2}}$ where a is a constant and $\nu = a\Gamma_0$. Γ_0 is the circulation about the vortex around a large circuit and t is the age of the vortex. The radius at which v_1 occurs increases asymptotically like $r_1 = (5.04a)^{\frac{1}{2}}(\Gamma_0 t)^{\frac{1}{2}}$. It can easily be seen that the circulation at the maximum velocity is constant in time. Saffman (Saffman, 1973) shows evidence that the constant a is in fact Reynolds number dependent-- varying by a factor of 10 when the Reynolds number increases from 2×10^3 to 10^7. Thus the decay rate of the maximum swirl velocity is

a Reynolds number dependent phenomenon. This must be considered in wind-tunnel modeling of vortex wakes.

A problem confronts the experimentalist attempting to measure the strength of a vortex with a fixed measurement probe. The position of a vortex in a turbulent flow is not fixed. Rather, the vortex will meander with the large scales of turbulence in which it is embedded. Thus any fixed probe placed in the flow will not be in the same position in the vortex at all times and will give a measure of the average swirl velocity at the point instead of the actual swirl velocity present at any instant in the vortex. When assessing the hazard a vortex presents to an aircraft it is the instantaneous strength of the vortex that is needed and not the spatial average of the vortex strength. Likewise, the inviscid theory of Hawthorne predicts the instantaneous strength of the vortex. For comparison of the theory with the observations it is desirable to have a method for determining the instantaneous vortex strength from the measured average vortex strength.

Corsiglia, Schwind and Chigier (1973) noted the importance of vortex meander when comparing their measurements in a wingtip vortex with measurements made by Mason and Marchman (1972) under conditions which were thought to be identical. The swirl velocities measured by Corsiglia, Schwind and Chigier were markedly lower than those observed by Mason and Marchman. It was determined that the ambient free-stream turbulence intensity was lower in the wind tunnel used by Mason and Marchman. In the lower level of ambient turbulence the excursions of the vortex away from its mean position were less and the measurement was more nearly of the instantaneous vortex strength. Quantitative comparisons or turbulence intensities are not given in the references.

Orloff and Grant (1973) used a scanning Laser Doppler Velocimeter to measure the true instantaneous swirl velocities in the vortex wake examined by Corsiglia, Schwind and Chigier. The laser system measured maximum swirl velocities approximately three times those measured with the fixed probe. Once again the ambient turbulence level is not specified in the references but it is presumably of the order of only 1 or 2 percent. Corsiglia, et al. (1973) used a three-sensor hot-wire probe on a large rotating arm to sweep through and measure the instantaneous vortex strength. Their measurements confirm that vortex meander can lead to very significant errors when measurements are made with a fixed probe.

Since the vortex meander is a result of the turbulence in the ambient flow, the meander will be more pronounced at higher turbulence intensities. Also, the meander will increase in amplitude with increasing distance from the body generating the vortex. Measurements with a fixed probe will not only yield values of swirl velocity lower than the instantaneous values, but will also result in observation of a vortex decay rate faster than the actual decay rate.

A method for correcting measurements with a fixed probe for vortex meander is presented by Baker, et al. (1974). Measurements were made in a vortex in a water channel with a laser anemometer system. This system made average measurements at a fixed point so it was capable of measuring only the average vortex strength. Dye was used for flow visualization to determine the instantaneous position of the vortex. From photographs of the flow it was possible to determine the amplitude of the excursions of the vortex. It was assumed that the vortex position fluctuated about its mean with a probability density

$$p(\eta,\zeta) = \frac{1}{2\pi\sigma^2} \exp\{- (\eta^2+\zeta^2)/2\sigma^2\} \quad \text{where} \quad \sigma^2 = 2\kappa x/U_o \quad \text{and} \quad \kappa \text{ is an}$$

eddy diffusivity. The value of σ was determined from the photographs of the vortex position. The mean swirl velocity can be calculated in terms of the probability density and the theoretical swirl velocity distribution in the instantaneous vortex. Thus,

$$\bar{v}(r,x) = \iint_{\infty} \frac{\eta-r}{[(r-\eta)^2 + \zeta^2]} \; v\{[(r-\eta)^2+\zeta^2]^{\frac{1}{2}},x\}p(\eta,\zeta)d\eta d\zeta \qquad (2\text{-}6)$$

In this expression r is measured from the mean position of the vortex axis. Calculation of the mean swirl velocity from the above expressions, using the observed values for σ, showed that the instantaneous swirl velocity was approximately 50 percent greater than the average swirl velocity. The free-stream turbulence intensity in the water channel was only 1/2 percent. The theoretical values of the swirl velocity, when corrected in the manner just described for vortex meander, agreed quite well with the measured values of swirl velocity.

The implication of this work is that, if a value of the standard deviation of the vortex axis displacement can be determined, then it is possible to infer the instantaneous values of vortex strength from the measured average values.

Investigations of Effects of Isolated Roughness Elements

A number of investigations have been performed into the effect of isolated roughness elements on boundary-layer transition. Since the emphasis of the research reported in the literature has been to determine the influence of the roughness element on the transition of the boundary layer there is very little quantitative information of interest

to the present wake study. However, the qualitative descriptions of wakes of surface obstacles in a laminar boundary layer are of use in interpreting or anticipating observations in wakes in a turbulent boundary layer.

Gregory and Walker (1951) observed a horseshoe vortex system in the wake of a cylinder submerged in a laminar boundary layer. Mochizuki (1961) presents a number of excellent photographs of smoke flow visualization of the vortex systems in the wake of a sphere mounted on the wall in a laminar boundary layer. The persistence of the horseshoe vortex is clearly evident in her photographs.

A survey paper by Tani (1969) on boundary-layer transition is a useful introduction and summary of the work that has been done on the transition problem. One item of particular interest reported by Tani is an observation by Klebanoff, Tidstrom and Sargent (1962) of span-wise variations of mean velocity and turbulence intensity in the wake of a vibrating ribbon. The variations observed are identified as being a result of the vertical convection of momentum and turbulent kinetic energy by longitudinal vortices generated by the vibrating ribbon.

Measurements of total pressure were made in the wake of a hemisphere in a turbulent boundary layer in 1938 by Jacobs (Jacobs, 1938). Jacobs discovered that the wake was unlike the momentum wake behind an obstacle in a uniform flow. The minimum velocity in the wake was observed not on the centerline but at points equally spaced on either side of the centerline. There was a velocity excess on the centerline of the wake. He attributed this unusual behavior, rather obscurely, to "enhanced turbulence behind the obstacle". No details are given about the approach flow characteristics, and the velocity

survey in the wake is rather limited. Nevertheless, the observations, if not the explanations, of Jacobs are certainly of historical interest.

Finally, an excellent review of the effects of small obstacles on boundary-layer flows is given by Sedney (1973). His review paper is a useful introduction to the wake problem and has an interesting discussion of some major differences between two- and three-dimensional wakes generated by obstacles.

Chapter III

THEORETICAL CONSIDERATIONS

Significant insight into the mechanisms acting in the vortex-containing wake can be attained through simple theoretical and intuitive considerations. These considerations, which were developed by this author, are detailed in the present chapter. Most important, a basic physical model of the vortex-containing wake is hypothesized to explain the effect a vortex may have on a momentum wake. Also recall that in the preceding chapter a brief outline was given of the theories available for the analysis of vortex and momentum wakes. The theory of Hunt predicts the linear interaction of the vortex with the momentum wake to describe the mean velocity behavior in the wake. But this theory requires as an input some knowledge of the strength and position of the vortex system shed from the obstacle. In this chapter a theory is presented which predicts the instantaneous and average horseshoe vortex strengths and position as a function of downwind distance in the wake of a hemisphere. The generation of the more complex roof-corner vortex system is not considered in this chapter, though the vortex meander theory will apply to any line vortex regardless of its origin.

The Vortex Wake Hypothesis

A schematic of the hypothesized horseshoe vortex-containing wake of a hemisphere submerged in a boundary layer is shown in Figure 4. Note that, as mentioned in Chapter II, there is a downward component of mean motion induced at all locations between the vortices. Also, since the wake is immersed in a shear flow, the mean velocity in the wake increases with height above the ground plane. Thus, the downwards

motion between the vortices carries high momentum fluid from the upper regions of the boundary layer toward the ground. This convection of momentum causes an increase in longitudinal mean velocity in the portion of the wake between the vortices. This can be seen mathematically by examining the convective terms in the equation of motion $(U \frac{\partial U}{\partial x} + W \frac{\partial U}{\partial z})$. In any region where W is negative and $\partial U/\partial z$ is positive, the change in U due to convection alone will be an increase in U.

Convection of turbulent kinetic energy by the motion induced by the vortices will, by similar reasoning, result in decreased turbulence intensity in the wake between the vortices. In the boundary layer the turbulent kinetic energy decreases with increasing height. Therefore, the downwards motion between the vortices will carry less turbulent fluid nearer the ground. At some distance downwind of the obstacle the convective motion will have acted long enough and the turbulence generated by the obstacle will have decayed sufficiently for the turbulence intensity in the wake to be less than the intensity at the same height in the undisturbed approach flow.

The persistence of a line vortex is well-known. (See Widnall, 1975, for example.) The swirl velocities in an instantaneous line vortex decay as $x^{-\frac{1}{2}}$ whereas the theory of Hunt (1974) predicts the wake strength decays as $x^{-3/2}$. Thus, the presence of a highly structured, highly persistent vortex in the wake can be expected to increase the persistence of a vortex-containing wake to downwind distances much greater than the extents of momentum wakes.

The Instantaneous Vortex Strength

It was pointed out in Chapter II that Hawthorne and Martin (1955) have developed a theory which predicts the streamwise vorticity field in the lee of a hemisphere in a shear flow. Two serious limitations in the theory were also pointed out, i.e., the theory neglects flow separation on the back half of the body and it predicts an infinite vorticity on the stagnation streamline. In the material that follows, both of these unrealistic conditions are removed from the theory to give a far more realistic prediction of the nature of the horseshoe vortex system in the hemisphere wake.

In the actual flow around a hemisphere there is a separation line which runs approximately down a meridian line from the top of the dome to the surface on which it rests. The exact position of this separation line depends on the Reynolds number and the approach-flow turbulence intensity as well as the nature of the surface of the hemisphere. As a good approximation the separation line can be taken as the 90-degree meridian line through the top of the body (in the plane $x = 0$). The approximate location of the separation line is shown in Figure 4. Sheets of streamwise vorticity will be shed at the separation line and this vorticity will roll up into a discrete line vortex at some distance downwind of the hemisphere. The rollup process is governed by the theorems of Betz which were discussed in Chapter II. Thus, if the distribution of streamwise vorticity in the vortex sheets shed from the body can be determined, the method of Betz can be used to calculate the center of gravity and circulation about the line vortex in the far wake of the hemisphere.

The theory of Hawthorne and Martin (1955) can be used to predict the streamwise vorticity at any point along the potential flow streamline by rewriting the integral of equation (2-5) in the form

$$M = \int_{x=-\infty}^{x} \frac{d\theta}{r/r_{\infty} \left(U(x,y,z)/U_{o}(r_{\infty})\right)^{2}} \quad . \qquad (3-1)$$

Integration to $x = 0$ will give the streamwise vorticity distribution in the flow as it separates from the body. Since the calculation is performed along the streamline upwind of the separation only, the potential flow approximation remains valid except very near the body.

The result of this alteration to the theory of Hawthorne and Martin is that the actual flow turns through only half the amount the ideal flow turns. This means the strength of the streamwise vorticity at separation is only half that predicted far downstream of the obstacle in the absence of separation. Results of the evaluation of the integral of equation (3-1) from the limit $x \to -\infty$ to $x = 0$ are shown in Figure 5. The streamwise vorticity distribution calculated in the plane $x = 0$ for a hemisphere in a boundary layer is shown in Figure 6.

The vorticity predicted by the inviscid theory is still infinite along the stagnation streamline (the surface of the body). In reality, the viscous effects become important in the boundary layer which develops on the body. In this region the vorticity will not be unbounded as predicted by the theory of Hawthorne and Martin but will approach some limiting value. In the calculation of the circulation about the vortex it is appropriate to assume that within a narrow region above the surface of the body the streamwise vorticity becomes constant and has the value predicted by the inviscid theory on the outer edge of this boundary layer.

With the assumption that all of the vorticity in the vortex sheet will roll up into the line vortex the circulation about the vortex is given by the simple relation

$$\Gamma = \iint_A \omega_s \, dydz \ . \qquad (3\text{-}2)$$

The area over which the vorticity is integrated is the entire area of the quarter plane $(x = 0, \ y \geq 0, \ z \geq 0)$. The integration was performed numerically with the assumption that

$$\omega_s(1.0 < \frac{r}{R} \leq 1.0 + \epsilon) = \omega_s(\frac{r}{R} = 1.0 + \epsilon) \ . \qquad (3\text{-}3)$$

Results of the integration for various values of ϵ are shown in Figure 7. It can be seen that the value of the circulation calculated is not highly sensitive to the value of ϵ. Over the region of interest a change of ϵ of one order of magnitude results in only a 34 percent change in Γ.

The value of ϵ can be approximated by the thickness of the mean velocity boundary layer on the hemisphere. The thickness of the boundary layer was estimated through a search of the literature. Schlichting reports that the thickness of a laminar boundary layer developing on a sphere in uniform flow is given by

$$\epsilon \sqrt{\frac{U_\infty R}{\nu}} = 2.6$$

on the 90-degree meridian (Schlichting, 1968). The value of ϵ obtained using this result is $\epsilon = 0.008$. Schlichting also reports data of Parr (1963) from boundary-layer-thickness measurements on a spherically blunted cylinder with flow along its axis. At a Reynolds number of

3×10^5 the momentum thickness (δ_2/R) is approximately 0.001. The actual boundary-layer thickness may be from 7 to 10 times the momentum thickness. This results in a value of ϵ in the range 0.007 to 0.010. The agreement between these two methods of obtaining the boundary-layer thickness in addition to the insensitivity of Γ to the value for ϵ chosen indicate with some confidence that the correct value for $\Gamma/U(R)R$ should be approximately 0.75. This is the strength of the instantaneous vortex after the rollup process is completed that is used in all subsequent calculations.

The Average Vortex Strength

The instantaneous vortex strength cannot measured by a fixed probe which relies on time-averaged quantities to measure mean swirl velocities. This is because of the vortex meander effect which was discussed in Chapter II. The vortex meander theory presented by Baker et al. (1974), relied on flow visualization to determine the value of σ. Since this is not feasible in a wind-tunnel study of a weak vortex, a new method for determining σ is proposed and described in this section. To calculate the effect of vortex meander it is assumed that the instantaneous vortex has the structure of a Rankine vortex of radius a. Then the average swirl velocity can be calculated by evaluating the integral in equation (2-6). The integral was evaluated numerically for various values of r/a and σ/a. The results are shown in Figure 8. The results are presented in the form of the ratio between the measured and instantaneous values of swirl velocity. It can be seen that the meander can have a very large effect when the standard deviation of the vortex lateral motion is of the order of or larger than the core

radius. As expected, the influence of meander is greatest near the edge of the vortex core where the velocity is highest.

To use the results shown in Figure 8 it is necessary to have an estimate for the value of σ/a. The lateral fluctuation of the vortex position are due to the lateral velocity fluctuations. The instantaneous slope of the vortex axis is given as $\frac{d\bar{y}}{dx} = \frac{V}{U}$. Over a distance x the rms of the lateral motion about the mean vortex position can be estimated as

$$\sigma = \frac{v'}{U} x \qquad (3-4)$$

where v' is the rms of the lateral velocity fluctuation and U is the average longitudinal velocity at the average vortex position. This form for σ for diffusion of passive particles was predicted theoretically by Taylor (see Hinze, 1959, for example) using Lagrangian velocity correlations. For diffusion times much less than the Lagrangian integral time scale (or downwind distances less than several Eulerian longitudinal scales of turbulence) the diffusion proceeds in direct proportion to the Lagrangian lateral velocity fluctuation and the time of flight (or x/U). For times greater than the Lagrangian integral time scale the diffusion proceeds only in proportion to $t^{\frac{1}{2}}$. Thus the expression (3-4) can only be applied when $x/U \ll T_L$, where T_L is the Lagrangian time scale. Additional support for this simple form for σ is found in the book on atmospheric diffusion by Pasquill (1962). The standard deviation of particle distributions about the center of a puff of passive particles in a turbulent flow is proportional to $x^{0.84}$. The motion of particles is exactly analogous to the motion of a weak vortex under the influence

of lateral velocity fluctuations. It is clear that the x dependence in the expression for σ is approximately correct. The proportionality to v' can be seen in Taylor's theory but must be verified experimentally. Note that this form for σ does not contradict that used by Baker et al. (1974). The eddy diffusivity used in their expressions must be a function of x.

As an illustration of the magnitude of the effect of vortex meander, results of a sample calculation are shown in Figure 9. The velocity profile of a Rankine vortex in a smooth flow is compared to the average profile that would be measured if the same vortex were in a turbulent flow with σ/a = 2.0. The effect of the meander is to give the appearance of a vortex with lower swirl velocities and a larger viscous core.

The Average Vortex Position

With the strength of the horseshoe vortex known as a function of downwind distance from the calculation of the instantaneous vortex strength, and the effect of vortex meander, the only major feature of the vortex yet to be determined is the position of the vortex axis as a function of x. According to the theory of Betz the position of the vortex after rollup is the same as the position of the "center of gravity" of the vorticity before rollup. This theory assumes, however, that the vortex is isolated in a uniform, smooth flow. In the wake of a surface-mounted obstacle in a wind-tunnel boundary layer there are several effects which can change the position of the vortex. The vortices and their images will induce convective velocities at the locations of all other vortices. In a boundary-layer flow there is a weak mean vertical motion due to the boundary-layer growth. This

motion will convect the vortices upward as they are carried downstream.
Also, in a turbulent boundary layer, there is vertical transport of vor-
ticity by diffusion. All of these effects combine to determine the
motion of a vortex in a turbulent boundary layer. In a wake in a
boundary layer the same effects will act on the vortex. If the wake is
only a small perturbation on the boundary layer the magnitudes of the
various effects can be estimated in the undisturbed boundary layer situa-
tion. Expressing the motion of a vortex in terms of the vortex-induced
motion, the mean motion due to boundary-layer growth, and vertical vor-
ticity transport (or diffusion) respectively, one obtains:

$$d\overline{y}/dx = (d\overline{y}/dx)_V \qquad\qquad (3\text{-}5a)$$

$$d\overline{z}/dx = (d\overline{z}/dx)_V + (d\overline{z}/dx)_W + (d\overline{z}/dx)_d \qquad (3\text{-}5b)$$

These terms will now be discussed individually in more detail.

A schematic of the horseshoe vortex pair and their image vortices,
with some nomenclature definitions, is shown in Figure 10. The view in
this schematic is downwind past the hemisphere. Note that each branch
of the horseshoe vortex induces a downward motion on the opposing branch
of the vortex, causing a descent of the vortex pair. Each image vortex
branch induces outward motion at the location of the corresponding real
vortex branch. Thus, in a uniform flow over a ground plane the vortices
would descend and spread laterally outwards as they approached the
ground plane. These effects are readily expressed quantitatively in the
following form (see Lamb, 1945, for example):

$$(d\overline{y}/dx)_V = \frac{\overline{\Gamma}}{4\pi\overline{z}} \quad \frac{\overline{y}^2}{\overline{y}^2+\overline{z}^2} \quad \frac{1}{U}$$

(3-6)

$$(d\overline{z}/dx)_V = \frac{-\overline{\Gamma}}{4\pi\overline{y}} \quad \frac{\overline{z}^2}{\overline{y}^2+\overline{z}^2} \quad \frac{1}{U} \quad .$$

The mean velocity U, can be expressed in terms of the power-law representation: $U = U(R) \, (\overline{z}/R)^n$. Then equations (3-6) can be written (in non-dimensional form) as

$$(d\overline{y}/dx)_V = \frac{\overline{\Gamma}}{4\pi\overline{z}^{-n+1}} \quad \frac{\overline{y}^2}{\overline{y}^2+\overline{z}^2}$$

$$(d\overline{z}/dx)_V = \frac{-\overline{\Gamma}}{4\pi\overline{y}\;\overline{z}^{-n}} \quad \frac{\overline{z}^2}{\overline{y}^2+\overline{z}^2} \quad .$$

(3-7)

Typically $\overline{y}$ may be approximately 1.1 or 1.2 and $\overline{z}$ may be approximately 0.1 or 0.2. $\overline{\Gamma}$ may be from 1/3 to 1/10 of Γ (which was calculated earlier in this chapter to be 0.75). Using typical values one sees that,

$$(d\overline{y}/dx)_V \sim 0.1$$

$$(d\overline{z}/dx)_V \sim - 0.001 \quad .$$

(3-8)

The vertical motion of the vortex due to the mean vertical velocity in the boundary layer is given as

$$(d\overline{z}/dx)_W = W/U \quad .$$

W/U can be estimated using the continuity equation and knowledge of the growth rate of the boundary layer. Integrating the continuity equation in the undisturbed, two-dimensional boundary layer one obtains

$$W(z) = - \int_0^z \frac{\partial U}{\partial x} \, dz \; . \qquad (3\text{-}10)$$

Using the power-law representation for U, and assuming U_∞ is constant

$$\frac{\partial U}{\partial x} = -nU \, \frac{1}{\delta} \, \frac{d\delta}{dx} \; . \qquad (3\text{-}11)$$

Integration of (3-10) using (3-11) yields the following result:

$$\frac{W}{U} = \frac{n}{n+1} \, \frac{z}{\delta} \, \frac{d\delta}{dx} \; . \qquad (3\text{-}12)$$

If the power-law exponent, n, is 0.12 and z/δ is approximately 0.2

$$\left(\frac{d\bar{z}}{dx}\right)_w = \frac{W}{U} \sim 0.02 \, \frac{d\delta}{dx} \; . \qquad (3\text{-}13)$$

The vertical transport of vorticity by diffusion away from the ground plane is another mechanism which might affect the motion of the weak vortex. A method has not been developed for directly calculating the vorticity transport but a phenomenological argument can be made for estimating $(d\bar{z}/dx)_d$. The turbulent boundary layer is a region containing vorticity which was generated as a result of the wall of the boundary layer. The growth of the boundary layer into the irrotational free-stream flow is a result of vertical transport of vorticity through the boundary layer. Thus, it is plausible to assume that the vertical transport, $(d\bar{z}/dx)_d$, is of the same order of magnitude as the boundary-layer growth $d\delta/dx$. Thus,

$$(d\bar{z}/dx)_d \sim d\delta/dx \; . \qquad (3\text{-}14)$$

A comparison of (3-14) and (3-13) shows that vorticity transport by diffusion dominates over the mean vertical motion term. Results of

Zoric (1969) and Tieleman (1967) indicate that, for the smooth-floor
boundary layer used in the present study, $d\delta/dx$ is approximately

$$d\delta/dx \sim 0.028 \ . \qquad\qquad (3\text{-}15)$$

Thus, the rate of vertical rise of the vortex due to vertical diffusion
of vorticity is of the order of 30 times greater than the rate of
descent due to vortex-induced motion (equation (3-8)). In equation
(3-5b), then, the vertical motion of the vortex is governed almost
entirely by the vorticity transport term:

$$\frac{d\bar{z}}{dx} \;=\; \left(\frac{d\bar{z}}{dx}\right)_d \sim \frac{d\delta}{dx} \ . \qquad\qquad (3\text{-}16)$$

Equation (3-16) can be integrated to yield

$$\bar{z}(x) = \delta(x) + \text{Constant} \ . \qquad\qquad (3\text{-}17)$$

Without details of the rollup process available to determine a boundary
condition for the problem, the constant in equation (3-17) is best deter-
mined by matching the solution with the results of the wind-tunnel
experiments.

The lateral motion of the vortex is governed by equation (3-5a).
Using equation (3-7) the form of $d\bar{y}/dx$ can be determined

$$\frac{d\bar{y}}{dx} \;=\; \frac{\bar{\Gamma}}{4\pi\bar{z}^{-n+1}} \; \frac{\bar{y}^2}{\bar{y}^2+\bar{z}^2} \ . \qquad\qquad (3\text{-}18)$$

With a solution for $\bar{z}$ available in equation (3-17), equation (3-18)
can be integrated numerically to determine $\bar{y}(x)$. Since the final solu-
tion depends on determining the boundary conditions from experimental
observations the results of these calculations will be presented in
Chapter V.

Chapter IV

DATA ACQUISITION AND ANALYSIS

Measurements in wakes require considerable care, both in their
acquisition and in their interpretation. In this chapter the methods
used to make measurements and the techniques used in converting directly
measured quantities to meaningful physical quantities are discussed.
Attention is drawn to the limitations in the techniques in an attempt
to prevent misinterpretation or misunderstanding of the results to be
presented in the next chapter.

Many of the methods used are very common and need little explanation.
However, particular attention is drawn to the rotating hot-film anemom-
eter system used to measure the three mean velocity components in the
vortices. This system was developed during the course of this research
at Colorado State University for high resolution measurements of cross
flows.

The Wind Tunnel Facility

The experiments were performed in the Meteorological Wind Tunnel
located in the Fluid Dynamics and Diffusion Laboratory at Colorado State
University. A plan view of the wind tunnel is shown in Figure 11. The
tunnel is a closed-circuit facility driven by a 250 hp variable-pitch,
variable-speed propeller. The test section is nominally two meters
square and 27 m long fed through a 9-to-1 contraction ratio. The test
section walls diverge 0.01 m/m and the roof is adjustable to maintain a
zero pressure gradient along the test section. The mean velocity can be
adjusted continuously from 0.3 to 37 m/sec. The wind speed in the test
section does not deviate from that set by the speed controller by more

than 1/2 percent. The tunnel is equipped with a refrigeration system
to maintain the air temperature at a constant level ($\pm\frac{1}{2}$°C). Though the
wind tunnel is capable of simulating thermally stratified planetary
boundary layers all tests reported in this dissertation used a neutral
boundary-layer stratification. The facility is described in detail by
Plate and Cermak (1963).

At the entrance to the wind-tunnel test section a 0.038 m high
sawtooth boundary-layer trip is installed to insure prompt formation
and growth of a turbulent boundary layer. A similarity profile is
attained in the boundary layer within 6.1 m of the test section
entrance (Zoric, 1969). All the measurements reported in this disser-
tation were made with the models at or beyond 11.3 m from the start of
the test section. Thus the approach-flow boundary layer had a simi-
larity velocity profile and changed very slowly along the test section.

The boundary layer continues to thicken at successive locations
along the test section. Over the smooth flat plate the thickness of
the boundary layer increases in proportion to $x^{.48}$ (Zoric, 1969).
However, in the region in which all measurements were made, the boundary-
layer growth was linear within the ability to measure the boundary-layer
thickness. Over the large distances the vortex wakes persist behind the
models, this change in boundary-layer thickness becomes significant. To
account for this difficulty all velocity deficits reported in this
research were calculated by finding the difference between the velocity
at a point in the wake and the velocity at the same point in the absence
of the model. This is not exactly identical to the deficit obtained by
finding the difference between the velocity at a point in the wake and
the velocity at the same height in the approach flow to the model.

Two different approach flows were used in various parts of this study. The boundary layer developed over the smooth flat plate floor of the wind tunnel had a thickness of 0.38 m at the location of the model and a power-law exponent of 0.12. The roughness height was 25μm. The flow was uniform along a lateral profile within ±1 percent of the free stream velocity. Mean velocity and turbulence intensity vertical profiles taken at the model location in the absence of the model are shown in Figure 12. The second boundary layer was developed over a shag carpet which was placed on the wind-tunnel floor. The boundary layer so obtained approximates that found over typical suburban terrain. The power-law exponent of this boundary layer was 0.25 and the thickness was 0.61 m at the model location (in absence of the model). Mean velocity and turbulence intensity profiles for this boundary layer are shown in Figure 13. The carpet used to generate this thick, rough wall boundary layer had an average strand length of 0.025 m and a strand density of 40,000 strands per square meter. The velocity profile along a lateral traverse over this carpet was uniform within ±2 percent. It was necessary to rake the shag carpet prior to each measurement and after persons walked on the carpet. But with these simple precautions the characteristics of the boundary layer were repeatable over several months of use and many removals and reinstallations of the carpet.

Models tested include plexiglas hemispherical shells of 0.076, 0.10, and 0.14 m radii and a heavily painted styrofoam block measuring 0.065 m high, 0.16 m long and 0.049 m wide. When placed on the carpet the models were attached to a 0.003 m thick steel plate which was simply set on the carpet without the necessity of further anchoring. The origin of the coordinate system was at the center of the base of the

hemisphere and at the intersection of the wind-tunnel centerline and the base of the rear face of the block building. The block building was rotated about its center to simulate different approach wind directions.

Velocity Measurements

Longitudinal velocities in the wakes were measured using two different systems. The first measurements were made using simply a pitot-static tube connected to an MKS Baratron Pressure Meter (Type 77). The pressure meter output and probe position output were connected to an x-y recorder to obtain a continuous profile of dynamic pressure in either a horizontal or vertical traverse of the wake. This preliminary survey of mean velocities was useful in determining the extent of the mean velocity wake and in identifying points where more detailed measurements should be made. More detailed measurements of mean and rms fluctuating velocities were made using a constant temperature hot-film anemometer system.

The pitot-static tube was used only in the wake beyond the separation bubble immediately behind the building. In this region the flow was essentially in the longitudinal direction--aligned sufficiently with the probe to eliminate any error due to misalignment. Another source of error in the pitot-static tube measurements was the effect of turbulence intensity on the mean velocity calculation. In the measurements over the carpet this error could be significant because the turbulence intensity was of the order of 30 to 40 percent at many measurement locations. For this reason later measurements with the hot-film anemometer are more reliable. However, in the boundary layer and wake over the smooth floor the turbulence intensity was only of the order of 20 percent, even

near the separated flow region. Thus the maximum error in the mean velocity of the order of two percent of the local mean velocity. Typical errors were approximately one percent. In the calculation of velocity deficits much of this systematic error was eliminated because it was of the same sense and roughly the same magnitude in both the disturbed and undisturbed flows. Thus a velocity deficit of less than one percent could be detected with the pitot-static tube.

The hot-film anemometer data was obtained using a Thermo-Systems, Inc., Model 1050 anemometer unit with a TSI-10 quartz coated cylindrical film. The unit was operated without linearization or filtering. The sensing element had a 25.4 μm diameter and a 0.00051 m sensing length. Calculations using the manufacturer's specifications (in a square-wave response test) indicated this film had a frequency response (down 3 db) up to 16 KHz. This was adequate in these measurements as the turbulent kinetic energy of the flow was down 5 orders of magnitude at a frequency of 2000 Hz (Tieleman, 1967). The small size sensing volume of the hot film permits detection of "eddies" with a frequency of approximately 5000 Hz in a stream moving at 7.6 m/sec. This was more than adequate for the flow of interest.

The hot films were calibrated daily using a Thermo-Systems, Inc., Model 1125 calibrator and the MKS Baratron Pressure Meter. The calibrator itself was calibrated using the same pressure meter and a pitot-static tube. The calibrator was accurate to within 1 percent of the velocity measured by the pitot-static tube. This small error was removed from the calibration during the data reduction.

Calibration data were fit to a variable exponent form of King's
Law

$$E^2 = A + BU^n \qquad\qquad (4\text{-}1)$$

using a least-square fitting program. From this equation it can be
shown that the local turbulence intensity is given, to a very good
approximation, by

$$\frac{U_{rms}}{U} = \frac{2EE_{rms}}{n(E^2-A)} \quad . \qquad\qquad (4\text{-}2)$$

Mean values of the anemometer bridge output were averaged over a
30 second period using a Hewlett-Packard integrating digital voltmeter
(Model 2401C). True root-mean-square voltages were read by averaging
for one minute the d-c output of a DISA Model 55D35 rms voltmeter with
the integrating voltmeter.

It was not feasible to calibrate the hot films in air at the same
temperature as the air in the tunnel test section. To avoid any error
due to the difference in calibration and test temperatures the method
of Bearman (1970) was used to correct the measured voltages to the
value that would be measured if the sensor were in air at the tempera-
ture of the calibrator flow. There are two basic conditions that must
be met to ensure accuracy of the Bearman correction. Temperature
differences must be small (less than approximately 12°C) and wind
speeds must be greater than 0.9 to 1.5 m/sec. Both of these conditions
were met in all tests performed.

To obtain an accurate measure of the influence of the building
model on the boundary-layer flow, it was necessary to take mean
velocity and turbulence intensity profiles both with and without the

model in place. The profile without the model in place was always
taken immediately before or after the measurement of the profile with
the model in the tunnel. Since the time required for significant drift
in the hot-film calibration is greater than the time required to measure
two velocity profiles the effect of any drift was negligible when the
velocity deficits and turbulence excesses were calculated.

On many days of testing the hot film was calibrated both before and
after the day's measurements. This was done both to verify the morning
calibration and also to obtain an indication of the system accuracy and
repeatability. The results of this procedure were quite acceptable.
Values of mean velocity deficit and turbulence intensity excess calcu-
lated from the same data but using the two different calibrations always
were in excellent agreement. Repeatability in mean velocity was typi-
cally of the order of 1/2 percent of the mean velocity and was never
observed greater than 1.5 percent in the data taken in the wake of the
hemisphere. Repeatability in turbulence intensity was better than that
in mean velocity. Since the calibrations on any given day were quite
often performed by different persons and at different temperatures these
results provide a partial check on the temperature correction scheme,
operator error, and the calibration stand setup.

It must be noted that neither the hot film itself nor the use of
the linearized King's Law is accurate in the highly turbulent flows in
and very near the separation bubble behind the buildings. Some data is
presented which was obtained in the separation bubble using the apparatus
and techniques just described. This data is presented only for complete-
ness and for the useful qualitative view it presents of the flow. The
values given are not accurate and should be used only to determine

trends along the very near wake profiles. Use of a pulsed hot wire such as Castro used (1973) or a laser doppler anemometer might be considered if quantitative measurements are needed in the separated flow.

Measurements in the Vortex

The need to measure the cross-flow components of mean velocity to locate and measure the strength of the trailing vortices necessitated use of a velocity transducer which has high resolution in a turbulent flow. A new rotating yawed hot-film probe designed by J. A. Peterka was developed and tested for use in the present research. Some details, in addition to those that will be given here, of the development, testing, and operation of the probe are given by Peterka and Cermak (1974).

The principle of operation of the rotating hot-film probe is the same as that for any other yawed hot-wire probe. Use is made of the fact that the hot-film cooling is sensitive not only to the magnitude of the velocity of the fluid passing over the wire but also to its direction. A discussion of this directional sensitivity can be found in Sandborn (1972). If a hot film is placed at a point in the flow and held at different orientations to the flow then information about the speed and direction of the flow can be extracted, using the calibration information of the probe, by straightforward mathematical techniques. This is precisely the principle of operation of the X-wire probe, except the X-film uses two films rather than using one film at two different orientations. Two mean velocity components are obtained for each orientation of an X-wire probe. Mathematically, two equations (one for each hot film) are needed to solve for the two components of mean velocity. When the rotating hot-film probe is used the hot film is set at several orientations to the flow (10 were used in this study).

The result is that one has more equations available than the three required for determining the three components of velocity. These equations can then be solved using a least-squares technique to find the three components of velocity that give the best solution to the equations. This reduces the error introduced into the calculations by the inevitable random errors of voltage measurement and positioning by "averaging out" these random errors with the least-squares fit. The result is a highly sensitive long-time average measurement of the three mean velocity components.

The probe is shown in Figure 14. An additional schematic of the probe showing some useful notation definitions is given in Figure 15. A 0.46 m long Thermo-Systems, Inc., probe support is mounted to a frame. A hot-film yawed 45 degrees to the probe support axis is installed on the probe support. The probe support is driven about its axis by a remotely controlled d-c motor. The angle of rotation of the probe support is measured remotely using a potentiometer. In operation the entire frame and probe support are placed in the flow at small angles of pitch and yaw. The probe support and hot-film probe are then rotated to, and held at, the several angles of incidence desired. At each angle of incidence, θ, a 30-second average of the anemometer bridge output is determined and the angle of orientation (ψ) of the hot film to some fixed reference coordinates is obtained from the potentiometer readout.

The angles of pitch and yaw of the entire probe support to the flow are quite important. If the angles are too small there will not be sufficient differences between the bridge voltages measured at the different hot-film orientations (different values of ψ). (If the angles of pitch and yaw are zero, of course, the hot film will be at $\theta = 45$ degrees to

the flow for all angles of rotation.) If the pitch and yaw angles are
too large there will be some angles of probe rotation where θ will be
near zero. This is more critical in highly turbulent flows because then
the instantaneous velocity vector may be directed along the film axis
even though the average velocity vector is several degrees from the axis.
Low angles of incidence must not occur if probe-tip effects are to be
avoided. In the tests reported in this dissertation the probe support
was rotated approximately 15 degrees out of alignment with the wake
centerline in a horizontal plane and then 15 additional degrees in the
vertical plane of the probe axis. In this orientation the average veloc-
ity vector formed an angle θ varying between 20 degrees and 70 degrees
with the hot-film axis at the various values of ψ.

The probe was calibrated over the required velocity range (7 to
16 m/sec) at angles between 20 degrees and 70 degrees in increments of
10 degrees. The 36 calibration points generated (6 velocities at each
of 6 angles) were fit to a surface of the form: $E^2 = A + BU^C f(\theta)$
where $f(\theta)$ is given by $f(\theta) = 1 + A_1\theta + A_2\theta^2 + A_3\theta^3$. The six con-
stants were determined by a least-squares fit method. This form for
$f(\theta)$ gives an excellent fit to the data over the range of θ con-
sidered. It has been found that this form of $f(\theta)$ may be inappro-
priate for a broader range of values of θ such as may be needed for
measurements in a more turbulent flow or a flow in which the direction
of the mean velocity vector is not known within approximately
10 degrees. The results of a typical calibration are shown in Figure 16.

Calculation of the mean velocity components from the 10 pairs of
voltage/hot-film orientation data is simple in concept, if not in detail.
Appendix A describes the calculations in detail. Values for the three

mean velocity components U, V, and W are assumed. For the
calculations the coordinate system is chosen such that U is in the
direction of the probe axis and V and W form an orthogonal set.
With the assumed values for the velocity components and the known
orientations of the hot film the values of θ for each of the 10 data
points can be calculated with simple geometrical considerations. These
calculated values of θ can then be used to calculate an anemometer
voltage corresponding to the assumed U, V and W using the calibra-
tion equation. The sum of the squares of the differences between the
measured and calculated values of E can be computed. Then the initial
guess for U, V, and W is altered with Newton's iterative method, the
calculations repeated, and the sum of the squares of the errors
obtained. This iterative process is repeated until the error is below
a specified minimum and the calculated corrections to the best values
of U, V, and W are also below a specified value. The resulting
solution gives the velocity components in the frame of reference of
the probe axis.

The velocity vector in the coordinate system of the wake and model
can be calculated by simple rotation of the velocity vector from the
probe coordinate system. In practice this angle of rotation was deter-
mined as follows: At the beginning of each day the rotating hot-film
would be calibrated and placed on the instrument carriage in the wind
tunnel. During the course of the day's measurements the velocity vector
at several points would be measured in the absence of the model. The
rotation angle would then be calculated such that the values of V and
W were zero (in the wake coordinate system), when averaged over all
the points in the undisturbed boundary-layer flow. (Though the vertical

velocity, W, in the undisturbed boundary layer, is of the order

W/U ~ (n/(n+1))(z/δ)dδ/dx   (see Chapter III) the interest is in the

vertical motion due to the vortex. Hence, it was desirable to "subtract"

the mean vertical motion in the undisturbed boundary layer.) Then all

the data for that same day in the wake of the models was reduced using

the same rotation angle. This, in a sense, is an additional step in the

probe calibration and insures that the data obtained indicates the effect

of the model on the flow and not simply an error in probe alignment or

the vertical velocity due to the boundary-layer growth.

Examining all the data taken in the undisturbed boundary layer

(where it is assumed V = W = 0) provides a measure of the accuracy of

the probe system. Refer once again to Figure 15. The angles ϕ and β

define the orientation of the velocity vector with respect to the wake

(or wind tunnel) coordinate system. If, as we assume, the cross-flow

components detected by the probe are both zero, then ϕ and β are

also identically zero. The measured values of ϕ and β are not always

identically zero though the average of all the values measured in one

day in the undisturbed flow is forced to zero. The standard deviations

of the values of ϕ and β are a measure of the resolution, or "noise

level" of the instrument. A total of 77 different measurements were

made in the course of the research in the undisturbed boundary layer

over the smooth floor. The standard deviations of the values for ϕ

and β were $\sigma_\phi = 0.39°$ and $\sigma_\beta = 0.63°$. It is shown in Appendix A,

using these values, that the rotating hot-film anemometer system is

capable of detecting a cross flow having a magnitude which is one

percent of the local longitudinal velocity. In fact the resolution of

the instrument may be better than this because of errors in the assumption of no cross flows in the undisturbed boundary layer.

The rotating hot-film anemometer offers high resolution and is necessary for measurements in the vortices in the wakes investigated. Although it is more reliable than conventional X-film systems its use is relatively complex and time consuming. Thus it was desirable to have a means of determining the points of interest in the wakes by making broad surveys of the wakes with a simple instrument. A "paddle-wheel vorticity meter" was constructed and used to determine regions of high streamwise vorticity in the wakes.

The vorticity meter is shown in Figure 17. The paddlewheel was constructed of 0.0016 m thick balsa wood and had a length of 0.025 m and a diameter of 0.019 m. The operation of this device was quick and simple and gave an excellent visualization of the vorticity distribution in the wakes. The paddlewheel turned slowly enough, except in the strongest regions of vorticity, to allow counting the revolutions visually for a 30 second period. With this survey of the entire wake it was possible to locate the points of interest and make the quantitative measurements with the rotating hot film.

The vorticity meter was intended only as a flow visualization device and no attempt was made to calibrate it. Construction of a more precise meter suitable for calibration may be of interest to persons embarking on an extensive study of many vortex wakes.

Measurement of Spectra and Correlations

Measurement technology has progressed to the point where digital techniques can replace many of the operations that previously could only be performed using analog techniques. Rather than passing an electronic signal through a series of filters to measure an energy

spectrum it is now possible to perform a discrete Fourier transform on a digital record to obtain the same energy spectrum. Correlations can be calculated from digital records on a digital computer to replace analog multiplication and summing circuits. An advantage of the digital data acquisition technique is that the use of anemometer linearizers, or the linearization error if they are not used, can be avoided by performing the spectrum or correlation calculation directly on the velocity record rather than on the voltage record.

For these reasons measurements of energy spectra and space correlations were made with a digital data-acquisition system. The system consists of an analog-digital converter, a mini-computer for control and formatting, and a digital tape recorder. The digital tape that is generated is compatible with the CDC 6400 computer for data reduction. The system is capable of sampling up to eight channels of data simultaneously. Sample rates can be as high as 16,000 samples per second. The resolution of the analog-digital converter is 0.691 mv. This is quite adequate for use with the hot-film anemometers in this study, with a typical sensitivity of 22 mv/m/sec at a velocity of 12 m/sec. Even at the locations of low velocity analyzed with the digital system the resolution is better than one percent of the mean velocity.

Measurement of space correlations of longitudinal velocity fluctuations was straightforward with the digital system. Two hot films were mounted on a portable carriage that could be oriented for a traverse in any direction in the wind tunnel. One film was held fixed at the end of the carriage while the second sensor could be moved up to 0.66 m from the first. One-minute recordings were made simultaneously of the two anemometer outputs at a sample rate of 2000 samples

per second. Thus 240,000 velocity data points were recorded to generate one point on the space correlation curve. To calculate the correlation the voltage values were converted to velocity values using King's Law. (This eliminated the linearization error.) Then the mean velocity was calculated and removed from each velocity record. The two channels of fluctuating velocity information were correlated by multiplying the two channels together, averaging, and normalizing.

Only 40 seconds of the 60-second record were required to arrive at a stationary result.

Measurement and calculation of the one-dimensional energy spectrum of longitudinal velocity fluctuations were accomplished using the digital data-acquisition system and a Fast-Fourier-Transform (FFT) subroutine. A detailed description and listing of the computation technique and computer code can be found in Akins (1975). A 30-second velocity record was recorded at a sample rate of 8000 samples per second. This sample rate corresponds to a Nyquist frequency of 4000 Hz. As already mentioned, the turbulent kinetic energy in the flow was at frequencies below 2000 Hz so this Nyquist frequency is adequate. The spectrum was calculated according to the method described in Bendat and Piersol (Bendat and Piersol, 1971). After removing the mean velocity from the record and tapering the data with a cosine function the FFT of the velocity fluctuations was computed. The FFT subroutine used (FOR2D, IBM Contributed Program Library, Program Order Number 360 D-13.4.006) was designed to employ external disc storage of data in the calculation. The advantage of this method was that the length of the record that could be analyzed (and hence the lower limit of frequency that could be calculated) was limited only by computing cost and not computer core storage

capability. This eliminated a past difficulty with the FFT method of spectrum calculation. From the Fourier Transform of the tapered velocity record the energy spectrum was calculated and then smoothed by averaging a specifiable number of adjacent points. The computed spectrum was output on a hard-copy plotter, a line printer, and magnetic tape for future access.

The FFT required a record length that is a power of two for efficient operation. For the calculations in this dissertation 131,072 points comprised one record. This corresponds to a record length of 16.384 seconds. On the CDC 6400 computer the calculation, plotting, and storage of one spectrum required approximately 340 seconds of computing time--or a cost, on a deferred basis, of roughly $20.00 per spectrum. This is not at all unreasonable considering the time and effort required to obtain an analog spectrum with such a broad frequency range.

Chapter V

RESULTS AND DISCUSSION

Results of the wind-tunnel measurements are reported and discussed in this chapter. The mean velocity measurements--both longitudinal and swirl velocities--are most useful in determining the physical model of the wake. Theoretical predictions of mean velocities have been proposed with the theories already available and those developed in this dissertation. For this reason the mean velocity observations will be discussed first and the physical model of the wake which was described in Chapter III will be verified. It is shown that the vortex-containing wake is very different in character from its momentum wake counterpart. The difference in character is shown to be a result of the presence of the longitudinal vortices as hypothesized in Chapter III. The longitudinal turbulence measurements are of interest for two reasons. Many of the practical applications of this work require knowledge of the turbulence field in the wake. Also, advancements and improvements in the theory of wakes will require details of the turbulence structure in the wake and how the turbulence interacts with the mean flow to alter the wake. Measurements of the turbulence statistics will be reported in the second section of this chapter.

Measurements by another researcher of mean surface pressures on a hemispherical model in the smooth floor boundary layer are presented in Appendix B. Though they are not the work of this author the measurements have not been reported elsewhere and are appropriate to the subject of this dissertation.

A summary of the various test conditions and measurements made is given in Table 1.

The Mean Velocity Field

Extensive surveys of the mean velocity field in the wakes of hemispherical and rectangular block models were made in the boundary layers over the carpet and the smooth floor. These measurements are presented and discussed in the following sub-sections.

Wakes downwind of hemispheres

Measurements of mean velocity in the wake of the hemisphere models provided much of the interest and motivation for continued study of the vortex-containing wake. After the first measurements were made the concept of the vortex wake (see Chapter III) was hypothesized as the possible explanation of the observations. In Figures 18a through 18f a series of lateral profiles of longitudinal mean velocity are shown. The velocity profiles were measured in the wake of the 0.14 m radius hemisphere in the boundary layer over the smooth floor. Measurements were made with a pitot-static tube. The free-stream velocity was 4.9 m/sec. These profiles are very similar to those reported by Jacobs (1938) (see Chapter II). They are different from the wake of a body in a uniform flow or a momentum wake behind a building in two important ways. First, in all the far wake profiles there is a relative maximum in the velocity (or a relative minimum in the velocity deficit) on the wake centerline. A significant portion of the wake contains velocity excesses. The minimum velocity in the lateral profiles is observed at points equally spaced on either side of the wake centerline. The near wake velocity profiles have the shape of a momentum wake. The minimum velocity is observed at the center of the wake. But this profile shape is quickly changed into the shape with a local maximum velocity on the wake centerline. Velocity profiles measured in the lower regions

of the wake show this transition, from a momentum wake profile to what can appropriately be called a vortex wake profile. The profiles measured above the height of the obstacle show a momentum wake character far downwind. But the region which contains the characteristic vortex wake velocity profiles slowly grows upward giving almost all of the far wake a vortex wake structure. The second, and at the time of its discovery most surprising, unique feature of the hemisphere wake is the extreme persistence of the wake. Recall that the mean velocity wakes of simple cubes and blocks in turbulent boundary layers reported by other researchers (Counihan (1971), Lemburg (1973), Colmer (1971), Castro and Robins (1975)) extended at most to distances of the order of 10-15H. But the wake of this hemisphere is clearly evident in Figure 18 at $x/R = 69.8$. The wake of the same hemisphere was also observed at $x/R = 96$. This was at the end of the wind-tunnel test section. It is not known how far the wake persisted downwind but it was apparently greater than 100 radii in the smooth-floor boundary layer.

These observations, both of the wake persistence and the regions of velocity excess were consistent with the vortex wake hypothesis. The wake persistence was caused by the vortex persistence and the velocity excesses were caused by the downwards convection of momentum by the horseshoe vortex pair. However, direct measurements of the vortex position, strength, and sense of rotation, in conjunction with theoretical arguments, were required to completely validate the vortex wake hypothesis.

Examination of the profiles at $x/R = 4.35$ shows that the influence of the vortices has not yet reached the centerline in the

near wake. The small regions of local minima in the deficit profiles on either side of the centerline support the hypothesis of vortex interaction. In the near wake the influence of each vortex is confined to its immediate vicinity. These regions of influence grow in the downwind direction until they meet on the wake centerline.

Measurements of longitudinal velocity were made in wakes of various hemispheres in both the smooth and rough wall boundary layers to determine if the flow were Reynolds number independent and to see the effect of a different approach velocity and turbulence profile on the extent of the wake. Figure 19 shows lateral profiles of mean velocity at four different Reynolds numbers. The profiles were all measured at the same relative location in the wakes in the smooth-floor boundary layer. The Reynolds number was varied both by changing the model size and the free-stream velocity. There is clearly a Reynolds number dependence in the flow. At low values of Re the wake (in the near wake region) resembles a momentum wake. As the Reynolds number increases the wake assumes more and more the character of the hypothesized vortex wake. At greater distances downwind the wakes at all the Reynolds numbers tested are more alike. In one possible explanation of the Reynolds number effect the vortex wake hypothesis is consistent with this observation. It is plausible that at higher Reynolds numbers separation is delayed and the horseshoe vortex pair is shed and carried nearer the centerline. Thus the influence of the horseshoe vortex becomes evident nearer the body. The vortex rollup process may also be Reynolds number dependent. A velocity profile at $Re = 2.3 \times 10^4$ at $z/R = 0.182$ is compared with

another profile at the same Reynolds number but behind a different size hemisphere in Figure 20. The two profiles are nearly identical though the models have different values of R/δ. On the plot it can be seen that profiles with identical values of R/δ but different Re are not alike. This demonstrates that the Reynolds number is the important parameter in the comparison of Figure 20 even though all other parameters are not equal for the four test conditions.

Measurements of mean velocity made with a hot-film anemometer are shown in Figure 21. These profiles are in the wake of the 0.14 m hemisphere in the smooth-floor boundary layer. The free-stream velocity was 16.2 m/sec. These conditions are the same used to obtain the turbulence intensity and mean swirl velocity data presented later in this chapter. These profiles are very similar to the profiles of Figure 18 except for the Reynolds number effect already noted.

The wake of a 0.076 m radius hemisphere in the rough-wall boundary layer was also surveyed with a pitot-static tube. In this approach flow the turbulence intensity is higher and thus one expects a wake with a shorter downwind extent (see the discussion of Chapter II). This was indeed the observation. The increased mixing due to the greater turbulence intensity diffuses the wake rapidly. This wake extended less than 60 radii. This persistence is still much greater than that of a momentum wake but less than that of the hemisphere wake in the smooth-floor boundary layer. The wake had the characteristic hemisphere wake velocity excess on the centerline, though the excess was lower than that observed in the smoother flow. At a height $z/R = 0.5$, the velocity excesses $(-\Delta U/U(R))$ at $x/R = 10$, 20, 40, and 60 were 0.063, 0.033, 0.005, and 0.0 respectively. In Figure 22 these

velocity excesses measured in the boundary layer over the carpet are compared to the centerline velocity excesses of Figure 18c. The wake over the smooth floor shows an increase in velocity excess due to the interaction of the vortex with the shear flow. This increase continues at height $z/R = 0.364$ downward to $x/R = 21.8$. But in the wake over the rough boundary the increase in velocity excess has stopped at or before $x/R = 10$ and the wake strength is decaying rapidly.

Wake behind the rectangular block building

During the same time period the hemisphere wake study was underway another study was begun on the wake of a simple rectangular block building. This work was directed at modeling in the wind tunnel a full-scale experiment being conducted at the NASA George C. Marshall Space Flight Center field site. This work is reported in more detail in another report (Hansen, Peterka and Cermak, 1974) and was described briefly in Chapter II. Primary interest was in examining the wake of the model when the wind was normal to the long side of the building ($\alpha = 0°$). But the opportunity presented itself for determining if the wake structure was significantly different from the momentum wake ($\alpha = 0°$) when roof-corner vortices were generated. Woo (1974) determined by observing smoke flow around the model that the roof-corner vortex pair appeared strongest when $\alpha = 47°$. Therefore this configuration was selected for further study. A photograph of the vortex pair when $\alpha = 47°$ is shown in Figure 23.

Mean velocity profiles were measured in the wake of the building oriented such that $\alpha = 47°$. The model was placed in the rough-wall boundary layer generated over the shag carpet. Lateral profiles of

longitudinal mean velocity are shown in Figure 24. The profiles show much the same character as the profiles in the hemisphere wakes. Once again there is a region of velocity excess in the wake and the wake is highly persistent. A velocity excess wake is observed in Figure 24 80 building heights downwind of the model. Measurements were not made further downwind than $x/H = 80$, thus the full extent of the wake is not known.

In this flow situation the vortex generated along the longer edge of the roof (on the side where $y/H < 0$) is stronger than the other vortex of the pair. The asymmetry of the wake reflects this inequality in the vortex strengths. All observations made in this wake are consistent with the hypothesis of the vortex wake applied to the hemisphere wake.

With the block model it is possible to compare the (hypothesized) vortex wake with the normal momentum wake. Velocity profiles taken in the normal wake $(\alpha = 0°)$ with the same model in the same boundary layer as the model of Figure 24 are shown in Figure 25. Comparison of Figures 24 and 25 shows dramatically the difference between the two wakes. Figure 26 compares the decay rates of the two wakes. The momentum mean velocity wake has the same strength 12 building heights downwind of the model as the vortex wake has at $x/H = 80$. The momentum wake compares favorably with the momentum wakes reported by Lemburg (1973), Counihan (1971) and Castro and Robins (1975). It can be concluded that the momentum wake is significantly different both in structure and persistence from the vortex wake.

Vortex strength measurements

The longitudinal mean velocity data all indicate that the vortex pair (the horseshoe vortex behind the hemisphere and the roof-corner vortices, perhaps combined with the horseshoe vortex, behind the block) is responsible for the difference between vortex wakes and the momentum wakes. But only measurements of the vortex positions and strengths can provide conclusive evidence for this simple model. Attempts to visualize the vortices in the wakes with smoke were all unsuccessful. The vortex strengths were too weak to render the vortex visible in the turbulent boundary layer. The vortices could be seen forming very near the bodies but at no time were they observed visually beyond the separation bubble behind the model. The paddlewheel vorticity meter and the rotating hot-film anemometer were required to detect the presence of the vortices.

Figure 27 shows contour plots of lines of equal streamwise vorticity in the wake of the 0.14 m radius hemisphere in the smooth-floor boundary layer. These contours were generated from the paddle-wheel vorticity meter data. Though the meter was not calibrated and cannot be used to give a quantitative measure of the vorticity the contour plot clearly gives the average location of the vortex and the sense of the rotation. Figure 28 shows a contour plot of streamwise vorticity in the wake of the block building with the wind approaching at $\alpha = 47°$. Similar results were observed for all values of α examined (between 37° and 57°). The vortex wake is generated behind the block building for a wide range of approach flow directions and not just near $\alpha = 47°$.

Quantitative measurements of swirl velocity were made using the rotating hot-film anemometer at locations the vorticity meter indicated to be of interest. Cross-flow velocities were measured in five data planes (at x/R = 8.73, 13.1, 17.5, 21.8, and 26.2) behind the 0.14 m radius hemisphere in the smooth-wall boundary layer, in one plane (at x/R = 8.7) in the wake of the 0.076 m radius hemisphere, also in the smooth-wall boundary layer, and in two planes (at x/H = 12.9 and 18.6) behind the block at α = 47° in the rough-wall boundary layer.

Cross-flow velocity vectors in the 0.14 m radius hemisphere wake are shown in Figure 29. The cross-flow vectors both with and without the model present are shown at many locations to verify the effect of the hemisphere on the flow. In Figure 29a the swirling motion is highly evident. Note that the rotation is such that there is a downward flow at the wake centerline as predicted by the theory of Hawthorne and observed with the vorticity meter. In Figure 29b the swirling motion is still apparent though considerably weaker than that shown in Figure 29a. Measurements in the three other planes indicated the same trends. In all five planes the swirling motion was present but the decay of the swirl velocities from one plane to the next was quite rapid. Neither the rotating hot-film nor the vorticity meter was sufficiently sensitive to detect the vortex beyond x/R = 26.2.

From the distribution of cross-flow velocities in the five data planes it was possible to calculate the circulation about the vortex as a function of x/R. Figure 30 shows the maximum circulations about any circuit in each of the data planes. The circulations about all closed rectangular paths through the data points were calculated. Then at each value of x/R the maximum value was selected. In all cases the

circuit which had the maximum circulation was at or near the outermost possible circuit through the data points.

Also shown in Figure 30 is the theoretical prediction of the vortex circulation obtained from the results of Chapter III. Recall that the inviscid theory of Hawthorne and Martin, which was modified by this author, predicts a normalized circulation around a large circuit of $\Gamma/U(R)R = 0.75$ for all x. This value in conjunction with the meander theory of Baker et al. was used to generate the curve shown in Figure 30. The value of σ was found from equation (3-4) to be $\sigma = 0.073$ m at $x/R = 8.7$. The vortex core radius, a, at $x/R = 8.7$ was selected to result in agreement between the theory and measurements at $x/R = 8.7$. The core radius at this location was found to be 0.019 m. At subsequent locations the value of a was calculated using the fact that a increases as $(x/R)^{\frac{1}{2}}$. The excellent agreement between the theory and observations at values of x/R greater than 8.7 indicates that the inviscid theory combined with the effect of meander is an adequate model of the flow. There is some uncertainty in the measured values of circulation at large values of x/R. But the trend indicated by the theory is certainly that indicated by the data and the numerical values are in quite good agreement also.

It is evident from these data that vortex meander is an extremely important feature of the vortex wake in a turbulent boundary layer. But it is seen in Figure 30 that the effect of meander can be calculated using a simple theory and the method described to determine the core radius. If the vortex were visible with smoke visualization, values of σ and perhaps a could be determined directly. But the indirect method gives good results when the vortex core radius can be determined empirically.

Application of the meander theory assumed a Rankine vortex structure in the instantaneous vortex. Figure 31 compares the measured swirl velocity distribution along a horizontal line through the vortex at x/R = 8.7 with the distribution calculated from the meander theory assuming a Rankine vortex. Though there is considerable scatter in the data there appears to be good agreement in the vortex core size and the velocity distribution. This serves to further confirm the method used to predict the average vortex strength.

In the one plane in which the cross flow was measured behind the 0.076 m radius hemisphere the maximum average circulation was $\overline{\Gamma}/U(R)R =$ 0.044. The hemisphere was placed in the wind tunnel where the boundary-layer thickness was 0.51 m. The thickness was 0.38 m at the location all other models were placed in the smooth-floor boundary layer. Thus it was expected that the circulation measured would be lower behind the 0.076 m model because the turbulence intensity was greater at the height of the vortex. This expectation was realized as the circulation was only approximately 20 percent of the value measured behind the 0.14 m model. This data provides another, however limited, check of the theory. The value of the instantaneous vortex strength predicted is still $\Gamma/U(R)R = 0.75$. When the meander theory is applied to obtain the average, or measured, circulation prediction a value of $\overline{\Gamma}/U(R)R =$ 0.135 is obtained. Calculation of this value required the assumption that the ratio a/R would be the same behind the 0.076 m model as it was behind the 0.14 m model. The validity of this assumption is open to question but no other method is available for estimating the core radius. The agreement between the measured value of $\overline{\Gamma}/U(R)R = 0.044$ and the predicted value of 0.135 is, at first glance, poor. But the

difference between the two values is only 12 percent of the instantaneous vortex strength. This agreement is as good as can be expected considering the uncertainty in the value of a and the measurement accuracy.

A final test of the theory predicting the instantaneous vortex strength was performed in a hemisphere wake. The hemisphere was mounted near the leading edge of a flat plate which was suspended in the free stream of the wind-tunnel test section. This was done to place the model in a uniform approach flow. According to the theory the vortex strength is directly related to the shear in the mean velocity profile approaching the model. In a uniform flow the horse-shoe vortex should not be generated. Observations with the vorticity meter showed a very weak vortex pair was generated. The average strength of the vortex pair was much less than that observed behind the model in a shear flow even though the turbulence intensity of the flow was much less. This weak vortex was most likely due to the small amount of shear generated by the leading edge of the flat plate and the boundary layer on the plate and model. The result is that the simple test also indicates the inviscid theory is adequate for predicting the vortex strength.

The final vortex strength measurements were made in the wake of the block building with the wind at an angle of approach of $47°$ in the boundary layer over the carpet. The results of these measurements are shown in Figure 32. The highly turbulent flow reduces the measured vortex strength to a level which is near the resolution limit of the instrument in the highly turbulent flow. Typical swirl velocities are of the order of three to five percent of the free-stream speed. But

the fact that the vortex can be detected at all in such a flow is a good indication that the instantaneous vortex strength is quite high. There is no prediction of the instantaneous strength available, and again there is no method to determine the core radius reliably. Therefore, a reliable quantitative application of the meander theory is not possible. Inspection of the meander theory indicates that the roof-corner vortex must be stronger than the horseshoe vortex behind the hemisphere. Indeed, visualization with the vorticity meter also indicated that the instantaneous roof-corner vortex was considerably stronger than the instantaneous horseshoe vortex. Unfortunately, a quantitative measure of the relative strengths of the instantaneous vortices is not possible with the instrumentation available for this study.

Vortex position behind the hemisphere

The position of the vortex behind the 0.14 m hemisphere was determined from the vorticity meter and swirl velocity data plots. The results are shown in Figure 33. Both methods for determining the vortex position agreed reasonably well. There is considerable scatter in the data because of the coarse spatial resolution between the swirl velocity data points and the sometimes asymmetric, weak distribution of swirl velocity. The trend of the motion is clear--the vortices rise and move outwards as they travel downstream. It was postulated in Chapter III that vortex rise is due to vertical transport of vorticity. The rate of rise of the vortex was then equated to the rate of growth of the boundary layer. The motion outwards was attributed to the interaction of the vortex with the surface (the induced motion due to the image vortex).

Also shown in Figure 33 is the predicted motion of the vortex. These curves were calculated by fitting the results of equation (3-17) with the observations, and then using this result for $\bar{z}(x)$ in conjunction with equation (3-18) to predict $\bar{y}(x)$. Two curves of $\bar{y}$ vs x are plotted. In one curve the boundary condition of equation (3-18) was selected to result in agreement between theory and observation at x/R = 8.73. In the other the boundary condition was selected to result in better overall agreement.

It can be seen that agreement between the phenomenological theory and the observations of vertical vortex motion is reasonably good. The vertical motion is slightly underpredicted. This may be due to error in the assumption that the obstacle is a disturbance to the boundary layer sufficiently small to allow equating the boundary layer growth in the wake to that in the undisturbed boundary layer. Agreement between the predicted and observed lateral motions of the vortex is not highly satisfactory. The theoretical curve is very sensitive to the selection of the boundary condition. But neither theoretical curve gives good agreement between the theory and the observations over a large range of x/R. It is apparent that either the physical mechanisms of vortex motion are not well understood or the mathematical model is not completely adequate.

It can be seen looking at Figure 34 that the vortex position is that required to satisfy the vortex wake hypothesis. The hypothesis requires that the vortex location be between the minimum and maximum of the velocity deficit profile. The points on the lateral profiles where the velocity deficit is a maximum are shown as the dashed line in

the figure. The vortex is always located inboard of this dashed line and not along the line as hypothesized by Castro and Robins (1975). Note that the growth of the vortex core can be seen in the divergence of the lines of minimum velocity and vortex location.

In a decaying line vortex which is very strong there is an axial flow in the core of the vortex towards the upwind (or younger) part of the vortex (toward the wingtip in a trailing vortex behind an aircraft) (Batchelor, 1964). This axial flow is a result of the pressure gradient from the weak, diffuse core of the decaying vortex to the tight, strong core of the upwind portion of the vortex. In the data obtained in the present study there is no indication of this phenomenon--which would appear as an increased velocity deficit at the location of the vortex. It can be concluded that the vortex is of insufficient strength to establish significant pressure gradients along the core of the vortex.

All of the observations of longitudinal and swirl mean velocities made in this study support the hypothesis that the vortices in the wake are responsible for the differences noted between the wakes reported in this research and the momentum wakes reported by others. The rotational sense and position of the vortices are precisely those required to support the hypothesis. The vortex meander results in observation of a weak, rapidly decaying vortex when in fact the instantaneous vortex is strong and only slowly decaying. It can be said with certainty the wakes in this investigation are combined vortex and momentum wakes and the vortex is responsible for the unusual features of the wakes.

Evaluation of the Hunt vortex wake theory

The combined vortex and momentum wake theory recently developed by Hunt can be tested by comparing some of Hunt's asymptotic solutions

for the vortex wake, combined with the momentum wake prediction, with the wind-tunnel observations in the hemisphere wake reported earlier in this chapter.

The experimental evidence of the importance of the vortex in determining the nature of the wake is clear. Thus it can be expected that Hunt's mathematical model, since it contains the basic physical model already described and verified, will present a reasonable prediction of the wake. The assumption of small velocity perturbations is valid in the hemisphere wake. The assumption that $n \ll 1$ is satisfied as is the assumption that $R/\delta \ll 1$. In the previous section it was shown that there are no significant velocity perturbations caused by pressure gradients along the vortex core. Therefore the assumption of a balance between inertial and Reynolds stresses in (V_+) and (V_-) is satisfied. There is insufficient data to test the turbulence model. It is unfortunate that only the asymptotic results are presently available. But several important conclusions can be drawn from comparing these results with the observations.

Evaluation of the theory is accomplished by comparing measurements on the wake centerline with the prediction of the asymptotic results for the inviscid region (E). On the centerline the effect of each branch of the horseshoe vortex is identical and additive. The effect of one branch can be calculated from the theory and then simply doubled to account for the other branch. Application of the theory requires a knowledge of the strength of the vortex at $x = 0$ and the vortex position for all x. The strength of the instantaneous vortex, $\Gamma/U(R)R = 0.75$, predicted by this author and verified earlier in this chapter is taken as the strength of the vortex at $x = 0$. The position

of the vortex is obtained from the observations already presented in Figure 33. An obvious problem is apparent in Hunt's model. He assumes the vortex position is constant (along the line $z = h$, $y = 0$). Actually h is a function of x and the vortex also moves laterally with increasing x. This may not be a serious problem because results of the theory can be applied using variable h and y values. But the solutions were obtained using an assumption which is not valid. The magnitude of the error introduced using this assumption should be examined in future refinements of the theory. In the calculations that follow h is taken as a constant, $h = 0.4R$, and the observed values for y are used.

The eddy viscosity $\tilde{v}/h = 2n\kappa^2$ is equal to $\tilde{v}/h = 0.038$ in the smooth-floor boundary layer. The regions (G) and (V_+) merge when $x/h \gg \sqrt{4\tilde{v}x/h^2}$. Therefore, for the present problem the regions merge directly beneath the vortex when $x/h \gg 6$. But on the wake centerline where y is typically equal to $4h$, the vortex core does not extend to the centerline until $x/h \gg (y^2/h^2)/(4\tilde{v}/h)$, i.e., $x/h \gg 100$. Thus along most of the wake centerline the assumptions valid in region (E) apply. Region (G) does extend quite high into region (E) on the wake centerline. But the effect of this boundary-layer region cannot be large away from the surface. The asymptotic results for region (E) should apply most correctly along the wake centerline though the damping influence of (G) will lead to actual values lower than the predicted values for large x/h.

Results of the calculations of the vortex wake on the wake centerline at four downwind positions are shown in Figure 35. The vortex wake results were calculated from equation (2-2). The momentum

wake velocity deficit profiles are also shown. These curves were
obtained using Hunt's momentum wake theory, choosing the strength of
the wake to result in agreement between theory and observations at
$x/R = 8.73$ for large z/R. The sum of the vortex wake velocity excess
and the momentum wake velocity deficit should agree with the observed
velocity profile. At $x/R = 4.36$ and $x/R = 8.73$ the agreement between
the observations and the predictions is quite good. For all x the
shape of the velocity profile is predicted very accurately though the
actual values are in error. Surprisingly, the vortex wake excesses
appear to be too weak near the ground and too strong far above the
ground. One would expect the influence of region (G) to have the
opposite effect. At great distance downwind the calculated vortex
wake is much stronger than the observed vortex wake. This is to be
expected because the regions (V_+), (V_-), and (G) have all merged and
asymptotic results for region (E) should not apply. Asymptotic results
have not been obtained by Hunt for the combined (V_+), (V_-), (G) region.

One of the most interesting predictions of Hunt's theory is the
slow decay of the wake strength. Recall that the vortex wake strength
first increases as $x^{\frac{1}{2}}$ and then decays as $x^{-\frac{1}{2}}$. This decay is very
slow compared to the $x^{-3/2}$ decay of a three-dimensional momentum wake
and the x^{-1} decay of a two-dimensional momentum wake. In Figure 36
the experimentally observed maximum vortex-induced velocity perturba-
tions on the wake centerline are plotted against x/R. The vortex-
induced perturbation was determined by adding the calculated momentum
wake velocity deficit already discussed to the observed velocity excess
(also shown on the figure). At $x/R = 26.2$ the maximum velocity excess
value is questionable. Therefore, at this location the two highest

observed values of $-\Delta U/U(R)$ are shown. It can be seen that the wake decay rate is approximately that predicted by Hunt. The increase in wake strength to $x/R = 21.8$ is not as rapid as predicted by Hunt's theory.

The results, though far from being completely satisfactory, are encouraging. The authors expect that agreement between theory and observations would be more complete if Hunt's complete results were available. But even the asymptotic results predict the shape of the velocity profiles quite satisfactorily. A wake with extreme persistence and a large region of net velocity excesses is also predicted. It appears that the theory contains many of the important physical concepts and is in need only of refinement.

Turbulence Measurements

Extensive measurements of longitudinal fluctuating velocities were made in the wakes of the block and the hemispheres. Only longitudinal velocity fluctuations were measured. Hence the word "longitudinal" will be omitted from the remaining discussion with the understanding that it is implied in all reference to turbulence measurements.

The turbulence intensity profiles in vortex wakes are quite different in character from their momentum wake counterparts. In Figures 37 and 38 the turbulence intensity wakes of the block building in the rough wall boundary layer at $\alpha = 47°$ and $\alpha = 0°$, respectively, are shown. In the vortex wake there is a large region where the turbulence intensity is lower than it would be at the same location in the absence of the model. This is due to the downwards convection by the vortices of less turbulent fluid from the upper portion of the

boundary layer. The turbulence vortex wake is also more persistent than the momentum wake--though the rms of the velocity fluctuations returns to the undisturbed state more rapidly than the mean velocity field. At x/H = 19 in the vortex wake of the block building the rms velocity fluctuations are uniform along a lateral profile. Variations in the turbulence intensity along the profile are due solely to variations in the local mean velocity.

The turbulence intensity wake of the 0.14 m radius hemisphere on the smooth floor is shown in Figure 39. Once again there is a large region of turbulence intensity deficit--as opposed to the more common excess in momentum wakes--and the unusual wake persistence. These observations confirm more strongly still the vortex wake hypothesis.

In none of the turbulence measurements is there any indication of turbulence damping in the vortex core by the rotational stabilization of the vortex. The rotation, which can act much like stable thermal stratification, is apparently not of sufficient magnitude to affect the turbulence.

Measurements of space correlation of velocity fluctuations were made in the wakes of the 0.076 m radius hemisphere and the block building at $\alpha = 0°$ and $\alpha = 47°$ in the boundary layer generated over the carpet. Additional measurements were made in the wake of a block building 0.15 m high (of the same proportions as the block building 0.065 m high) to see if the turbulence scales in the near wake are completely determined by the building size.

Counihan (1971) reported that all integral scales of turbulence are reduced in a momentum wake of a three-dimensional obstacle from their value in the undisturbed boundary layer. Figure 40 shows two-point

velocity correlation coefficients as a function of lateral separation distance in a vortex wake. Obviously the correlation is better in the vortex wake than it is in the undisturbed boundary layer for a given separation distance. This may be due to the decreased turbulence intensity in the vortex wake and the improved correlation due to the presence of the more highly structured vortex (see Townsend, 1956, for example). Figure 41 shows a similar series of plots in the momentum wake of the block building at $\alpha = 0°$. In this wake, as in Counihan's measurements, the scale of turbulence is reduced. It can be seen from a comparison of Figures 40 and 41 that the vortex wake is more highly structured than the momentum wake. At $x/H = 20.0$, in the vortex wake, the correlation is higher in the wake than in the undisturbed boundary layer. At $x/H = 20.0$ the wake of the building at $\alpha = 0°$ is not observed. Presumably the correlation would be the same at $x/H = 20.0$ as it is in the undisturbed boundary layer. Correlations as a function of longitudinal separation distance in the vortex wake of the block are shown in Figure 42. The vortex wake has better longitudinal correlation for large separation distances than the undisturbed boundary layer or the momentum wake.

Lateral correlations in the hemisphere wake are shown in Figure 43. Here the correlations are very similar in and out of the wake. But in the wake there is a slight rise in the correlation at $y/R = 1.0$. This may be a weak indication of the presence of the vortex. If the vortex strength were higher in proportion to the turbulence intensity the evidence of the vortex would likely be more pronounced.

A tabulation of the integral scales of turbulence at all measurement locations is given in Table 2. Note that at all locations in the

momentum wakes the scales are reduced from their values in the undisturbed boundary layer. But in the vortex wakes many of the scales increase.

It might be expected that in the near wake of a body the scales of turbulence, particularly the lateral scales, are determined solely by the dimensions of the body. Comparison of lateral scales measured at $x/H = 2.55$ behind the 0.065 m block and the 0.15 m block shows that this is not the case. The ratio Λ_y/H is 0.34 behind the small model and 0.21 behind the large model. At $x/H = 7.17$ the ratios are 0.55 and 0.30 behind the small and large models respectively. The ratios of the longitudinal scale of turbulence to the building height at $x/H = 2.55$ are 1.67 and 0.64 behind the small and large models. Obviously the scales of turbulence in the wakes of bodies in the rough-wall boundary layer are not determined solely by the scale of the body--even in the very near wake.

One-dimensional turbulent kinetic energy spectra were calculated at several points in the wakes and at the corresponding heights in the approach flow in the rough-wall boundary layer. There were two purposes in this. One was to determine how the energy was redistributed in the wake. The other was to determine if there is a discrete meander frequency to the motion of the wake or the vortex. It was found that there was little difference between the normalized spectra in and out of the wakes and there was no meander frequency evident in any of the spectra calculated. Spectra were measured throughout the wakes-- including points at the edge of the wake and at the location of the vortices. Figure 44 shows a comparison of a spectrum in the wake of the block at $\alpha = 47°$ to the spectrum of the undisturbed boundary layer

at the same height. There is the expected shift of energy to the higher frequencies in the wake. Both spectra show a distinct inertial subrange region and viscous dissipation region. A spectrum at $x/H = 20$ was virtually indistinguishable from the approach flow spectrum. There is some scatter in the points at the low frequency end of the spectrum. This scatter could be reduced by lengthening the duration of the velocity record.

Figure 45 compares spectra in and out of the hemisphere wake. Again there is little difference between the two curves. At $x/R = 20$ the hemisphere wake spectrum, too, is indistinguishable from the approach flow spectrum. It can be concluded that the structure of turbulence in the wake returns to its undisturbed state far more quickly than the mean velocity distribution returns to its undisturbed state.

The absence of evidence of a discrete vortex meander frequency lends further support to the assumption of a Gaussian probability distribution in the vortex meander theory.

All of these turbulence measurements indicate that the vortex wake has turbulence characteristics quite different from the momentum wake. The turbulence deficit and wake persistence, not observed in a momentum wake, are due to the presence of the vortices in the combined vortex and momentum wake. The turbulence wake is not as persistent as the mean velocity vortex wake. The opposite is true in a momentum wake.

Chapter VI

CONCLUSIONS AND RECOMMENDATIONS

An obstacle wake unlike any reported previously in the literature has been recognized and investigated using wind-tunnel tests and theoretical analyses. The new type of wake is a vortex-containing wake behind a bluff body mounted on a plane surface in a thick, turbulent boundary layer. Several conclusions can be drawn from the results of the study of the vortex-containing wakes which were presented in the foregoing chapters.

The vortex-containing wakes have a character quite unlike that of their momentum wake counterparts. Two major differences were noted between the two types of wakes: 1) vortex-wake persistence is much greater than momentum-wake persistence and 2) the vortex wake contains large regions of mean velocity excess and turbulence intensity deficit not observed in momentum wakes. A vortex wake hypothesis was developed to explain the differences between the two types of wakes. Briefly, the hypothesis states that the longitudinal vortices in the vortex wake induce a downwards motion in the center of the wake which carries high momentum fluid from the higher portions of the boundary layer toward the ground plane. This results in the velocity excesses noted in the wakes. The remarkable wake persistence is a result of the persistent nature of a trailing line vortex. The vortex wake hypothesis was verified by measurements of the location, sense of rotation, and strength of the vortices in the wake.

The extent of the vortex wake, just as that of the momentum wake, is decreased with increasing turbulence intensity in the approach flow at the height of the obstacle. However, there is not sufficient data

over a wide range of approach flow and obstacle configurations to permit development of an empirical expression relating the wake parameters to the approach flow parameters for even simply shaped obstacles.

The inviscid secondary-flow theory of Hawthorne and Martin (1955) was modified by this author to give a realistic prediction of the instantaneous strength of the horseshoe vortex in the wake of a hemisphere. The effect of flow separation was considered in the new model, as was the effect of viscosity in the boundary layer on the hemisphere. The average vortex strength in the turbulent wake was calculated using a Gaussian probability distribution to describe the lateral and vertical meander of the vortex core. The selection of one free constant in the meander theory to give agreement between the predicted and observed vortex strengths at one location in the hemisphere wake also resulted in good agreement at all other locations in the wake. The vortex meander phenomenon is of major importance in understanding the decay of the average vortex strength in a turbulent flow.

The mean motion of the trailing vortices in the hemisphere wake was upwards away from the ground and outwards from the centerline of the wake. Theoretical prediction of this motion models correctly the trend of the motion but does not give highly satisfactory agreement between the observed and predicted vortex motions. The mean vortex motion is not completely understood at this time.

The integral scales of turbulence in the vortex wake were often larger than the corresponding scales in the undisturbed approach flow. This is not the case in a momentum wake--where integral scales of turbulence are reduced in the wake. It was also observed that even

in the near wake of an obstacle the integral scales of turbulence were
not determined solely by the dimensions of the obstacle.

It was found that the combined vortex- and momentum-wake theory of
Hunt predicts the velocity excess character and $x^{-\frac{1}{2}}$ decay law observed
in the wind-tunnel simulation of the vortex-containing wake. The theory
is in need of refinement--particularly regarding addition of a vortex
strength and position prediction--but even the simple asymptotic results
predict the correct vortex-wake character. In a limited region the
theory also predicted the correct mean velocity deficits in the vortex
wake.

Finally, a rotating hot-film anemometer for sensitive measurements
of cross-flow velocities in a turbulent flow has been developed. This
anemometer makes possible the detection of weak vortices in the vortex
wakes.

REFERENCES

Akins, R. E., 1975, "Computation of Power Spectral Densities and Correlations using Digital FFT Techniques," Fluid Dynamics and Diffusion Laboratory Report CER75-76REA13, Colorado State University.

Baker, G. R., Barker, S. J., Bofah, K. K., and Saffman, P. G., 1974, "Laser Anemometer Measurements of Trailing Vortices in Water," Journal of Fluid Mechanics, Vol. 65, Part 2, pp. 325-336.

Batchelor, G. K., 1964, "Axial Flow in Trailing Line Vortices," Journal of Fluid Mechanics, Vol. 20, Part 4, pp. 74-87.

Bearman, P. W., 1970, "Corrections for the Effect of Ambient Temperature Drift on Hot-Wire Measurements in Incompressible Flow," Disa Information Bulletin No. 11.

Bendat, J. S. and Piersol, A. G., 1971, Random Data: Analysis and Measurement, Wiley-Interscience, New York.

Betz, A., 1932, "Behavior of Vortex Systems," NACA Technical Memo 713.

Blessman, J., 1971, "Pressures on Domes with Several Wind Profiles," Proc. 3rd Int. Conf. Wind Effects on Buildings and Structures, Tokyo.

Cass, S. D., Scoggins, J. R., and Chevalier, H. L., 1973, "Low-Altitude Atmospheric Turbulence Around an Airport," Journal of Aircraft, Vol. 10, No. 3.

Castro, I. P., 1973, "An Experimental Investigation of the Flow Around a Surface Mounted Cube in a Uniform Free Stream," Central Electric Generating Board Report R/M/N 687.

Castro, I. P. and Robins, A. G., 1975, "The Effect of a Thick Incident Boundary Layer on the Flow Around a Small Surface Mounted Cube," Central Electricity Generating Board Report R/M/N 795.

Cermak, J. E., 1975, "Applications of Fluid Mechanics to Wind Engineering," 1974 Freeman Scholar Lecture, ASME Journal of Fluids Engineering, Vol. 97, Ser. 1, No. 1, March.

Colmer, M. J., 1971, "Some Full-Scale Measurements of the Flow in the Wake of a Hangar," ARC-CP-1166.

Corsiglia, V. R., Schwind, R. G., and Chigier, N. A., 1973, "Rapid Scanning Three-Dimensional Hot-Wire Anemometer Surveys of Wing-Tip Vortices," Journal of Aircraft, Vol. 10, No. 12, December. Also AIAA Paper 73-681.

Counihan, J., 1971, "An Experimental Investigation of the Wake Behind a Two-Dimensional Block and Behind a Cube in a Simulated Boundary Layer Flow," CERL Lab. Note RD/L/N 115/71.

Counihan, J., Hunt, J. C. R., and Jackson, P. S., 1974, "Wakes behind Two-Dimensional Obstacles in Turbulent Boundary Layers," Journal of Fluid Mechanics, Vol. 64, Part 3, pp. 529-563.

Crow, S. C., 1970, "Stability Theory for a Pair of Trailing Vortices," AIAA Journal, Vol. 8, No. 12, pp. 2172-2179.

Donaldson, C.DuP., 1971, "A Brief Review of the Aircraft Trailing Vortex Problem," AFOSR-TR-71-1910. Also ARAP Report No. 155.

Donaldson, C.DuP., 1973, editor, "Vortex Wakes of Large Aircraft," AIAA Professional Study Series.

Frost, W., 1973, "Review of Data and Prediction Techniques for Wind Profiles Around a Manmade Surface Obstruction," paper presented at NATO meeting at Woburn Abbey.

Frost, W., Fichtl, G., Connel, J. R., and Hutto, M. L., 1975, "Mean Horizontal Wind Profiles Measured in the Atmospheric Boundary Layer About a Simulated Block Building," Proceedings of the Second U. S. National Conference on Wind Engineering Research, Fort Collins, Colorado.

Frost, W., Maus, J. R., and Simpson, W. R., 1973, "A Boundary Layer Approach to the Analysis of Atmospheric Motion Over a Surface Obstruction," NASA CR-2182.

Govindaraju, S. P. and Saffman, P. G., 1971, "Flow in a Turbulent Trailing Vortex," The Physics of Fluids, Vol. 14, No. 10, October 1971, pp. 2074-2080.

Greeley, R., Iverson, J. D., Pollack, J. B., Udovich, N., and White, B., 1974, "Wind-Tunnel Simulations of Light and Dark Streaks on Mars," Science, Vol. 183, March 1, 1974, pp. 847-849.

Gregory, N. and Walker, W. S., 1951, "The Effect of Isolated Surface Excrescences in the Boundary Layer," ARC R&M 2779, October.

Hansen, A. C., Peterka, J. A., and Cermak, J. E., 1975, "Wind-Tunnel Measurements in the Wake of a Simple Structure in a Simulated Atmospheric Flow," NASA CR-2540.

Hawthorne, W. R., 1951, "Secondary Circulation in Fluid Flow," Proc. Roy. Soc. London, Ser. A, Vol. 206, p. 374.

Hawthorne, W. R. and Martin, M. E., 1955, "The Effect of Density Gradient and Shear on the Flow Over a Hemisphere," Proc. Roy. Soc. London, Ser. A, Vol. 232, pp. 184-195.

Hinze, J. O., 1959, Turbulence, McGraw-Hill Book Co., New York.

Hirt, C. N. and Cook, J. L., 1971, "Calculating Three-Dimensional Flows Around Structures and Over Rough Terrain," Los Alamos Scientific Laboratory, LA-DC-13289.

Hunt, J. C. R. and Smith, G. P., 1969, Central Electric Research Laboratory Report RD/L/N31/69.

Hunt, J. C. R., 1970, "Further Aspects of the Theory of Wakes behind Buildings and a Comparison of the Theory with Experimental Results," Central Electric Generating Board Report RD/L/R 1665.

Hunt, J. C. R., 1971a, "The Effect of Single Buildings and Structures," Phil. Trans. Roy. Soc. London, Ser. A, Vol. 269, pp. 457-467.

Hunt, J. C. R., 1971b, "A Theory for the Laminar Wake of a Two-Dimensional Body in a Boundary Layer," Journal of Fluid Mechanics, Vol. 49, Part 1, pp. 159-178.

Hunt, J. C. R., 1972, "Some Theories for the Mean and Turbulent Velocity Distributions in Flows around Bluff Bodies," Symposium on External Flows, University of Bristol, July.

Hunt, J. C. R, 1974, "Wakes behind Buildings," paper presented to the Atmospheric Environment Committee of the Aeronautical Research Council, October.

Hunt, J. C. R., 1975, Personal Communication.

Jacobs, W., 1938, "Flow behind a Single Roughness Element," Ing.-Archiv., Vol. 9, pp. 343-355.

Klebanoff, P. S., Tidstrom, K. D., and Sargent, L. M., 1962, "The Three-Dimensional Nature of Boundary Layer Instability," Journal of Fluid Mechanics, Vol. 12, Part 1, pp. 1-34.

Lamb, H., 1945, Hydrodynamics, Dover Press, 6th ed., New York.

Lemburg, R., 1973, "On the Wakes Behind Bluff Bodies in a Turbulent Boundary Layer," University of Western Ontario Report BLWT-3-73.

Lin, J. T., 1969, Personal Communication.

Mair, W. A. and Maull, D. J., 1971, "Aerodynamic Behavior of Bodies in the Wakes of Other Bodies," Phil. Trans. Roy. Soc. London, Ser. A, Vol. 269, pp. 425-437.

Mason, W. H. and Marchman, J. F., 1972, "Farfield Structure of an Aircraft Trailing Vortex, Including Effects of Mass Injection," NASA CR-62,078.

Mochizuki, M., 1961, "Smoke Observation on Boundary Layer Transition Caused by a Spherical Roughness Element," Journal of the Physical Society of Japan (Nippon Batsuri Gakkai), Vol. 16, No. 5, May, pp. 995-1008.

Munn, R. E. and Cole, A. F. W., 1967, "Turbulence and Diffusion in the Wake of a Building," Atmospheric Environment, Vol. 1, pp. 33-43.

Olsen, J., Goldburg, A., and Rogers, M., Editors, 1971, Aircraft Wake Turbulence and Its Detection, Plenum, New York.

Orloff, R. L. and Grant, G. R., 1973, "The Application of Laser Doppler Velocimetry to Trailing Vortex Definition and Alleviation," NASA TM-X 62243, February.

Ostrowski, J. S., Marshall, R. D., and Cermak, J. E., 1967, "Vortex Formation and Pressure Fluctuations on Buildings," Proc. of the International Seminar on Wind Effects on Buildings and Structures, Ottawa, Canada, September. Also Fluid Dynamics and Diffusion Laboratory Report CEP67-68JSO-RDM-JEC80, Colorado State University.

Parr, O., 1963, Ing.-Arch., Vol. 32, pp. 393-413.

Pasquill, F., 1962, Atmospheric Diffusion, van Nostrand Co., London.

Peterka, J. A., 1975, "Turbulence in Building Wakes," 4th International Conference on Wind Effects on Buildings and Structures, London, September.

Peterka, J. A. and Cermak, J. E., 1974, "A Wind Model for an Elevated STOL-Port Configuration," NASA CR-2450.

Plate, E. J. and Cermak, J. E., 1963, "Micrometeorological Wind Tunnel Facility, Description and Characteristics," Fluid Dynamics and Diffusion Laboratory Report CER63EJP-JEC9, Colorado State University.

Saffman, P. G., 1973, "The Structure of Turbulent Line Vortices," The Physics of Fluids, Vol. 16, No. 8, August, pp. 1181-1188.

Sandborn, V. A., 1972, Resistance Temperature Transducers, Metrology Press, Fort Collins, Colorado

Schlichting, H., 1968, Boundary-Layer Theory, McGraw-Hill Book Co., New York.

Sedney, R., 1973, "A Survey of the Effects of Small Protuberances on Boundary-Layer Flows," AIAA Journal, Vol. 11, No. 6, June, pp. 782-792.

Styles, K. F. and McCallum, J. A., 1972, "A Visual Indication of a Steady Wind," Weather, Vol. 27, No. 4, April, 1972.

Tani, I., 1969, "Boundary-Layer Transition," Annual Review of Fluid Mechanics, Vol. 1.

Tieleman, H. W., 1967, "Viscous Region of Turbulent Boundary Layer," Fluid Dynamics and Diffusion Laboratory Report CER67-68HWT21, Colorado State University.

Townsend, A. A., 1956, The Structure of Turbulent Shear Flows,
    Cambridge University Press, pp. 7-20.

Widnall, S. E., 1975, "The Structure and Dynamics of Vortex Filaments,"
    Annual Review of Fluid Mechanics, Vol. 7.

Wise, A. F. E., 1971, "Effects Due to Groups of Buildings," Proc. Roy.
    Soc. London, Ser. A, Vol. 269, pp. 469-485.

Woo, H. G. C., 1974, Personal Communication.

Zoric, D. L., 1969, "Approach of Turbulent Boundary Layer to Similarity,"
    Fluid Dynamics and Diffusion Laboratory Report CER68-69DLZ9,
    Colorado State University.

Appendix A

MEAN VELOCITY CALCULATIONS FROM THE ROTATING
HOT-FILM DATA

Calculation of the three mean-velocity components in the probe

coordinate system from the ten pairs of mean anemometer bridge voltage

(E_i) and wire orientation (ψ_i) data is accomplished using a least-

squares technique. The hot-film calibration equation constants are

determined by a simple least-squares fit to the daily calibration data.

This equation is then used to relate the velocity vector to the

anemometer bridge voltage. The calibration equation has the form:

$$E^2 = A + B \, U_T^C \, f(\theta) \tag{A.1}$$

where $f(\theta) = 1 + A_1\theta + A_2\theta^2 + A_3\theta^3$ and $U_T = (U^2 + V^2 + W^2)^{\frac{1}{2}}$. With reference

to Figure 14 and simple geometrical considerations it can be seen that

angle θ is given by the relationship

$$\cos\theta = \frac{U \cos 45° + V \sin 45° \cos\psi + W \sin 45° \sin\psi}{U_T} \tag{A.2}$$

Defining the quantities $s_i (i=1,2,\ldots 10)$

$$s_i = (E_i^2 - A)\frac{1}{B} \tag{A.3}$$

and

$$S = \sum_{i=1}^{10} (U_T^C \, f(\theta_i) - s_i)^2 \tag{A.4}$$

the solution (U,V,W) (or U_j) is selected as the vector which minimizes

the value of S. The conditions required for minimizing S are that

$$\frac{\partial S}{\partial U} = 0, \qquad \frac{\partial S}{\partial V} = 0, \qquad \frac{\partial S}{\partial W} = 0 \tag{A.5}$$

These conditions (A.5) applied to equation (A.4) result in the following equations:

$$\frac{\partial S}{\partial U_j} = 0 = \sum_{i=1}^{10} [U_T^c f(\theta_i) - s_i] U_T^{c-2} [cU_j f(\theta_i) + f'(\theta_i) \frac{\partial \theta}{\partial U_j}] = F_j \quad (A.6)$$

This is a system of three equations in the three unknowns U, V, and W. The quantities F_j are defined here for later convenience. This system of equations is best solved through numerical application of Newton's iterative technique. Values for U, V, and W are assumed and then F_1, F_2, and F_3 can be calculated. First order corrections to U_k are computed using the relation

$$F_{j_{new}} = F_{j_{old}} + \frac{\partial F_j}{\partial U_k} \Delta U_k \quad (A.7)$$

The concept involved in this calculation is straightforward. But the details become quite involved. It is convenient for programming purposes to rewrite equations (A.6) in the form

$$F_1 = \sum_{i=1}^{10} X_{1_i} X_2 X_{3_i}$$

$$F_2 = \sum_{i=1}^{10} X_{1_i} X_2 X_{4_i} \quad (A.8)$$

$$F_3 = \sum_{i=1}^{10} X_{1_i} X_2 X_{5_i}$$

where the definitions of X_{ℓ_i} are obvious by comparison of (A.8) with (A.6). From (A.8) it can be seen that

$$\frac{\partial F_1}{\partial U_k} = \sum_{i=1}^{10} \left\{ \frac{\partial X_{1_i}}{\partial U_k} X_2 X_{3_i} + X_{1_i} \frac{\partial X_2}{\partial U_k} X_{3_i} + X_{1_i} X_2 \frac{\partial X_{3_i}}{\partial U_k} \right\} \quad (A.9)$$

Similar expressions are obtained for $\partial F_2/\partial U_k$ and $\partial F_3/\partial U_k$. The quantities that are contained in (A.9) are listed below:

$$\frac{\partial X_1}{\partial U_k} = cU_k U_T^{c-2} f(\theta) + U_T^c f'(\theta) \frac{\partial \theta}{\partial U_k} \tag{A.10}$$

$$\frac{\partial X_2}{\partial U_k} = (c-2)U_k U_T^{c-4} \tag{A.11}$$

$$\frac{\partial X_3}{\partial U} = cf(\theta) + (c+2)Uf'(\theta) \frac{\partial \theta}{\partial U}$$

$$+ U_T^2 f''(\theta) \left(\frac{\partial \theta}{\partial U}\right)^2 + U_T^2 f'(\theta) \frac{\partial^2 \theta}{\partial U^2} \tag{A.12}$$

$$\frac{\partial X_3}{\partial V} = cUf'(\theta) \frac{\partial \theta}{\partial V} + U_T^2 f''(\theta) \frac{\partial \theta}{\partial U} \frac{\partial \theta}{\partial V}$$

$$+ U_T^2 f'(\theta) \frac{\partial^2 \theta}{\partial U \partial V} + 2Vf'(\theta) \frac{\partial \theta}{\partial U} \tag{A.13}$$

$$\frac{\partial X_3}{\partial W} = cUf'(\theta) \frac{\partial \theta}{\partial W} + U_T^2 f''(\theta) \frac{\partial \theta}{\partial U} \frac{\partial \theta}{\partial W}$$

$$+ U_T^2 f'(\theta) \frac{\partial^2 \theta}{\partial U \partial W} + 2Wf'(\theta) \frac{\partial \theta}{\partial U} \tag{A.14}$$

Similarly,

$$\frac{\partial X_4}{\partial U_j} = cf(\theta)\delta_{2j} + cU_2 f'(\theta) \frac{\partial \theta}{\partial U_j} + U_T^2 f''(\theta) \frac{\partial \theta}{\partial U_j} \frac{\partial \theta}{\partial U_2}$$

$$+ U_T^2 f'(\theta) \frac{\partial^2 \theta}{\partial U_j \partial U_2} + 2U_j f'(\theta) \frac{\partial \theta}{\partial U_2} \tag{A.15}$$

and

$$\frac{\partial X_5}{\partial U_j} = cf(\theta)\delta_{3j} + cU_3 f'(\theta) \frac{\partial \theta}{\partial U_j} + U_T^2 f''(\theta) \frac{\partial \theta}{\partial U_j} \frac{\partial \theta}{\partial U_3}$$

$$+ U_T^2 f'(\theta) \frac{\partial^2 \theta}{\partial U_j \partial U_3} + 2U_j f'(\theta) \frac{\partial \theta}{\partial U_3} \tag{A.16}$$

The derivatives of θ with respect to U_j contained in equations (A.10) through (A.16) are given below:

$$\frac{\partial \theta}{\partial U} = \frac{U \cos \theta - U_T \cos 45°}{U_T^2 \sin \theta} \tag{A.17}$$

$$\frac{\partial \theta}{\partial V} = \frac{V \cos \theta - U_T \sin 45° \cos \psi}{U_T^2 \sin \theta} \tag{A.18}$$

$$\frac{\partial \theta}{\partial W} = \frac{W \cos \theta - U_T \sin 45° \sin \psi}{U_T^2 \sin \theta} \tag{A.19}$$

The six second-order derivatives contained in (A.12) through (A.16) are readily calculated from (A.17) through (A.19).

The solution for U, V, and W is obtained through repeated use of (A.7) to calculate corrections to the assumed values of U, V, and W. Equation (A.7) is solved for ΔU_k using Gaussian elimination. The terms contained in (A.7) are evaluated using (A.8) through (A.19). The solution is accepted when the values of ΔU_k are below a specified minimum ($|\Delta U_k| < 0.0005$). Though the computations seem complex the mean velocities at a point can be calculated (using up to 15 iterations) in approximately one to two seconds of computing time on the CDC 6400 computer. Thus the computing cost of data reduction is quite insignificant in comparison to other costs involved in the experiment procedure.

Error Analysis

The uncertainty in the swirl velocity measurement can be estimated from the standard deviations σ_ϕ and σ_β presented and explained in Chapter IV. The swirl velocity vector magnitude, U_s, is given by

$$U_s = (V^2 + W^2)^{\frac{1}{2}} \tag{A.20}$$

The uncertainty in U_s, defined as ΔU_s, is determined from the uncertainties in V and W. Thus,

$$\Delta U_s = \frac{\partial U_s}{\partial V} \Delta V + \frac{\partial U_s}{\partial W} \Delta W \ . \qquad (A.21)$$

This simplifies, using (A.20), to the form

$$\frac{\Delta U_s}{U_s} = \frac{V \Delta V + W \Delta W}{U_s^2} \qquad (A.22)$$

Since

$$\phi = \tan^{-1} W/U$$

$$\beta = \sin^{-1} V/U_T \qquad (A.23)$$

and $U \gg V, W$

$$\phi \simeq W/U$$

$$\beta \simeq V/U \qquad (A.24)$$

Therefore $\Delta W \simeq U \Delta \phi$ and $\Delta V \simeq U \Delta \beta$ $\qquad (A.25)$

Equation (A.22) can now be rewritten

$$\frac{\Delta U_s}{U_s} = \frac{1}{(U_s/U)^2} \ [(V/U) \Delta \beta + (W/U) \Delta \phi] \ . \qquad (A.26)$$

Typical values for V/U and W/U are 0.03. Using $\Delta \phi = \sigma_\phi = 0.39°$ and $\Delta \beta = \sigma_\beta = 0.63°$ the typical uncertainty in U_s is $\Delta U_s/U_s = 0.30$. In terms of the local longitudinal velocity the uncertainty is $\Delta U_s/U = 0.01$. Thus, as stated in Chapter IV, the anemometer system is capable of detecting with confidence a cross-flow which has a magnitude of one percent of the local mean velocity.

These results were obtained in the low turbulence intensity flow of the smooth floor boundary layer. It was observed that the uncertainty

was greater in the more turbulent boundary layer over the carpet. Over
the carpet the cross-flow velocity in the undisturbed boundary layer
was measured at 12 locations. The values of σ_ϕ and σ_β for these
12 data points were $\sigma_\phi = 0.38°$ and $\sigma_\beta = 1.86°$. Using the same values
for V/U and W/U as in the example in the smooth-floor boundary layer
an uncertainty in U_s of $\Delta U_s/U_s = 0.66$ is calculated. The uncertainty
in terms of the local longitudinal velocity, $\Delta U_s/U$, is equal to only
2.8 percent. The reason for the increased variance in the horizontal
angle β with an increased ambient turbulence intensity is not known
at this time.

APPENDIX B

PRESSURE MEASUREMENTS ON THE HEMISPHERE SURFACE

Another researcher at Colorado State University (J. T. Lin, 1969)
made measurements of the static pressure distribution on the surface
of the 0.14 m radius hemisphere in the 0.38 m thick boundary layer over
the smooth floor of the wind-tunnel test section. These results have
not been published previously and are relevant to the present study.
Therefore they are presented here though they are not the work of the
present author.

Figure 46 shows contours of constant pressure on the surface of
the hemisphere. The pressure coefficient is defined as

$$C_p = \frac{P-P_s}{\frac{1}{2}\rho U^2 (R)}$$

where P is the pressure at the point in question and P_s is the static
pressure in the free-stream above the boundary layer. In the region
marked $-0.7 \geq C_p \geq -0.9$ the values measured by Lin (1969) were somewhat
unreliable. It can only be said with assurance that the pressure
coefficients were between -0.7 and -0.9 in this region.

In the x-z plane the pressure becomes negative at a latitude of
approximately 45°. This is very near the location of the change in
sign of pressure coefficients on a sphere in a uniform flow. A pres-
sure coefficient of 1.0 is not observed on the hemisphere because of
the shear in the approaching flow. Separation is seen to occur some
distance before or very near the 107° meridian (where C_p = -0.70).
Somewhat preceding this meridian and beyond it an adverse pressure

gradient acts to cause separation. The precise separation line is difficult to locate using these pressure measurements.

A drag coefficient was calculated from the pressure distribution. The drag coefficient is defined as

$$C_D = \frac{\text{Drag Force}}{\frac{1}{2}\rho U_\infty^2 A_b}$$

where A_b is the dome base area. This is the form used by Blessman (1971) in reporting pressure distributions and drag coefficients on domes in various simulated planetary boundary layers. The present measurements yield a drag coefficient $C_D = 0.094$. Blessman, in a boundary layer similar to that used in these measurements, obtained a value of $C_D = 0.109$ at a Reynolds number of 2.1×10^6. Unfortunately, Blessman does not define the Reynolds number he used nor does he define the reference pressure used. He merely states that the pressure coefficients represent normalized "effective pressures".

TABLE 1 SUMMARY OF WIND-TUNNEL MEASUREMENTS AND CONDITIONS

Test Series	Model	H (or R) (m)	Boundary Layer	U_∞ (m/sec)	H/δ	Re [†] ($\times 10^{-4}$)	$\dfrac{U_{rms}(H)}{U(H)}$ (%)	Measurements
1	Hemisphere	0.14	Smooth (n=0.12)	16.2	.37	10.7	5	U, U_{rms}, swirl velocity
2	Hemisphere	0.14	Smooth	4.9	.37	3.2	5	U
3	Hemisphere	0.14	Smooth	3.3	.37	2.3	5	U
4	Hemisphere	0.14	Smooth	6.1	.37	4.0	5	Surface static pressure distribution
5	Hemisphere	0.10	Smooth	4.9	.27	2.2	6	U
6	Hemisphere	0.10	Smooth	3.3	.27	1.6	6	U
7	Hemisphere	0.076	Smooth	16.2	.20	5.5	8	Swirl velocity
8	Hemisphere	0.076	Carpet (n=0.25)	16.2	.13	4.0	17	U, U_{rms}, correlations and spectra
9	Block (α=0°)	0.065	Carpet	16.2	.11	3.3	19	U, U_{rms}, correlations and spectra
10	Block (α=47°)	0.065	Carpet	16.2	.11	3.3	19	U, U_{rms}, correlations and spectra, swirl velocity
11	Block (α=0°)	0.15	Carpet	16.2	.25	9.4	14	U, U_{rms}, correlations and spectra

[†] Re $= \dfrac{U(H)H}{\nu}$ or $\dfrac{U(R)R}{\nu}$

TABLE 2   RATIOS OF INTEGRAL LENGTH SCALES OF TURBULENCE IN THE WAKE TO
THE CORRESPONDING SCALES IN THE UNDISTURBED BOUNDARY-LAYER

	Rectangular Block H=0.065m, $\alpha=0°$*	Rectangular Block H=0.15m, $\alpha=0°$†	Rectangular Block H=0.065m, $\alpha=47°$*	Hemisphere R=0.076 m*
Longitudinal Scales				
x/H = 2.55	.52	.37	--	--
x/H = 7.17	.73	.58	1.2	1.11
x/H = 20.	--	--	1.13	1.19
Lateral Scales				
x/H = 2.55	.52	.51	--	--
x/H = 7.17	.84	.73	.95	.93
x/H = 20.	--	--	1.36	.99
Vertical Scales				
x/H = 2.55	.35	.47	--	--
x/H = 7.17	.59	.62	.93	.93
x/H = 20.	--	--	1.04	1.04

*In the undisturbed boundary layer Λ_x = 0.21 m, Λ_y = 0.043 m, Λ_z = 0.088 m.

†In the undisturbed boundary layer Λ_x = 0.27 m, Λ_y = 0.063 m, Λ_z = 0.10 m.
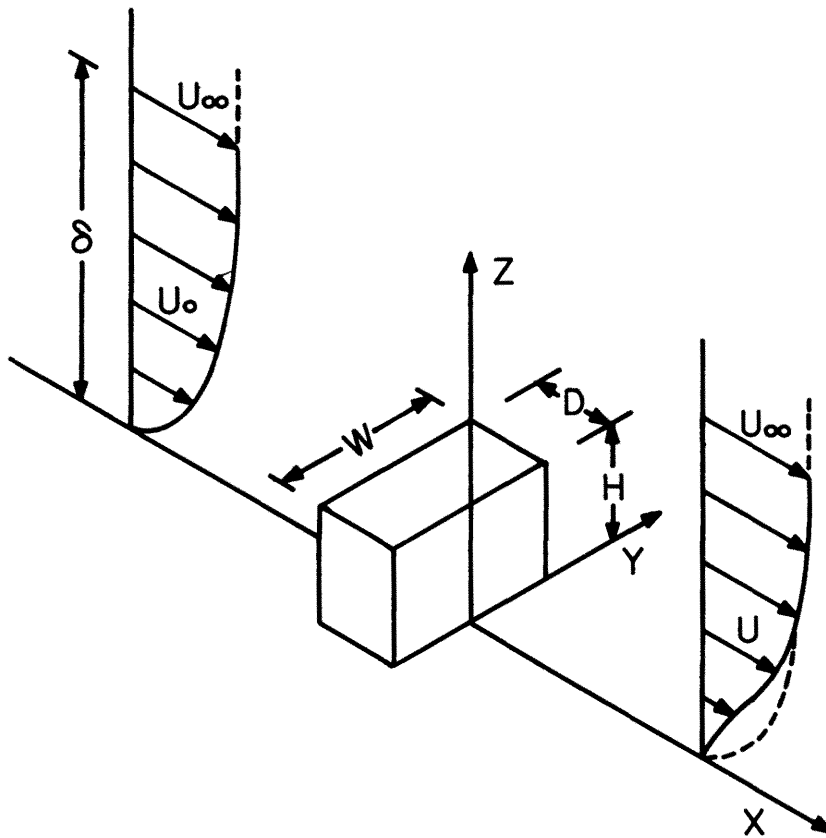
Figure 1. Schematic of the experiment configuration showing the coordinate system and symbol definitions.
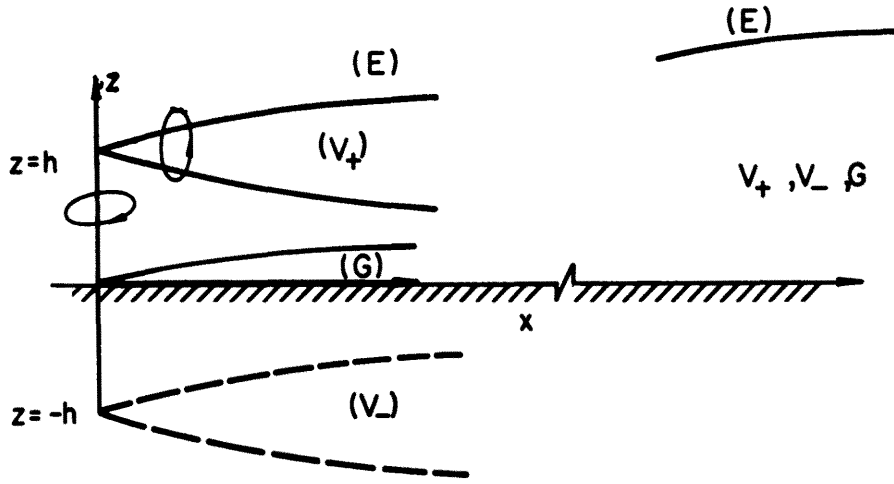
(a) Side View
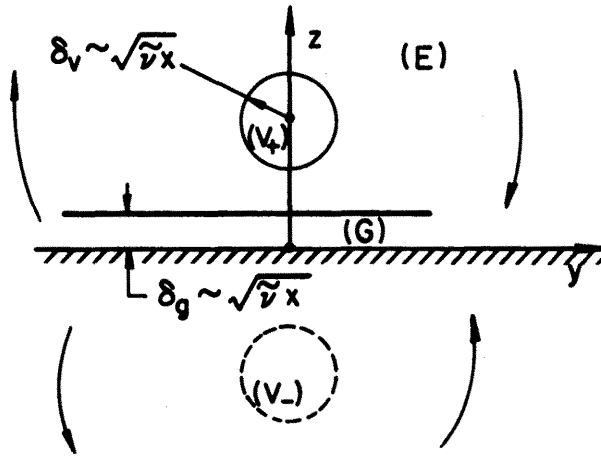
(b) Looking Upwind $h \gg \sqrt{\tilde{\nu} x}$
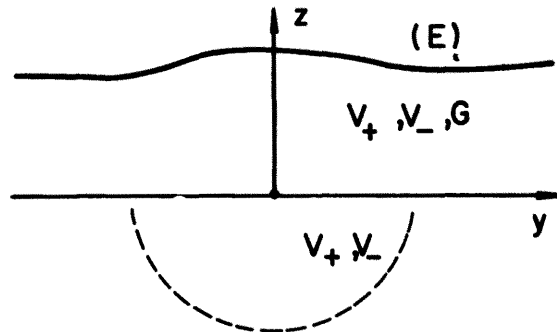
(c) Looking Upwind, $h \ll \sqrt{\tilde{\nu} x}$

Figure 2. Schematic of the regions of influence of the vortex cores and the vortex-induced boundary layer from the vortex wake theory of Hunt (Hunt, 1975).
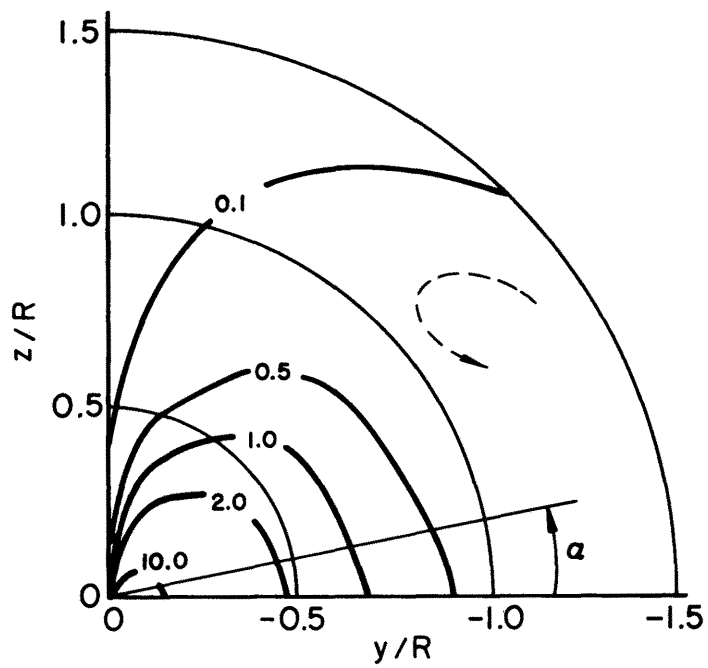
Figure 3. Lines of constant $\omega_s/U_o'(r_\infty)$ at infinity downstream of a hemisphere in a shear flow. (Viewed looking downwind with the hemisphere center at y=0, z=0.) From Hawthorne and Martin, 1955.
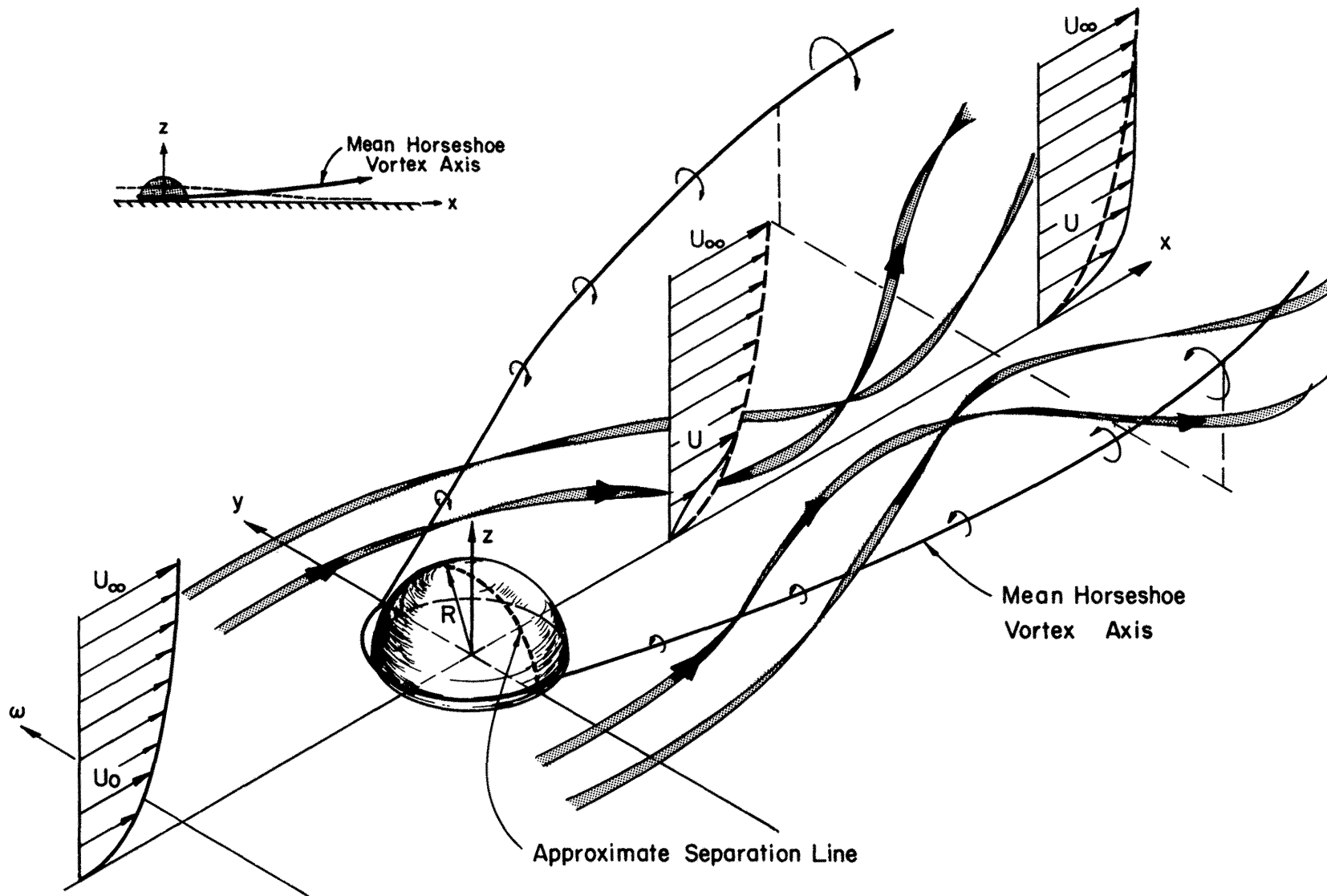
Figure 4. Schematic of the vortex-containing wake of a hemisphere.
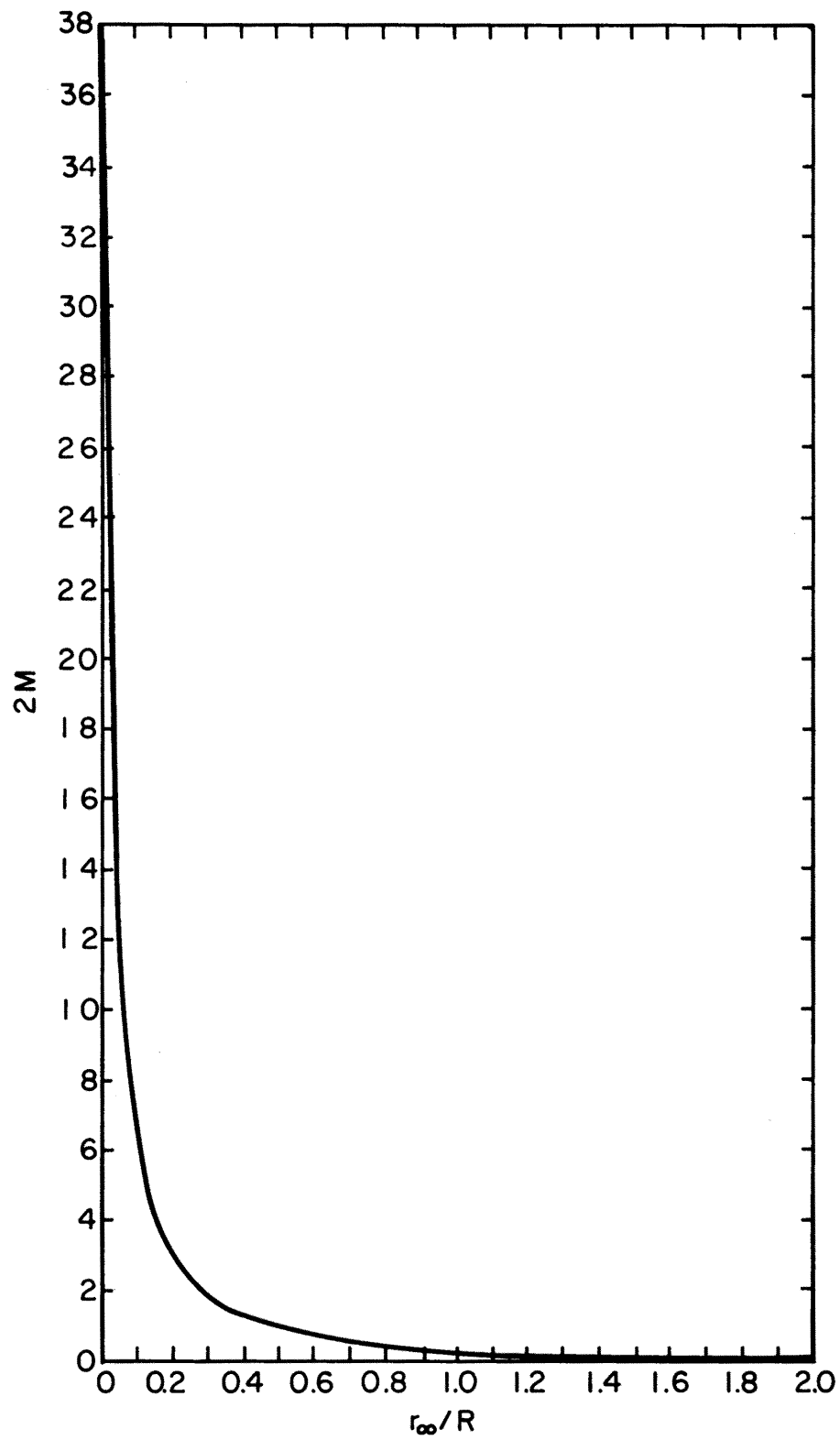
Figure 5. Results of evaluation of the integral of equation (3-1).
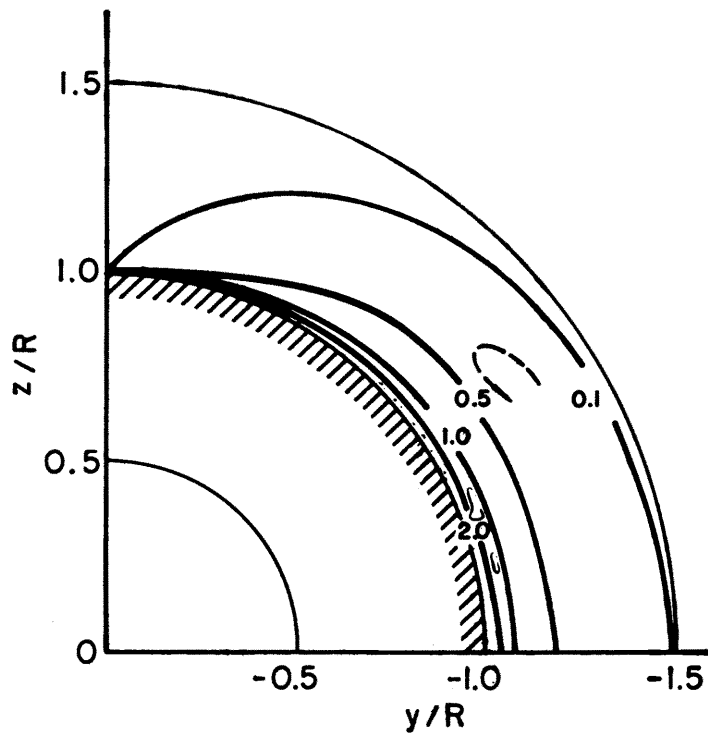
Figure 6. Lines of constant $\omega_s/U_o^{'}(r_\infty)$ shed from a hemisphere in a shear flow. Viewed looking downwind past the hemisphere.
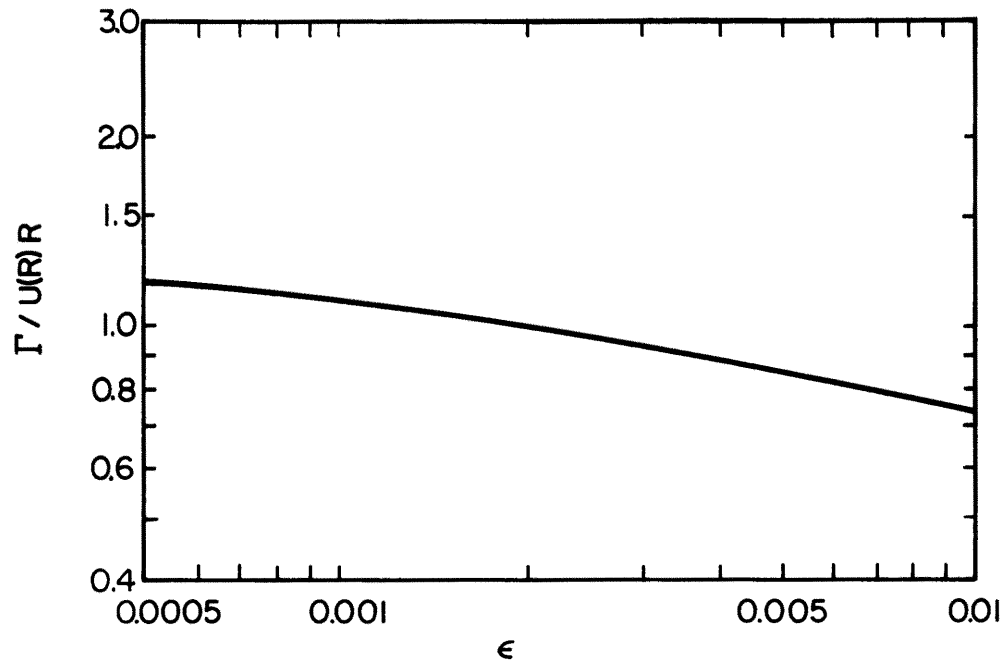
Figure 7. The instantaneous strength of the horseshoe vortex
           formed by the hemisphere as a function of the thick-
           ness of the boundary layer on the hemisphere at x=0.
           n = 0.12.
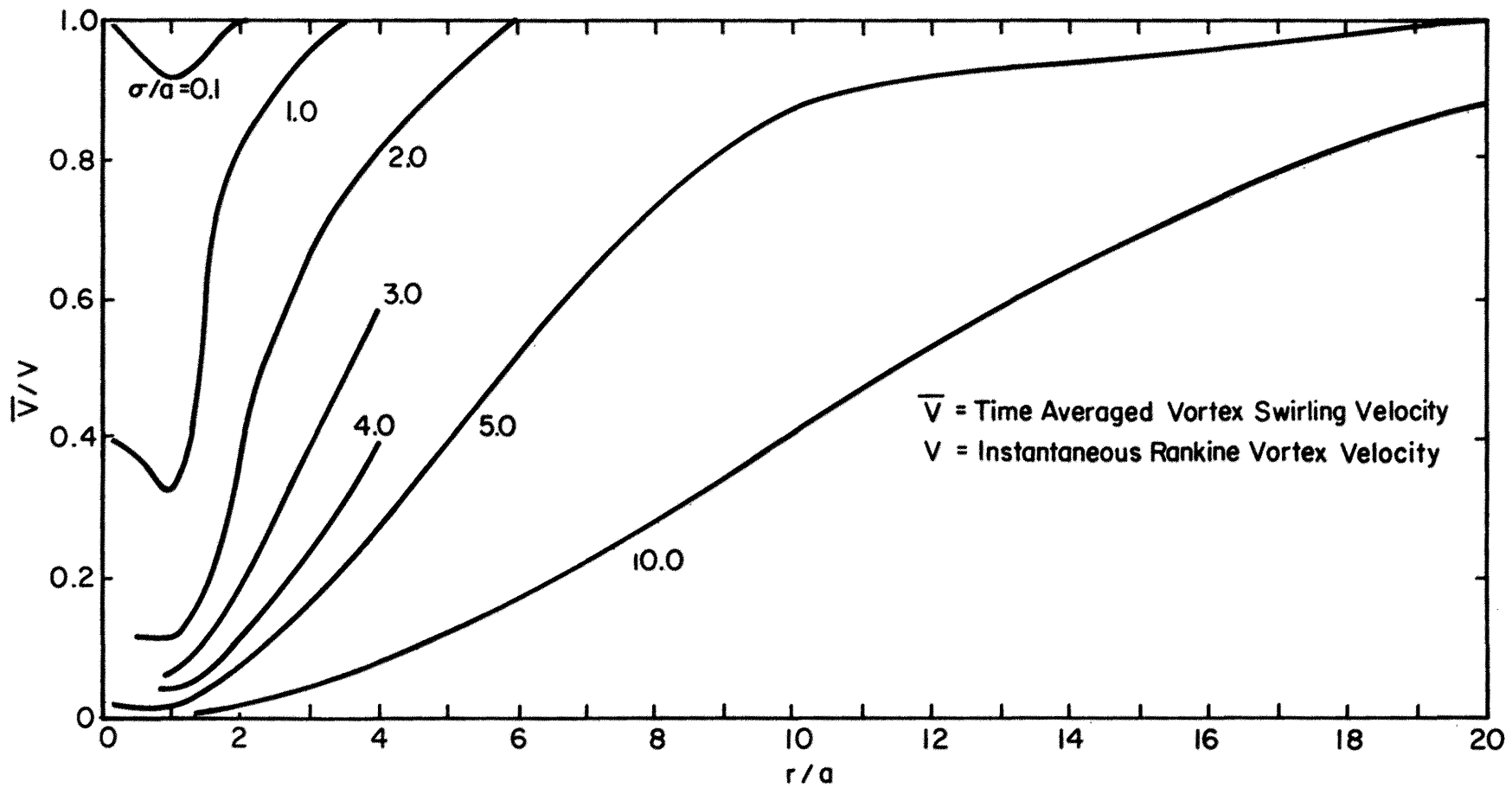
Figure 8.   The effect of vortex meander in terms of the meander
amplitude and the distance from the center of the
average vortex.
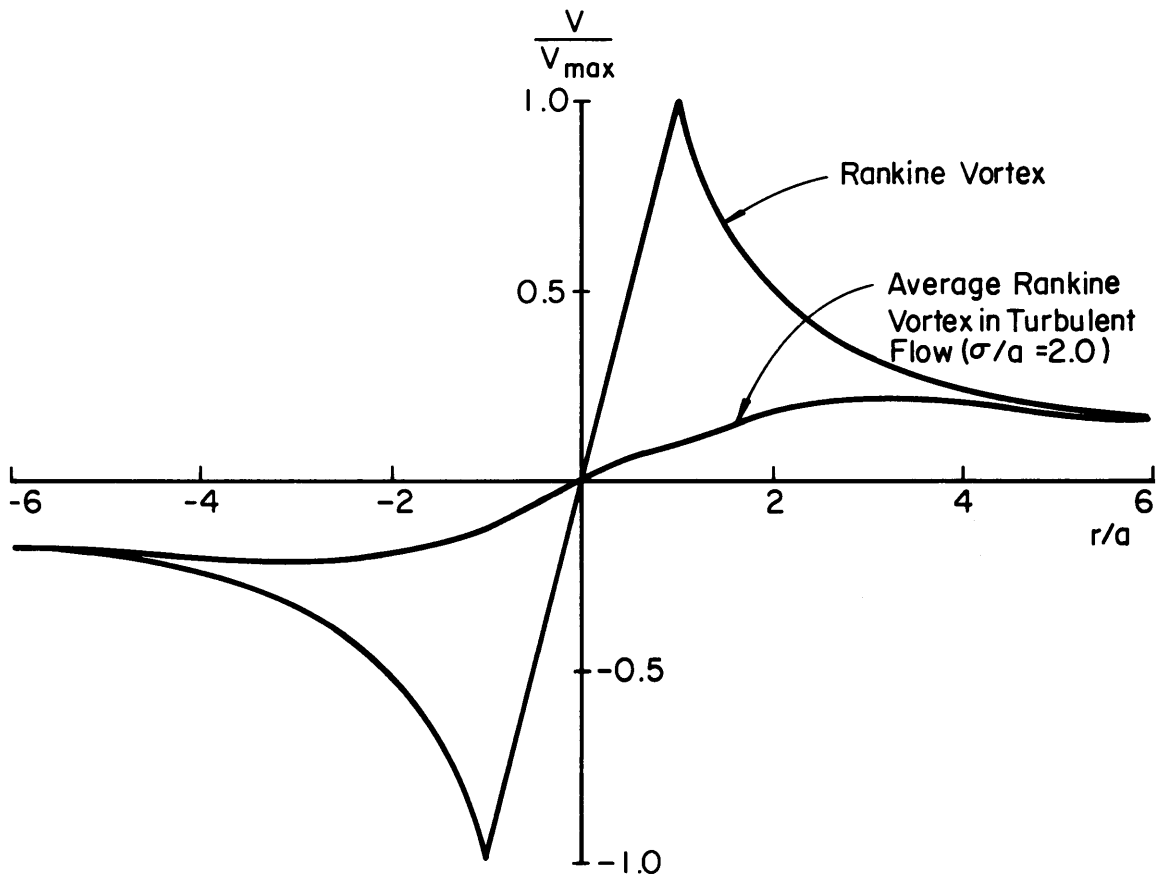
Figure 9.   A comparison of the instantaneous and average Rankine
vortex in a turbulent flow.
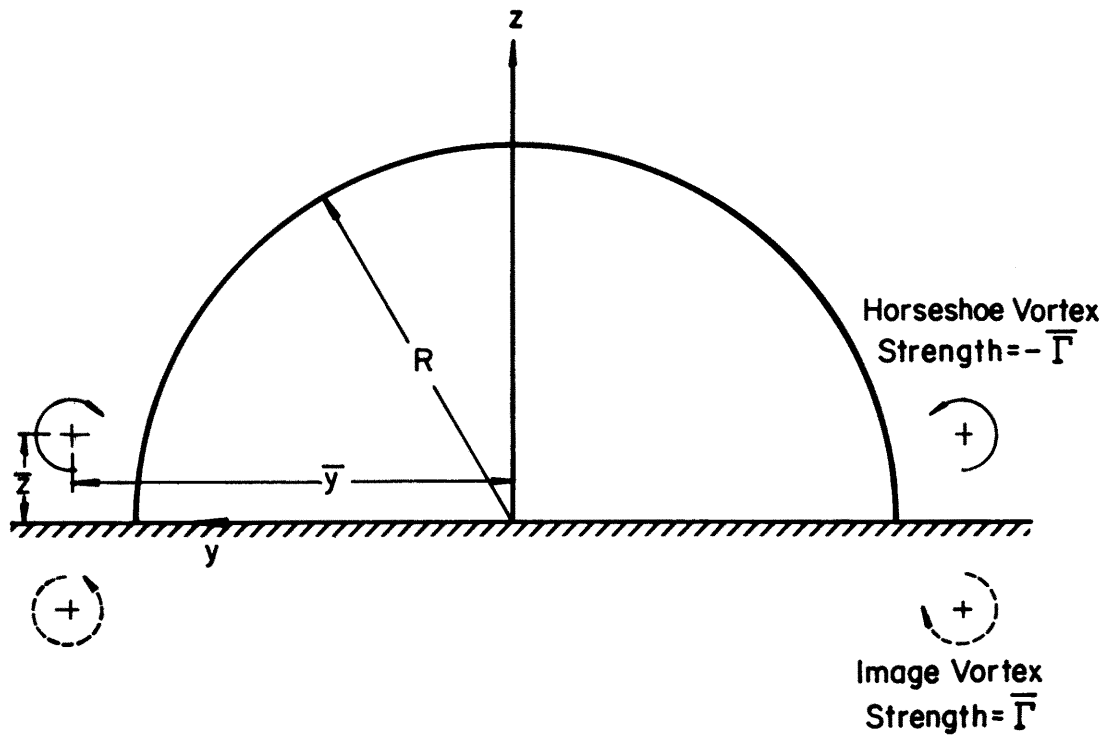
Figure 10. Schematic of the horseshoe vortex system generated by passage of a shear flow around a surface mounted hemisphere. Viewed looking downwind.
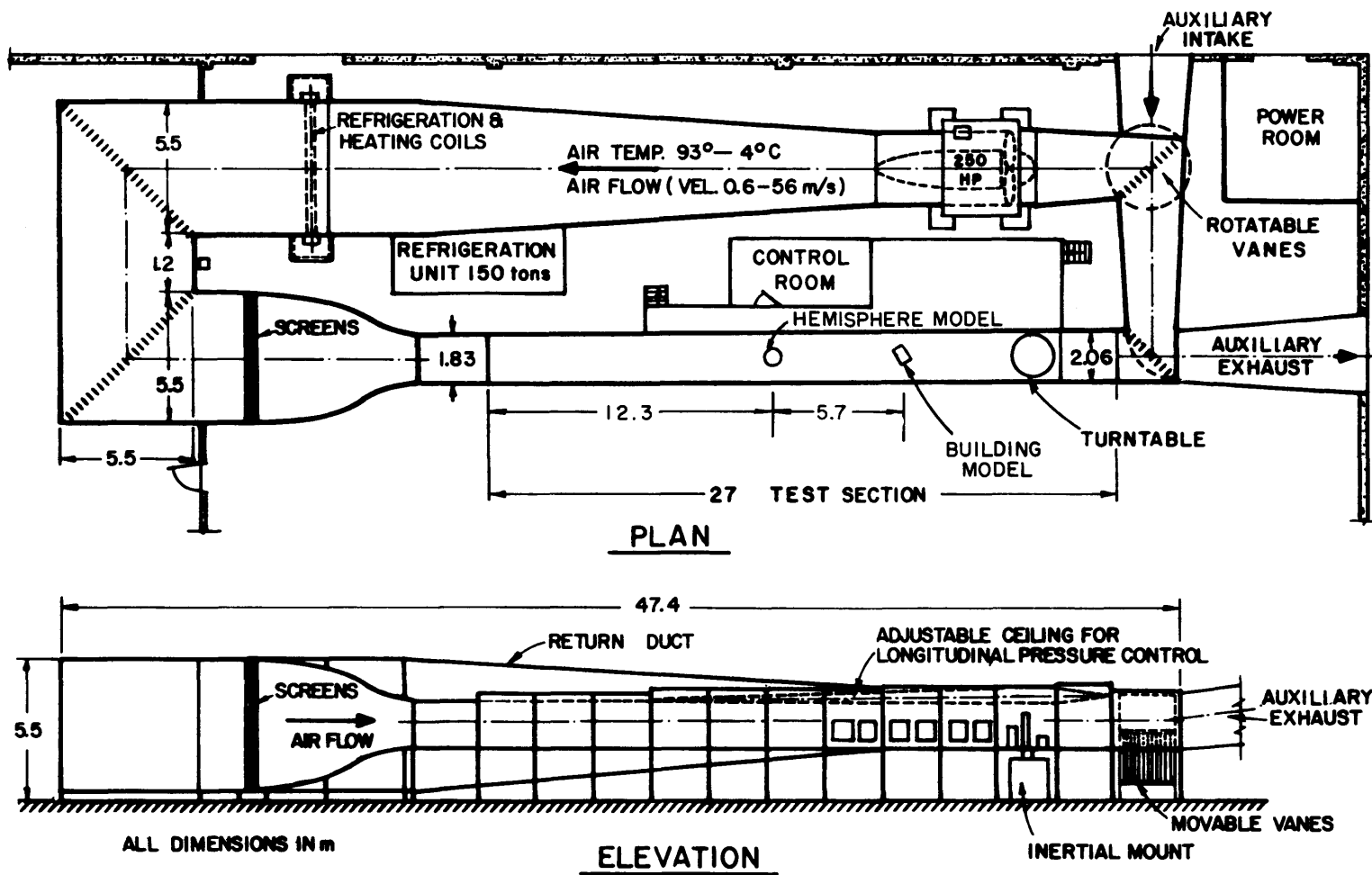
Figure 11.   Meteorological Wind Tunnel, Fluid Dynamics and Diffusion
Laboratory, Colorado State University.
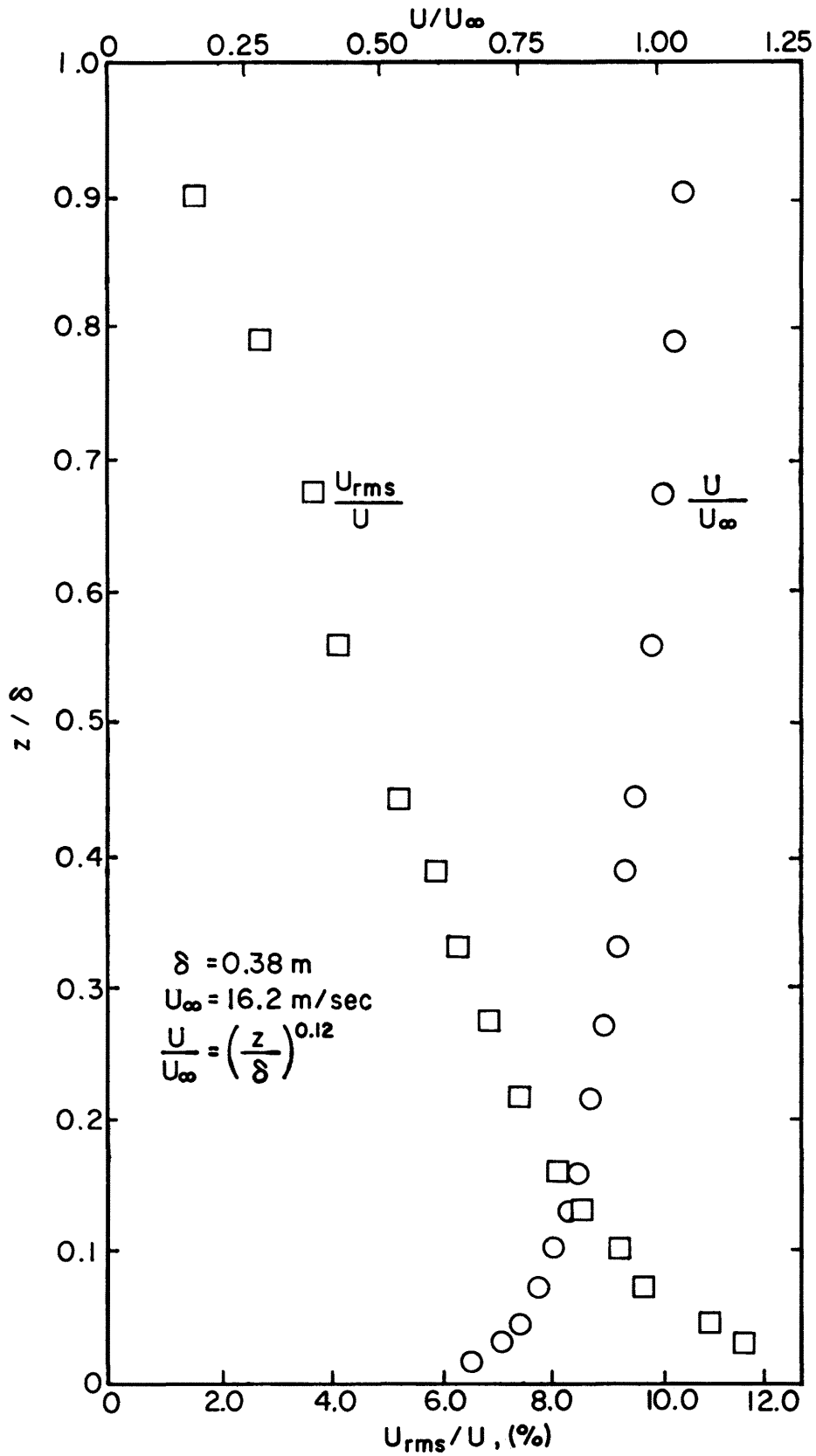
Figure 12. Mean velocity and turbulence intensity vertical profiles in the smooth floor boundary layer.
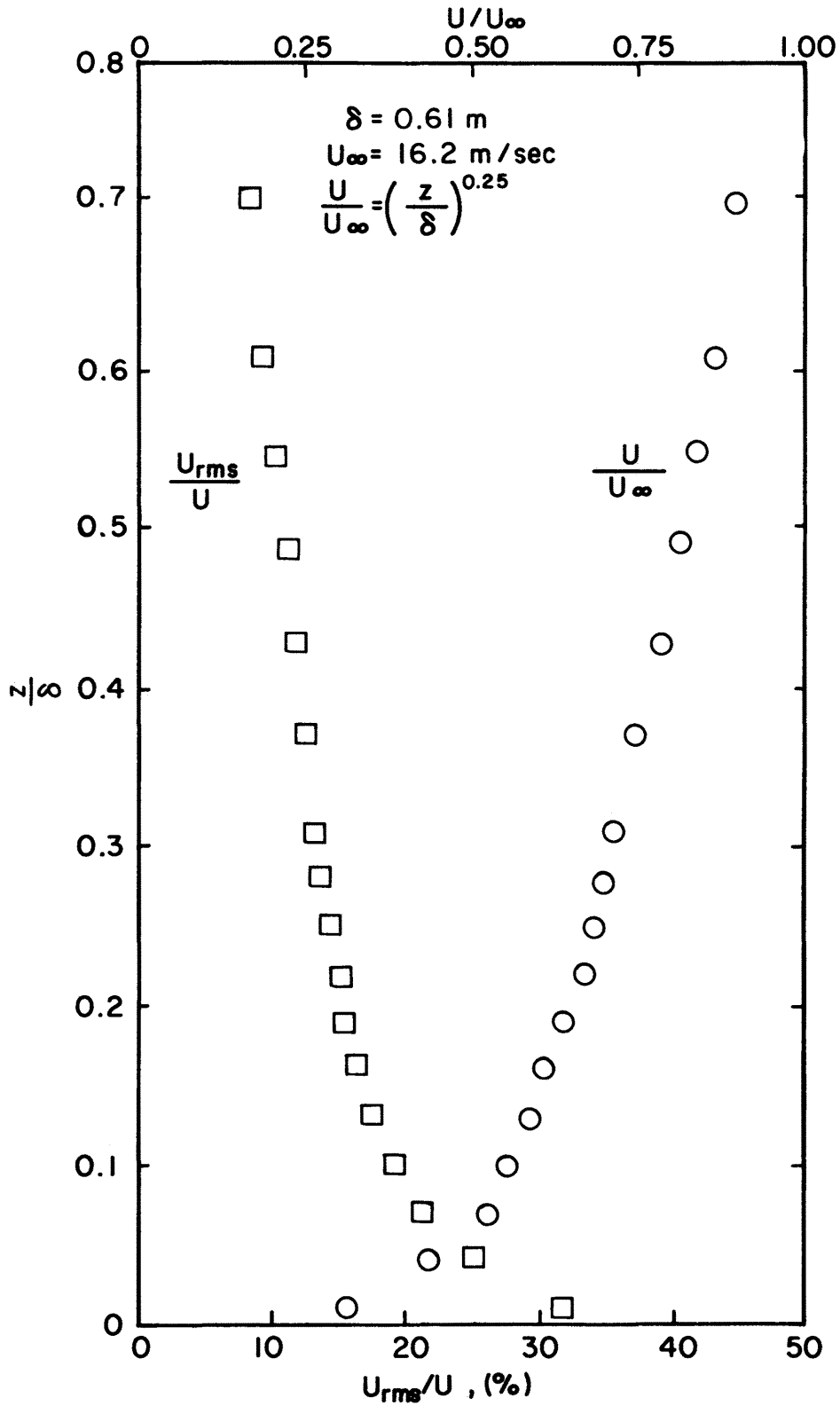
Figure 13.   Mean velocity and turbulence intensity vertical
profiles in the boundary layer over the carpet.

Figure 14. Rotating hot-film probe.

(a)

(b)
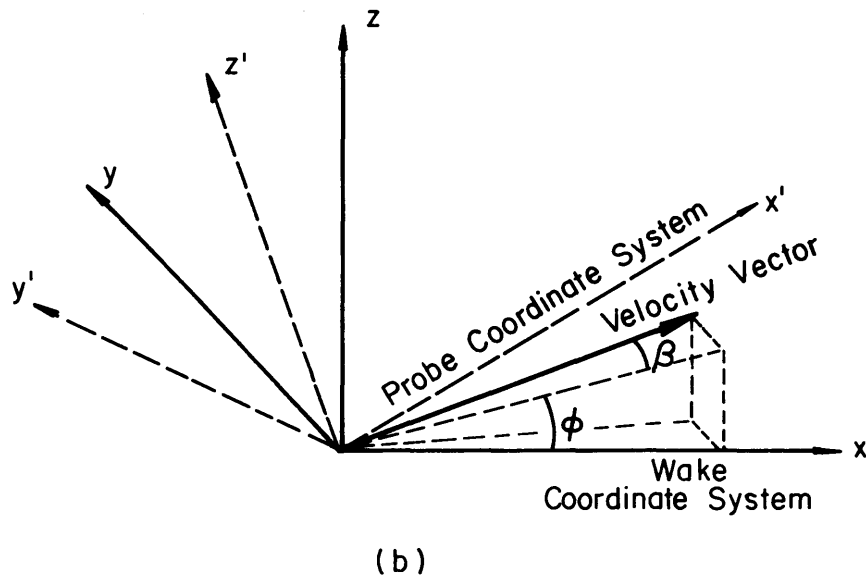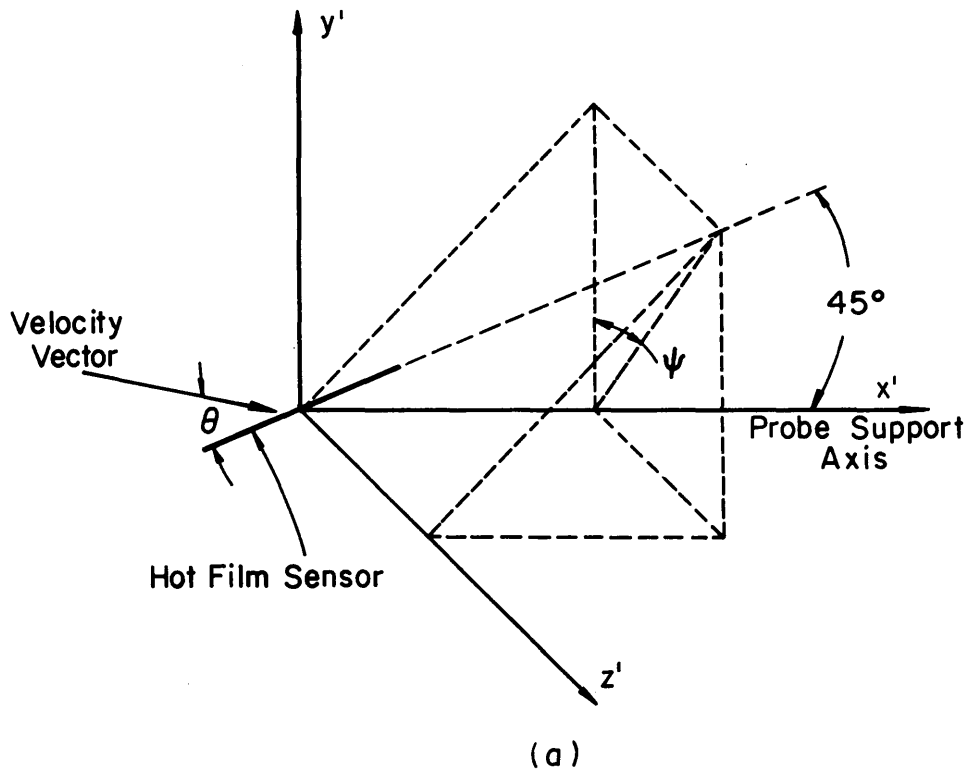
Figure 15. (a) Schematic of the probe coordinate system and
(b) Definition of the angles ϕ and β in the
wake coordinate system.
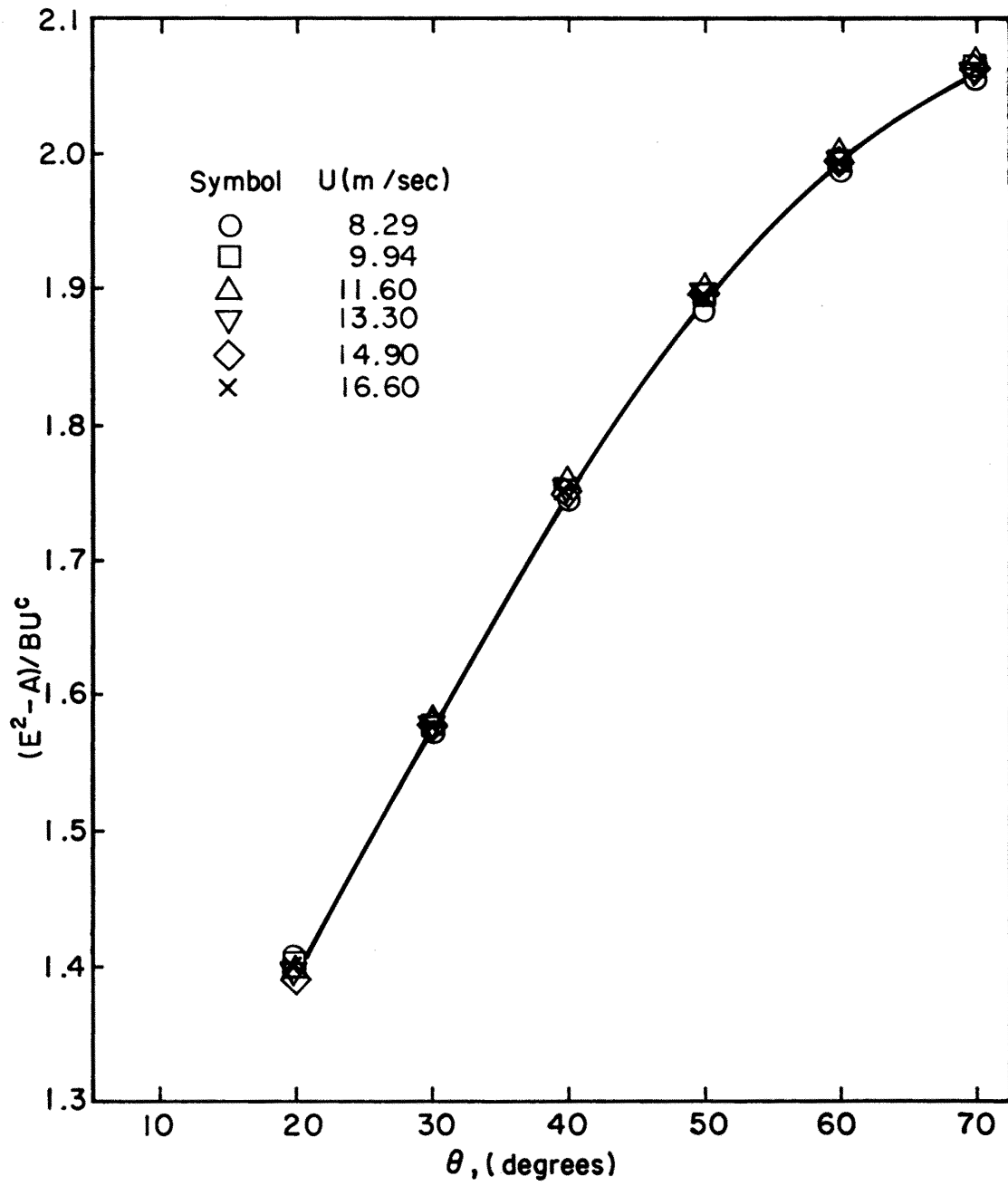
Figure 16. A typical rotating hot-film anemometer calibration.
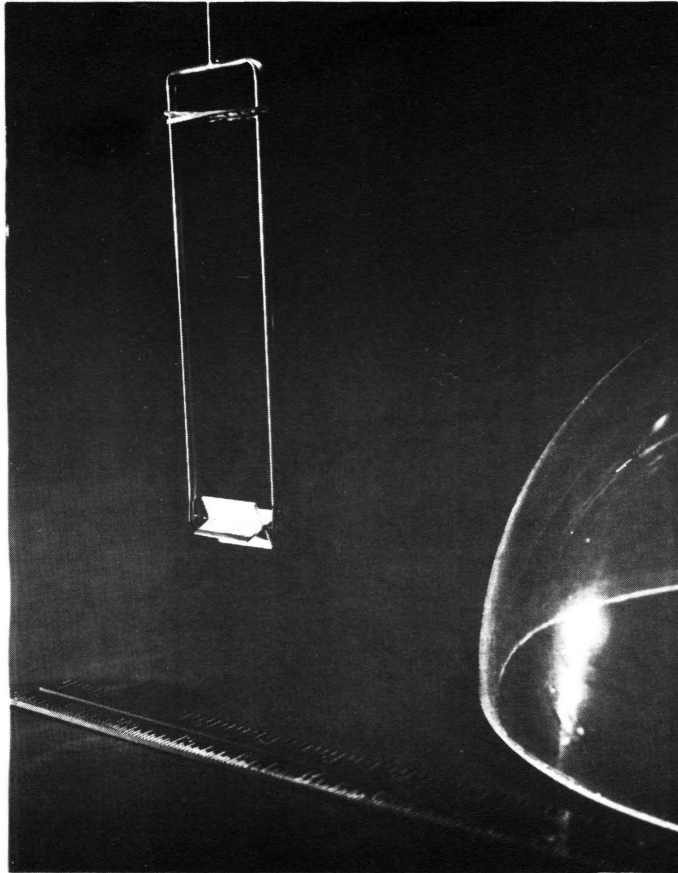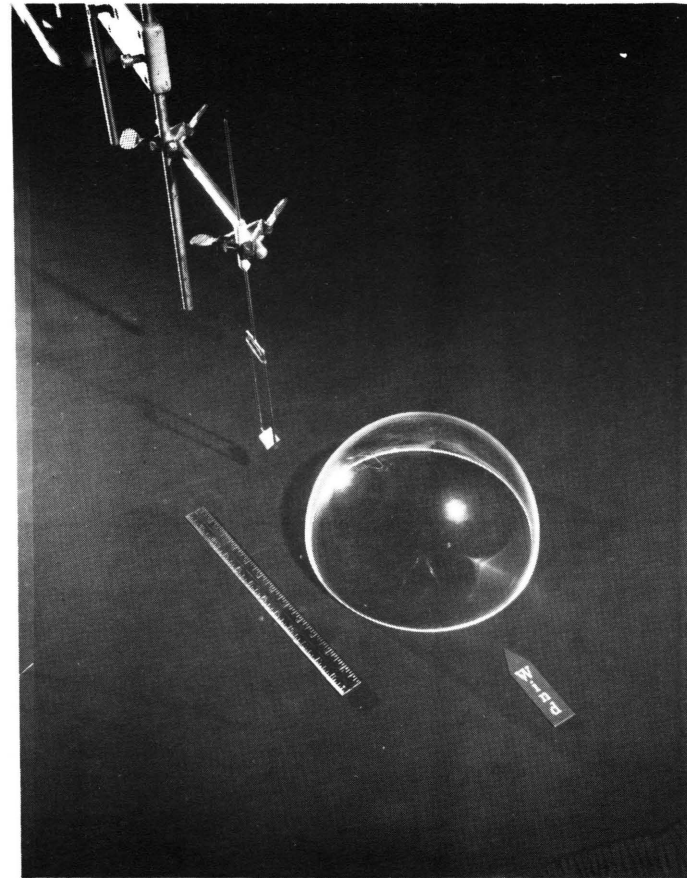
(a)   (b)

Figure 17.   Photographs of the paddlewheel vorticity meter in
a) a close-up view and b) a typical operating
configuration in the near wake.
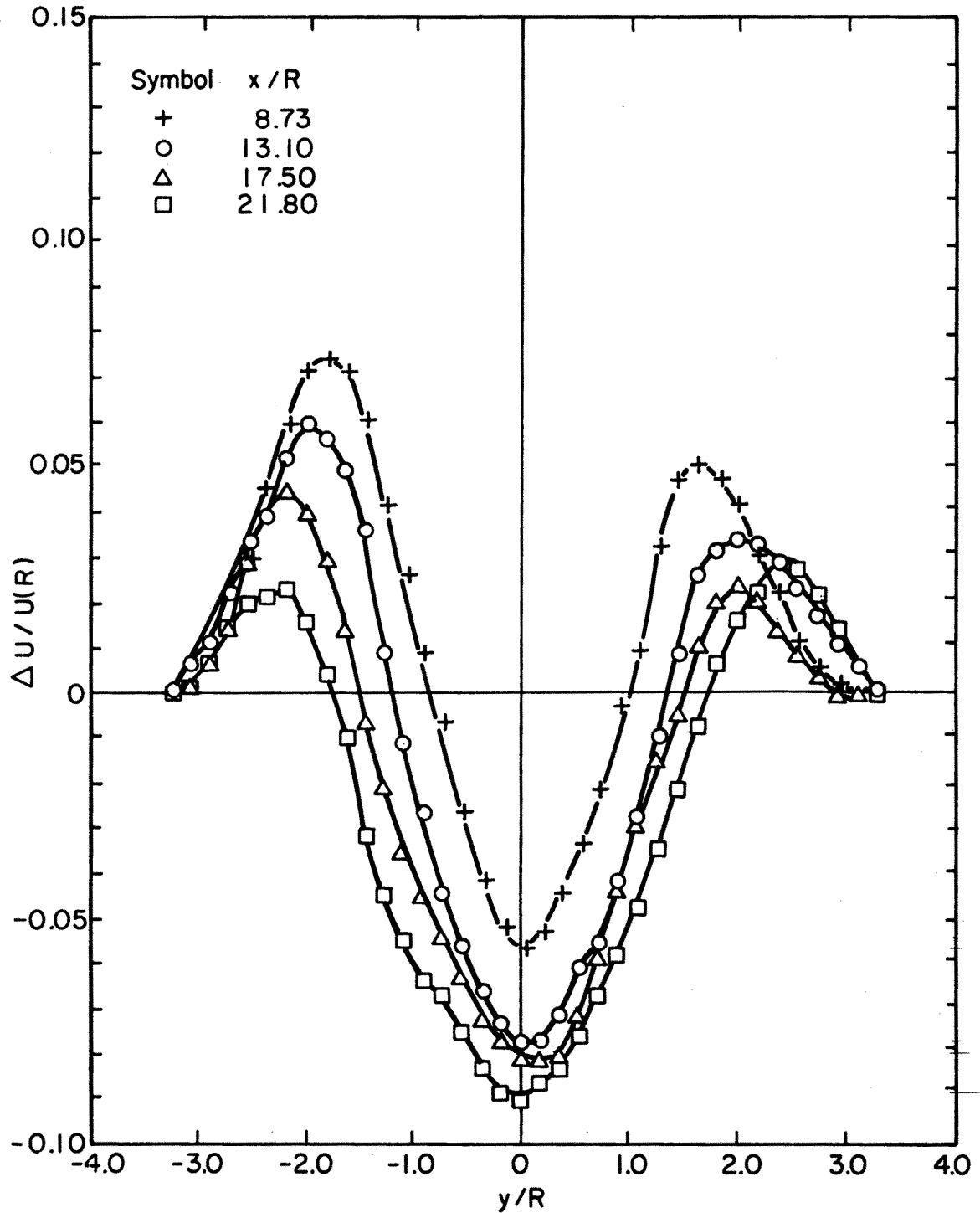
Figure 18. Lateral profiles of mean velocity deficit in the wake of a hemisphere. Test series 2.

(a) z/R = 0.091.
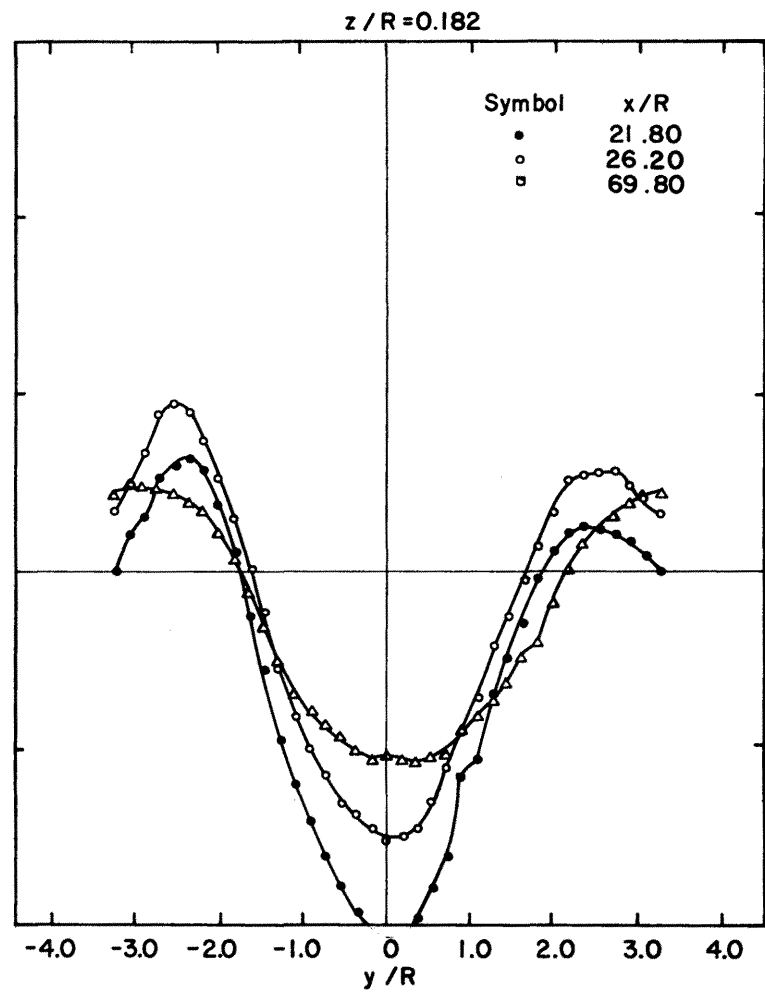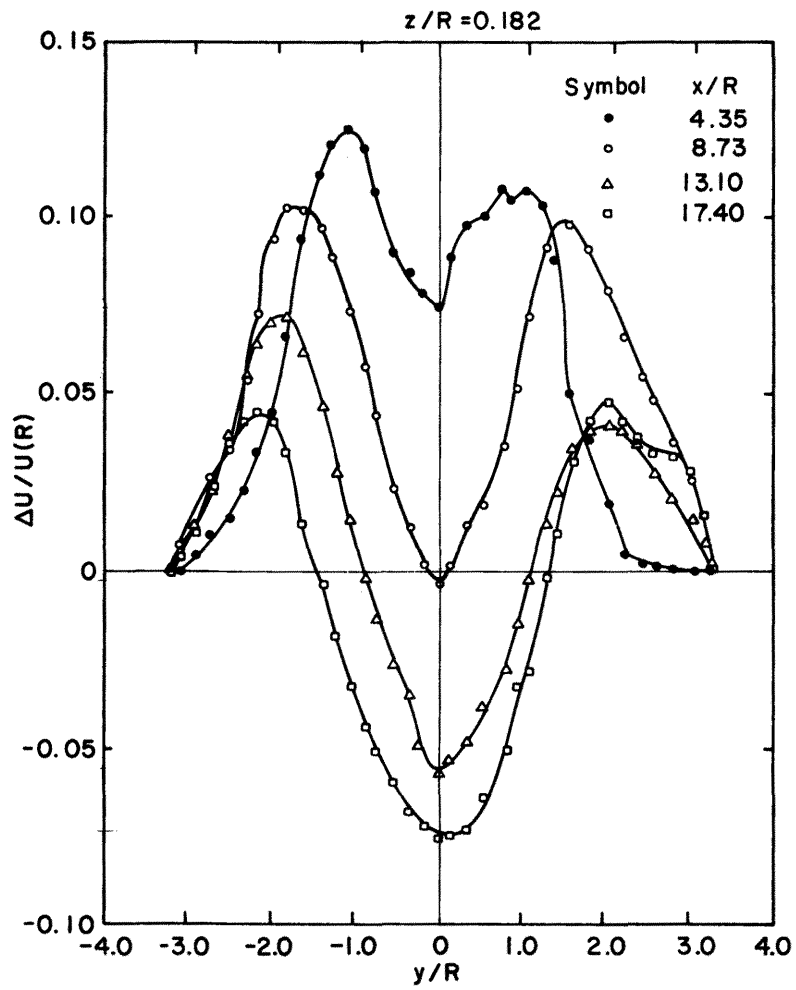
Figure 18 (b)   z/R = 0.182.
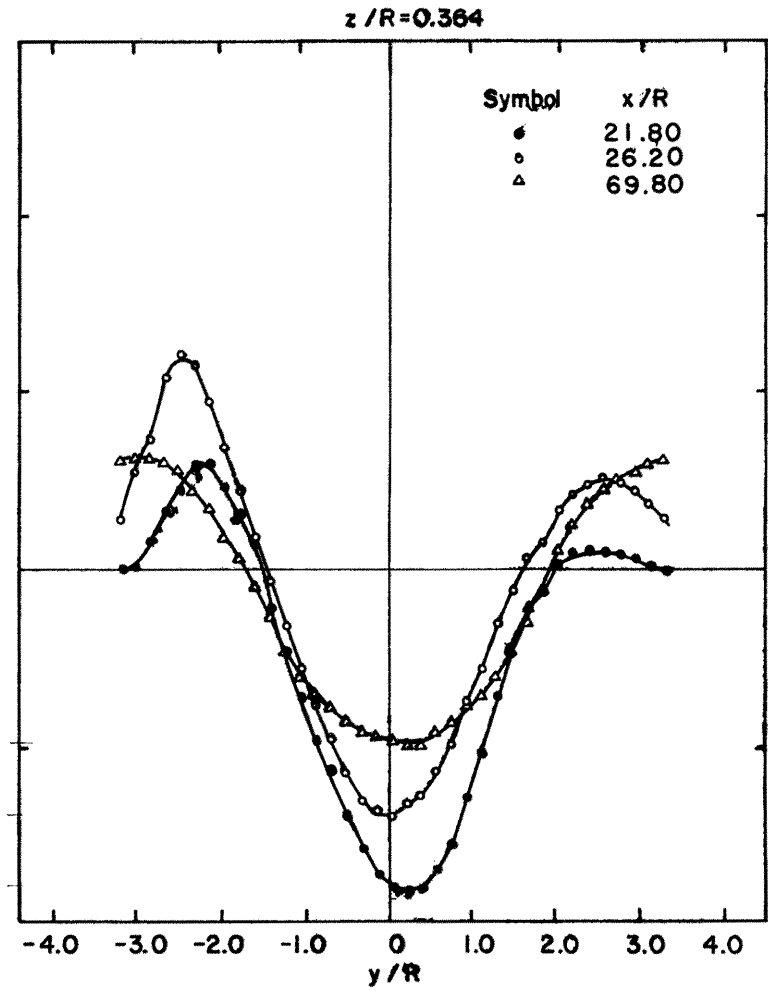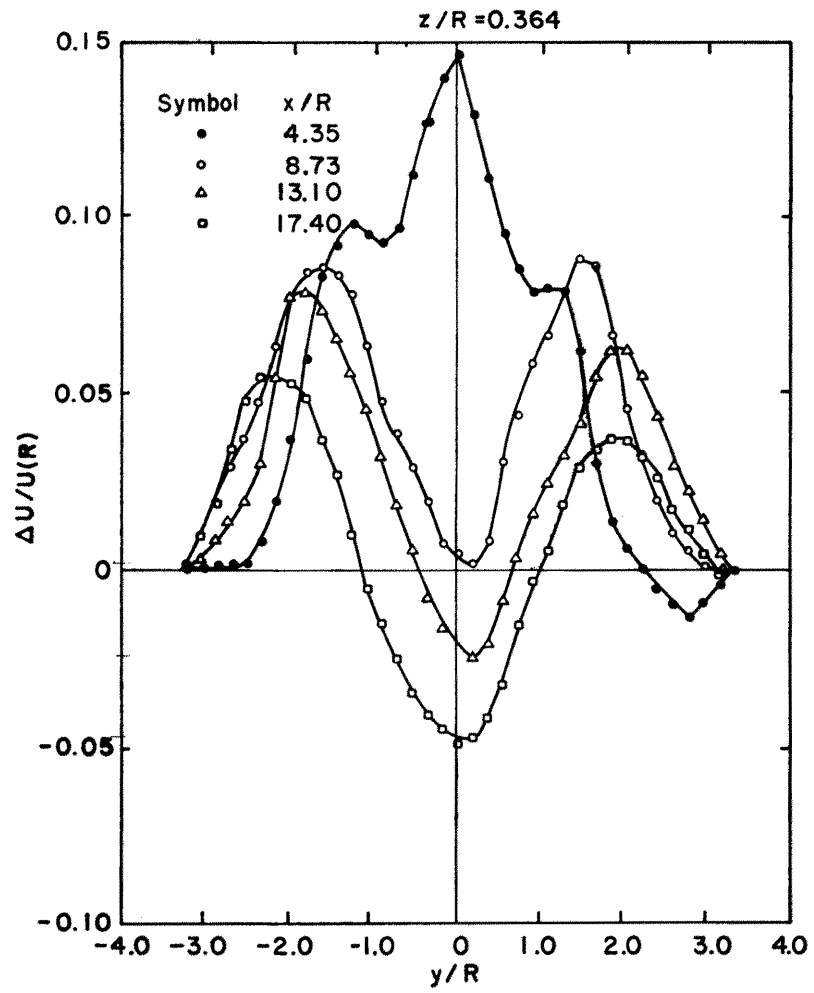
Figure 18 (c)   z/R = 0.364.
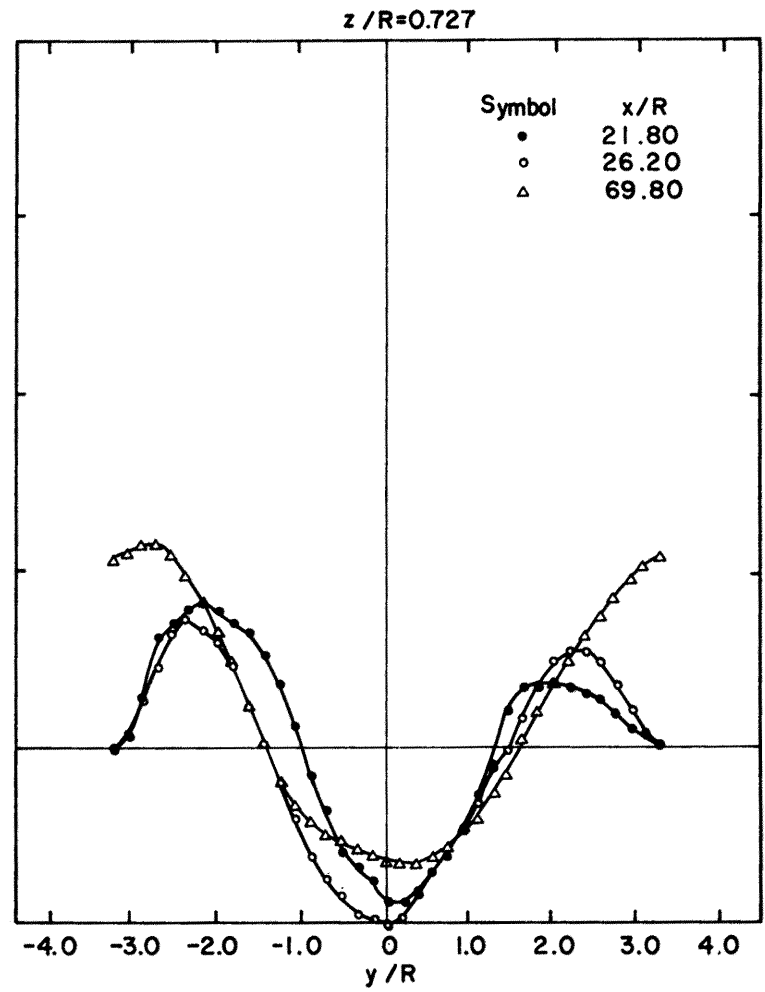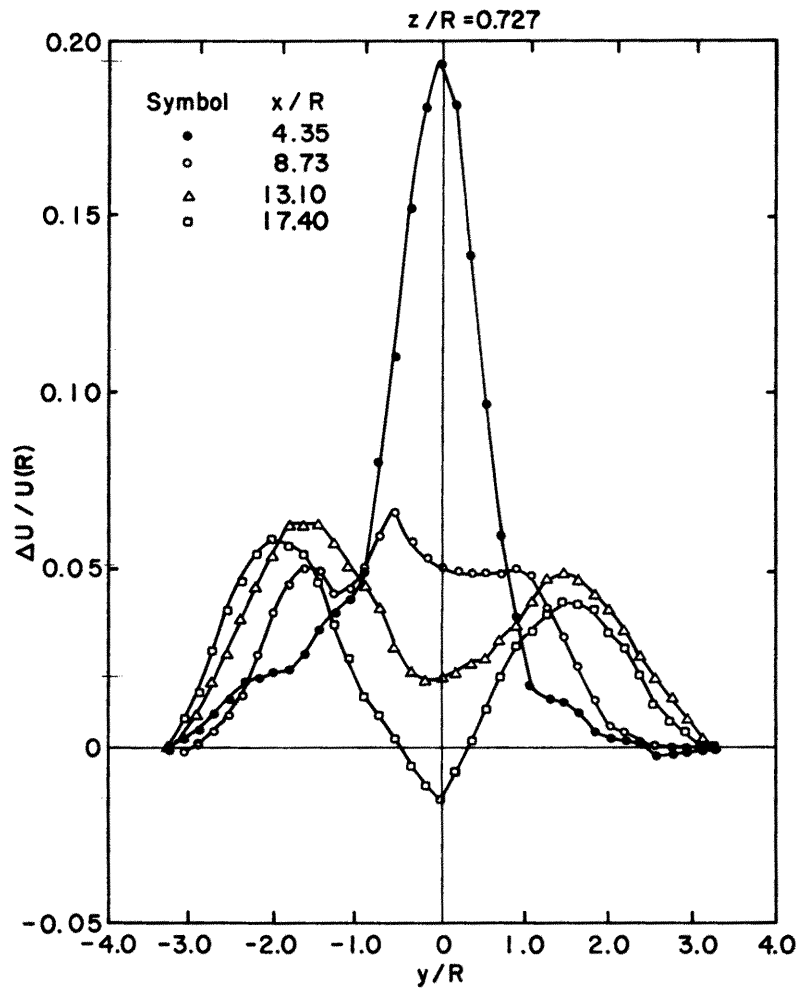
Figure 18 (d)   z/R = 0.727.
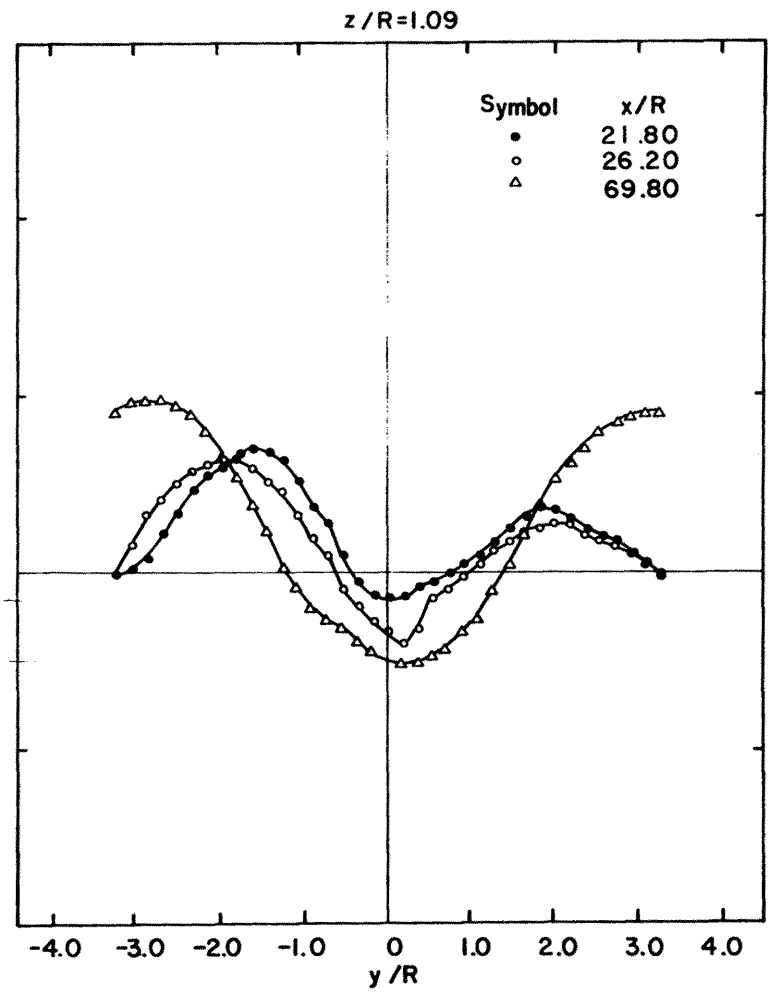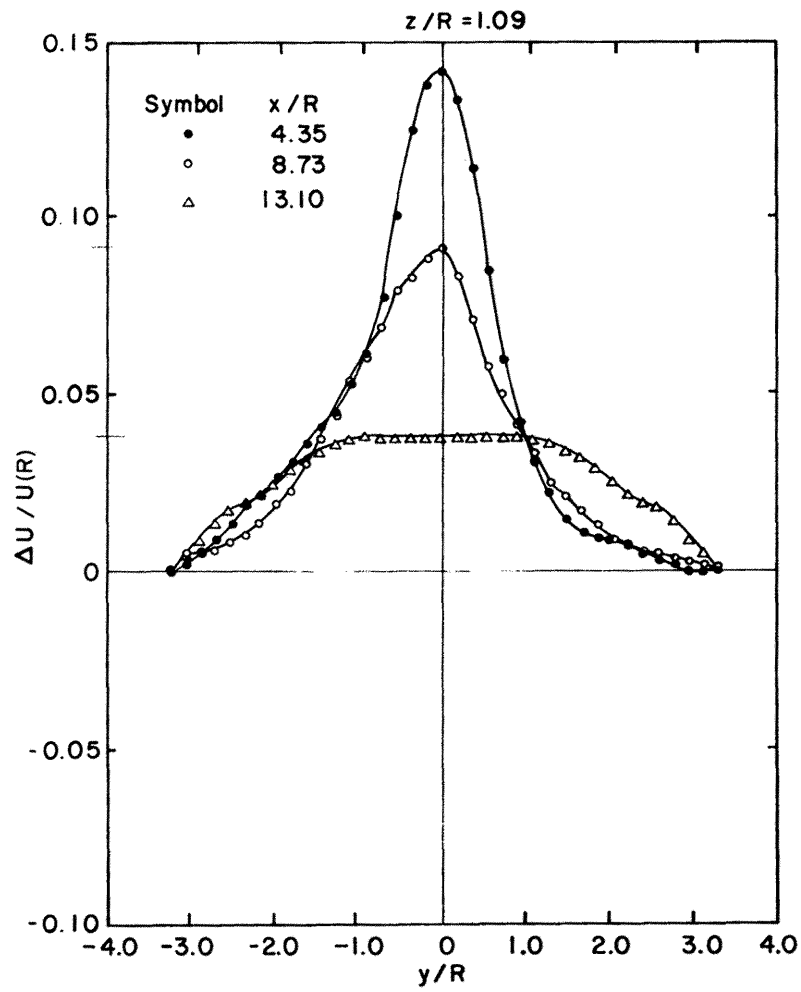
Figure 18 (e)   z/R = 1.09.
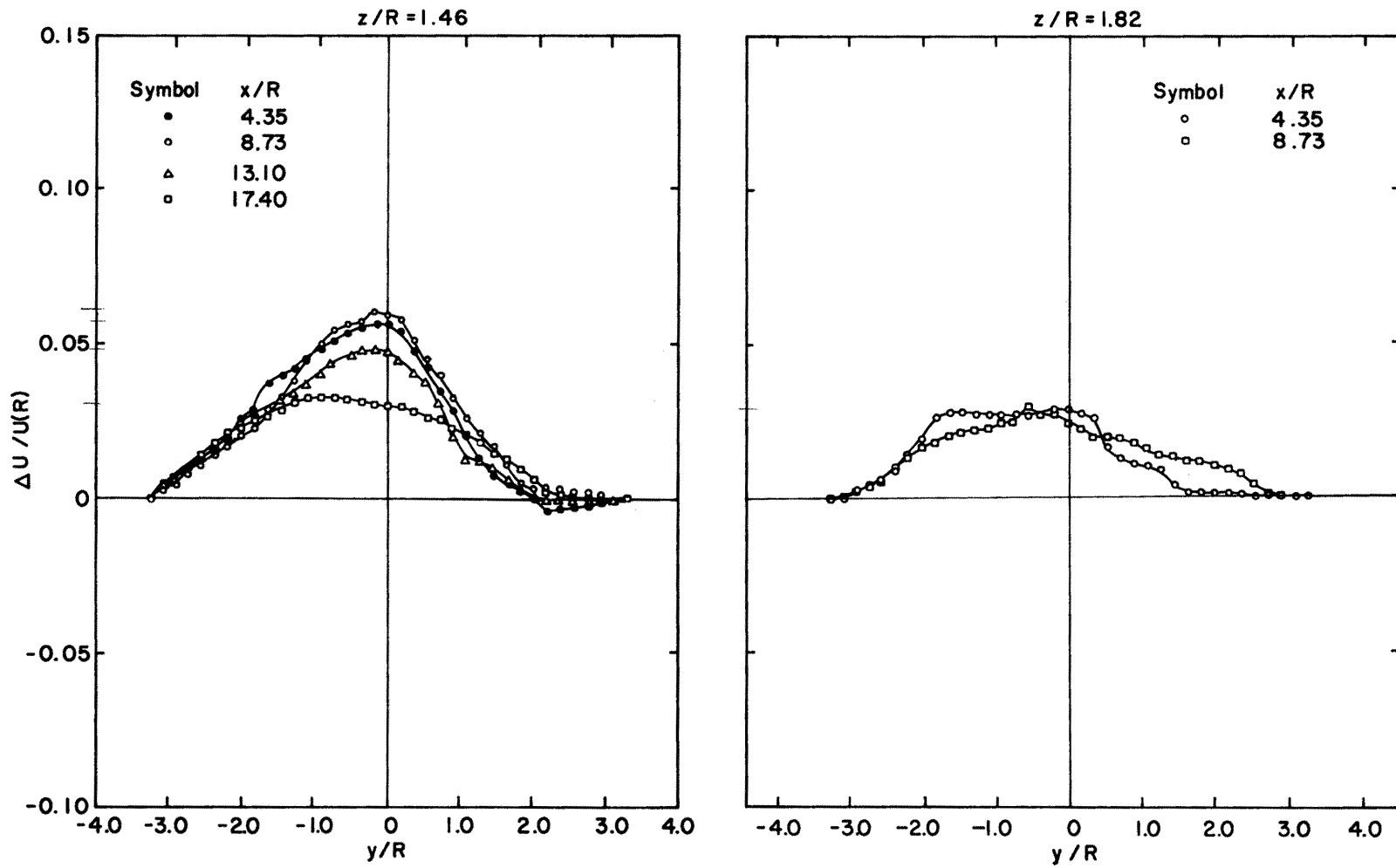
Figure 18 (f)   z/R = 1.46 and 1.82.
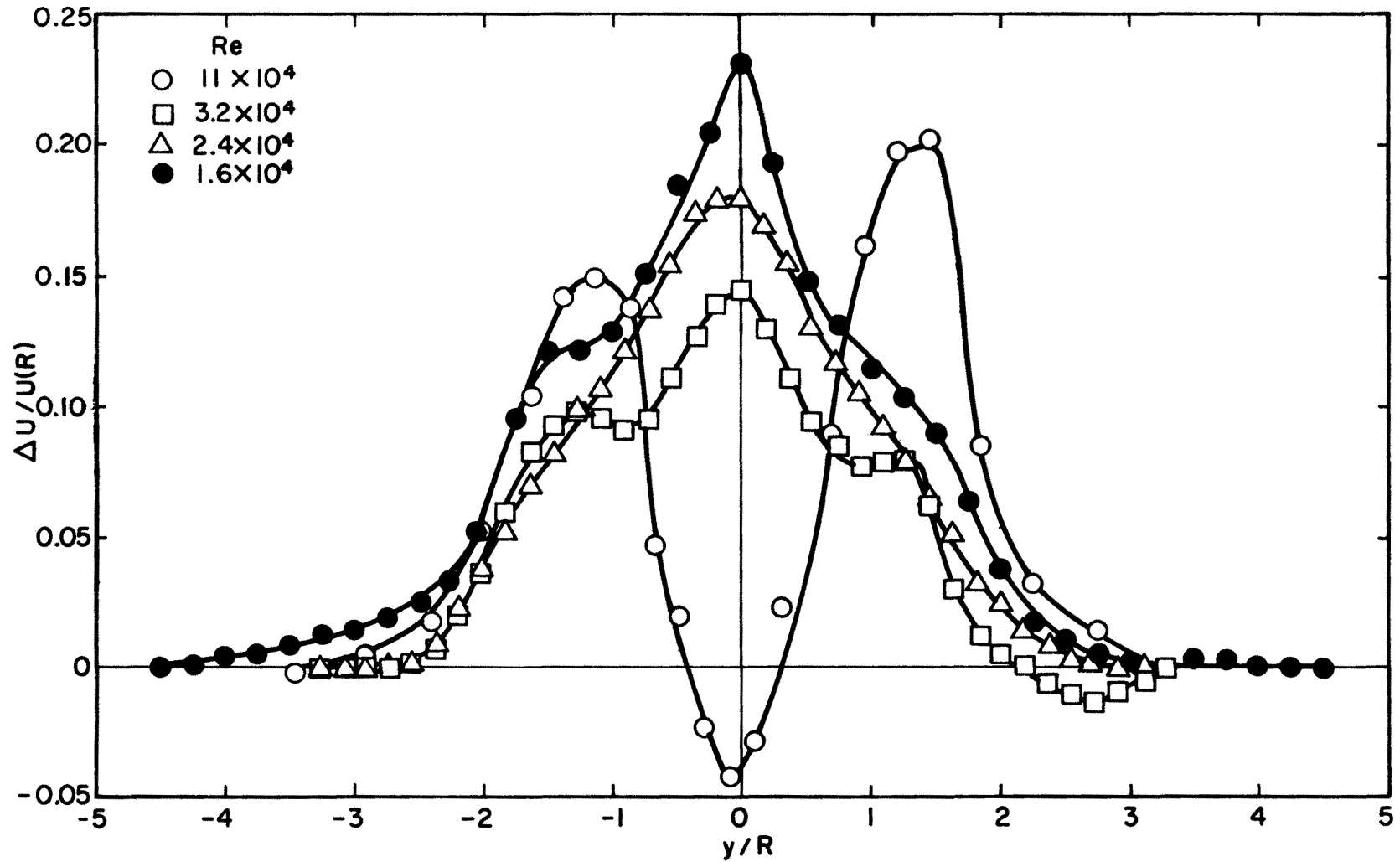
Figure 19. Lateral profiles of mean velocity deficit in the wakes of hemispheres at x/R = 4.36, z/R = 0.364; showing the effect of Reynolds number on the near wake character in the smooth floor boundary layer.
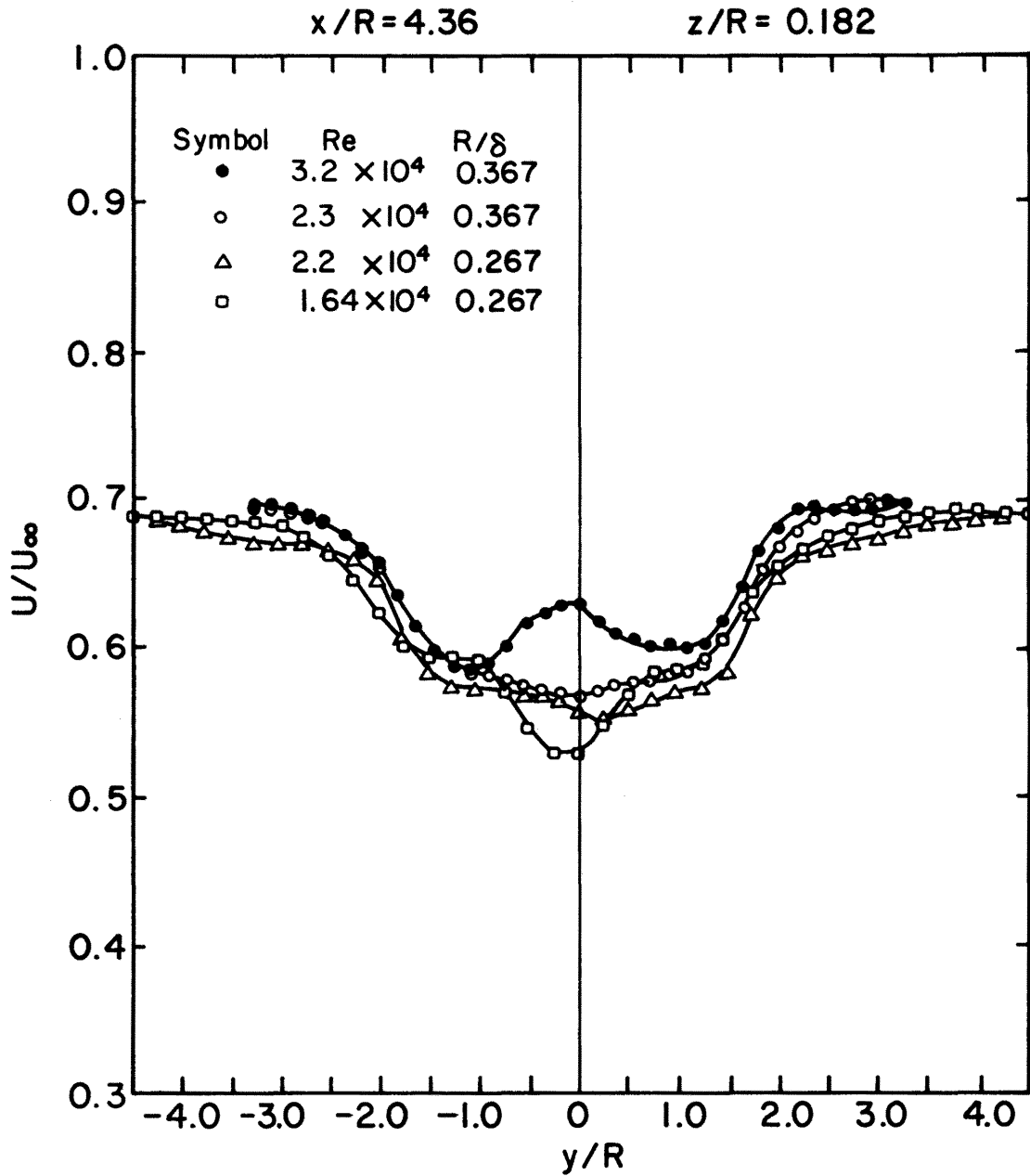
Figure 20. Lateral profiles of mean velocity in the wakes of
hemispheres. x/R = 4.36, z/R = 0.182, smooth floor
boundary layer.
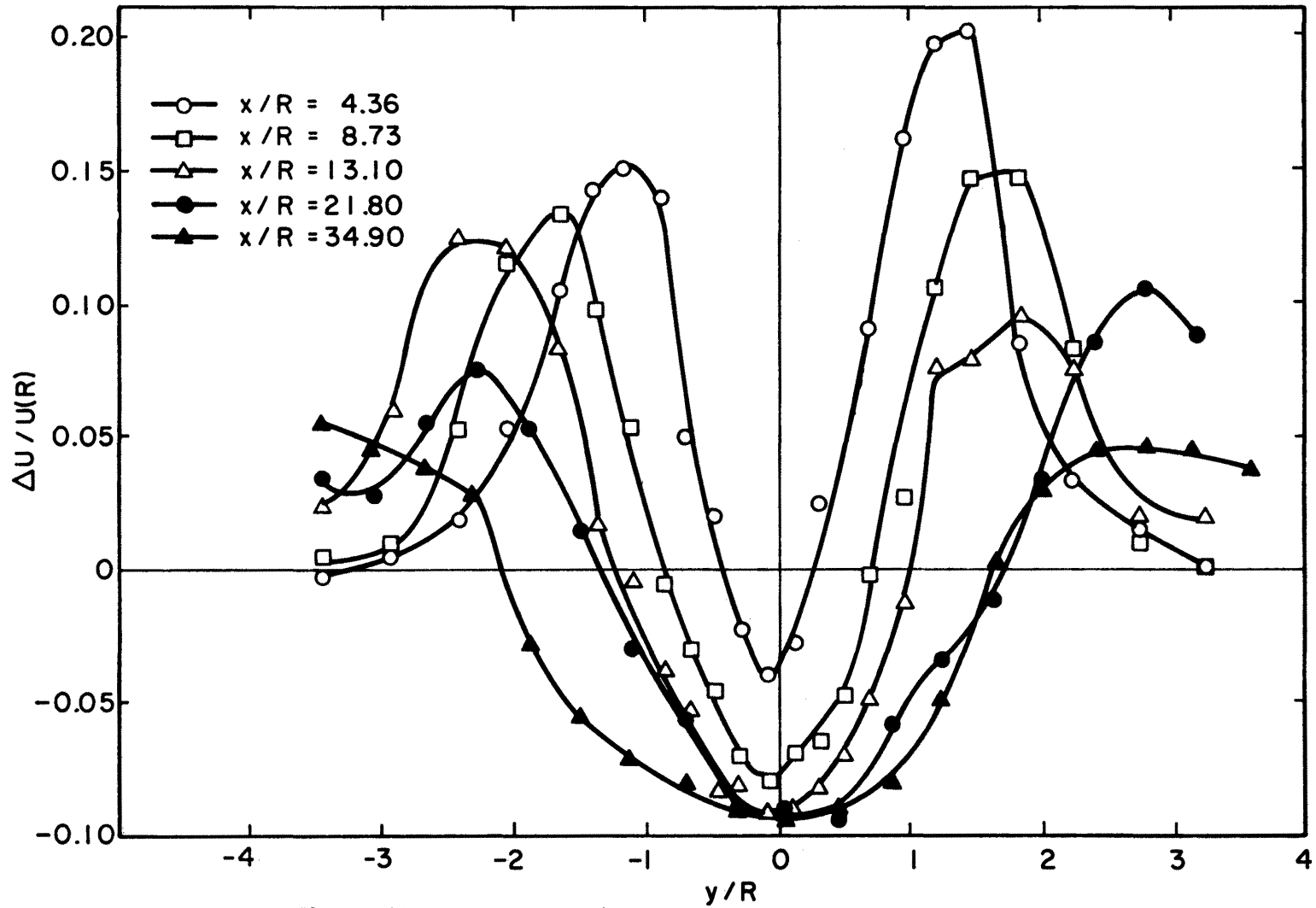
Figure 21. Lateral profiles of mean velocity deficit measured with a hot-film anemometer in the wake of a hemisphere at height z/R = 0.364. Test series 1.
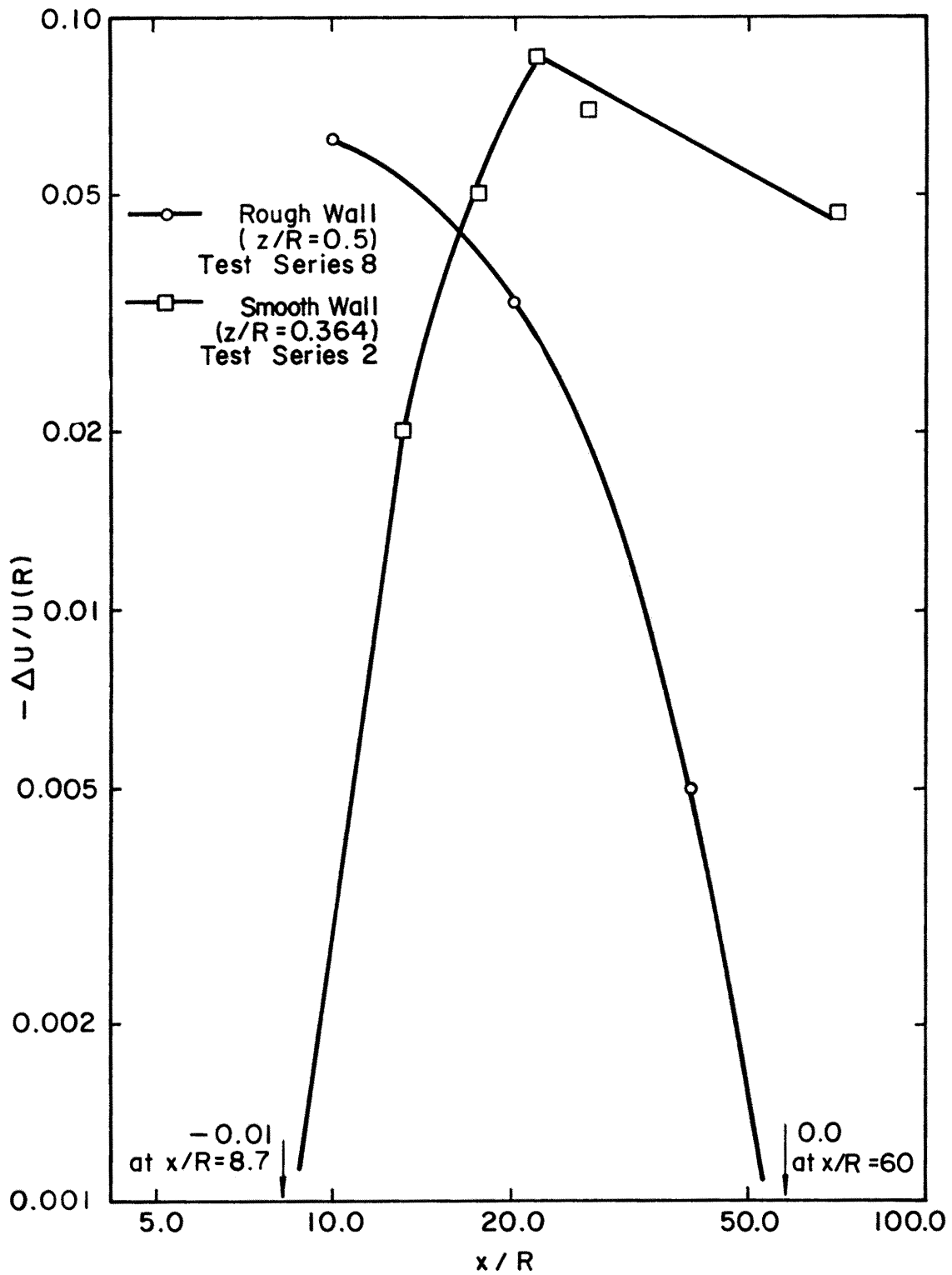
Figure 22. Comparison of the decay of the centerline velocity
excess in the wakes of hemispheres in the smooth-
and rough-wall boundary layers.
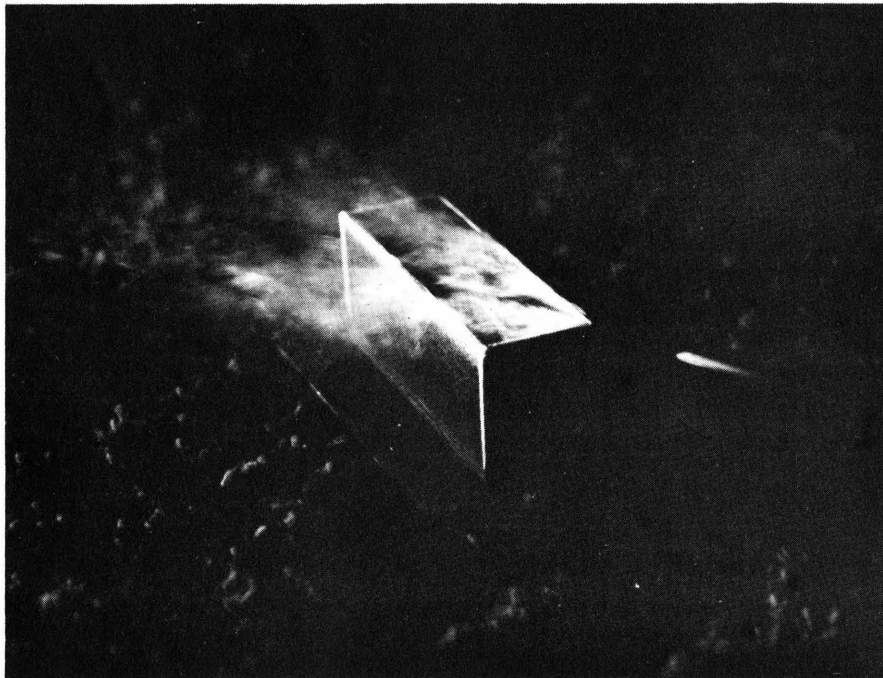
Figure 23. Flow visualization of the roof-corner vortices with
the wind approaching at 47 degrees to the normal to
the long face of the building. ($\alpha = 47°$)
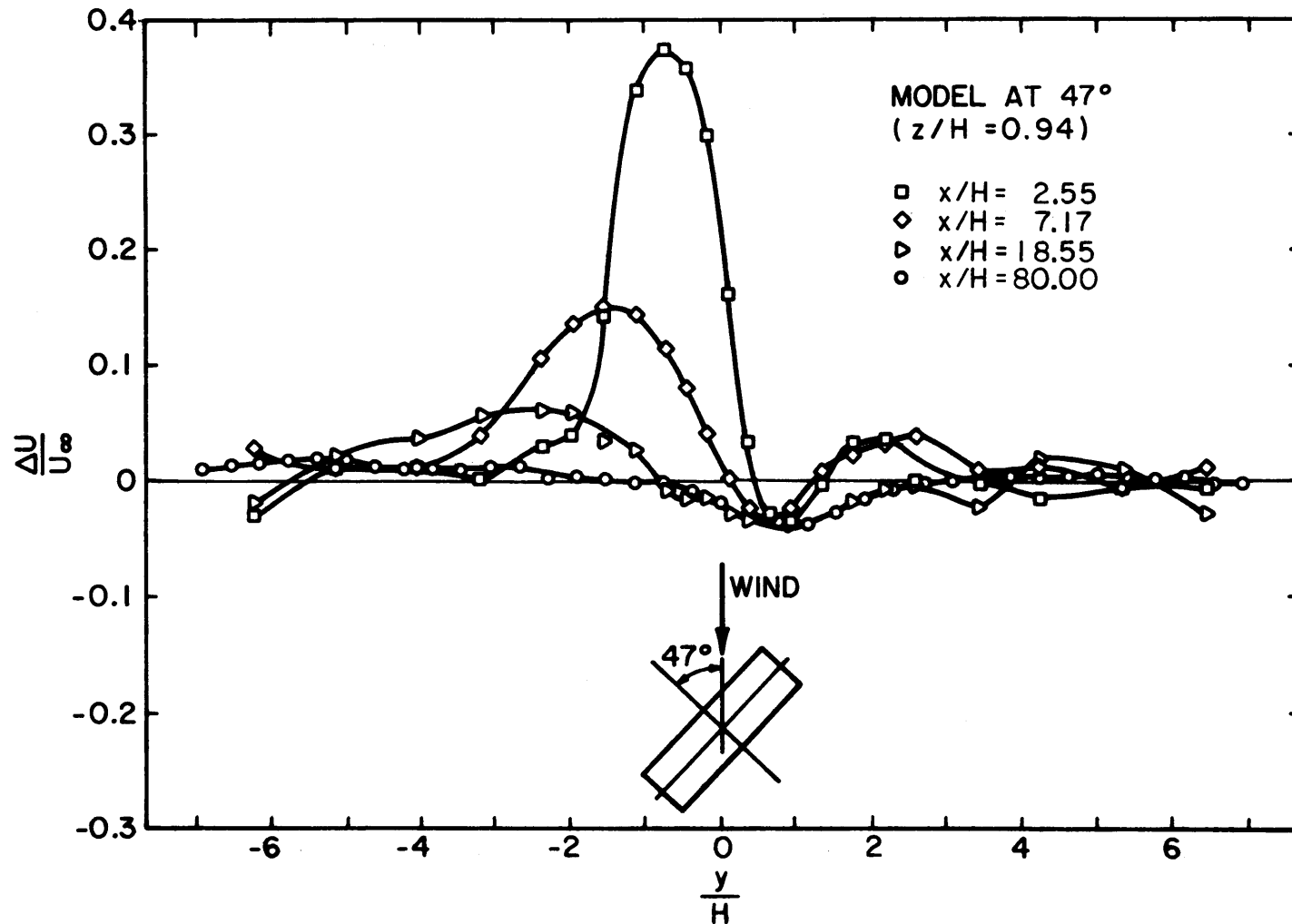
Figure 24. Lateral profiles of mean velocity deficit in the wake of the building at 47 degrees. Test series 10.
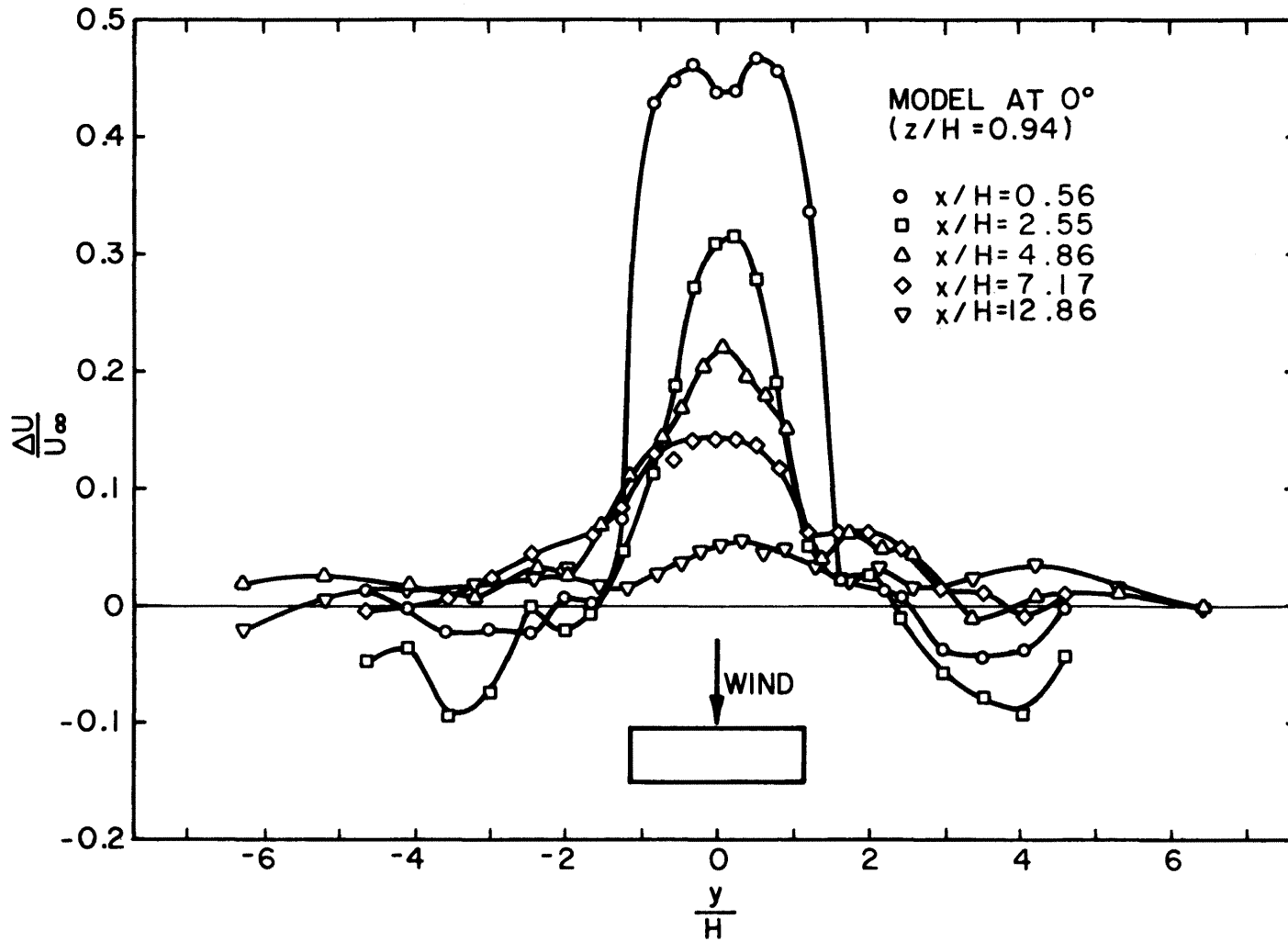
Figure 25. Lateral profiles of mean velocity deficit in the
wake of the building at 0 degrees. Test series 9.
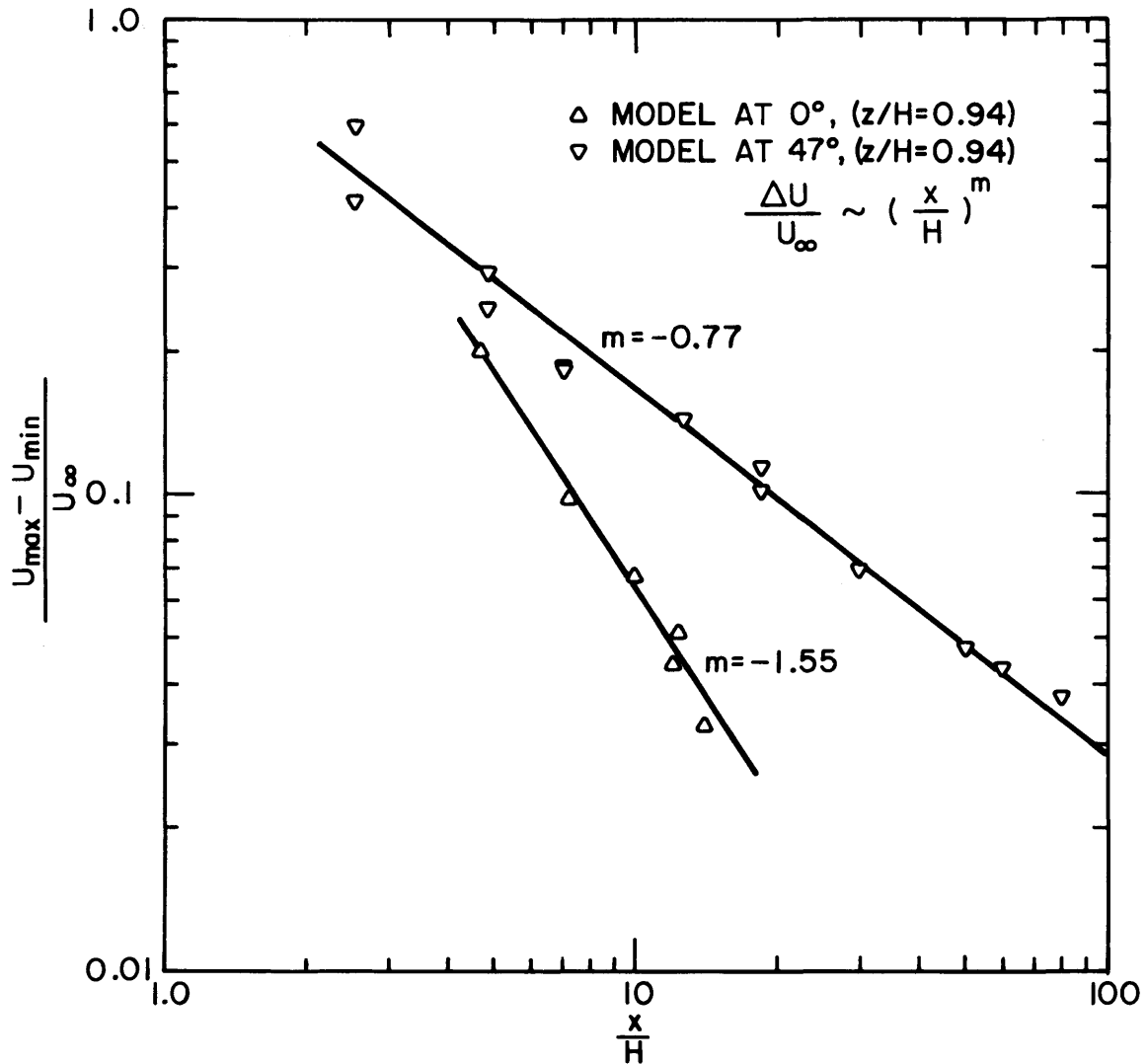
Figure 26. Decay of the maximum mean velocity difference
(across a lateral profile) behind the block
building with downwind distance for two wind
directions. Test series 9 and 10.
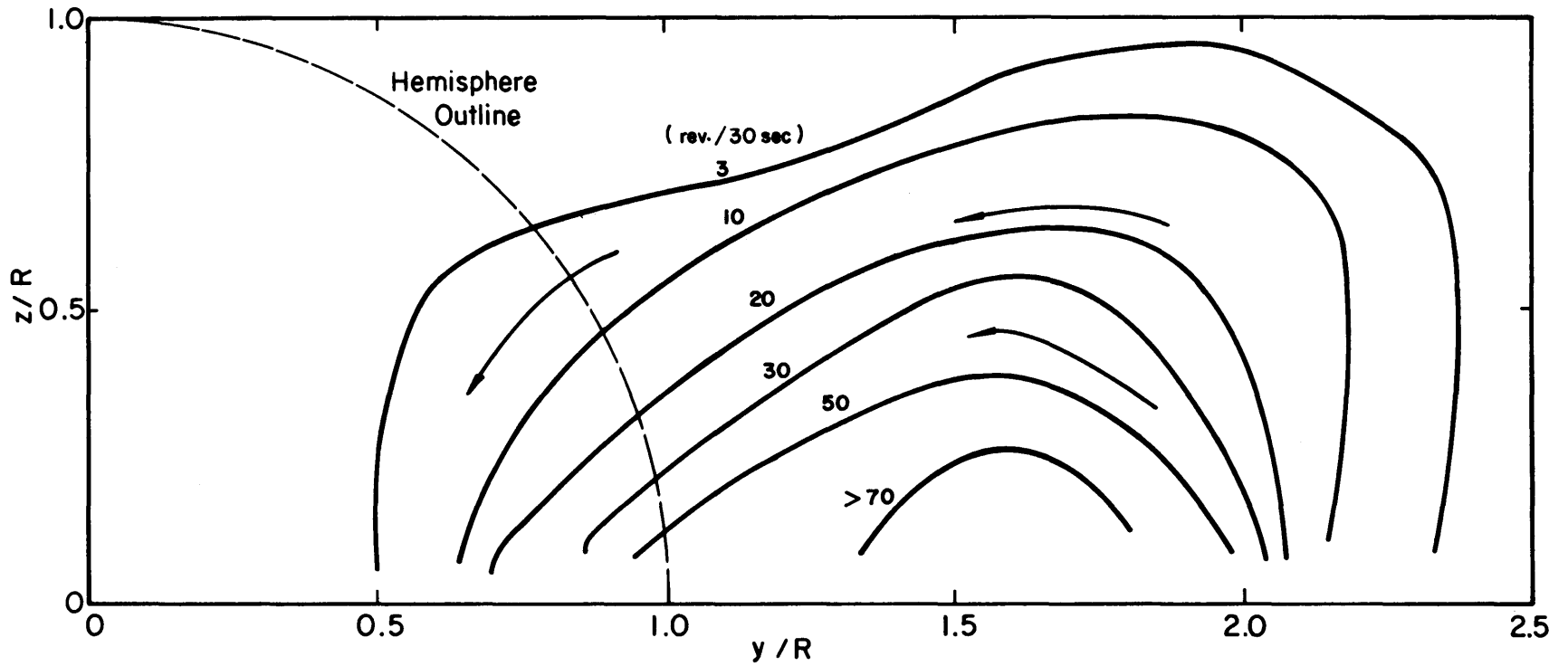
Figure 27a. Contours of constant streamwise vorticity in the wake of a hemisphere at x/R = 8.73. Test series 1. (Viewed looking downstream.)
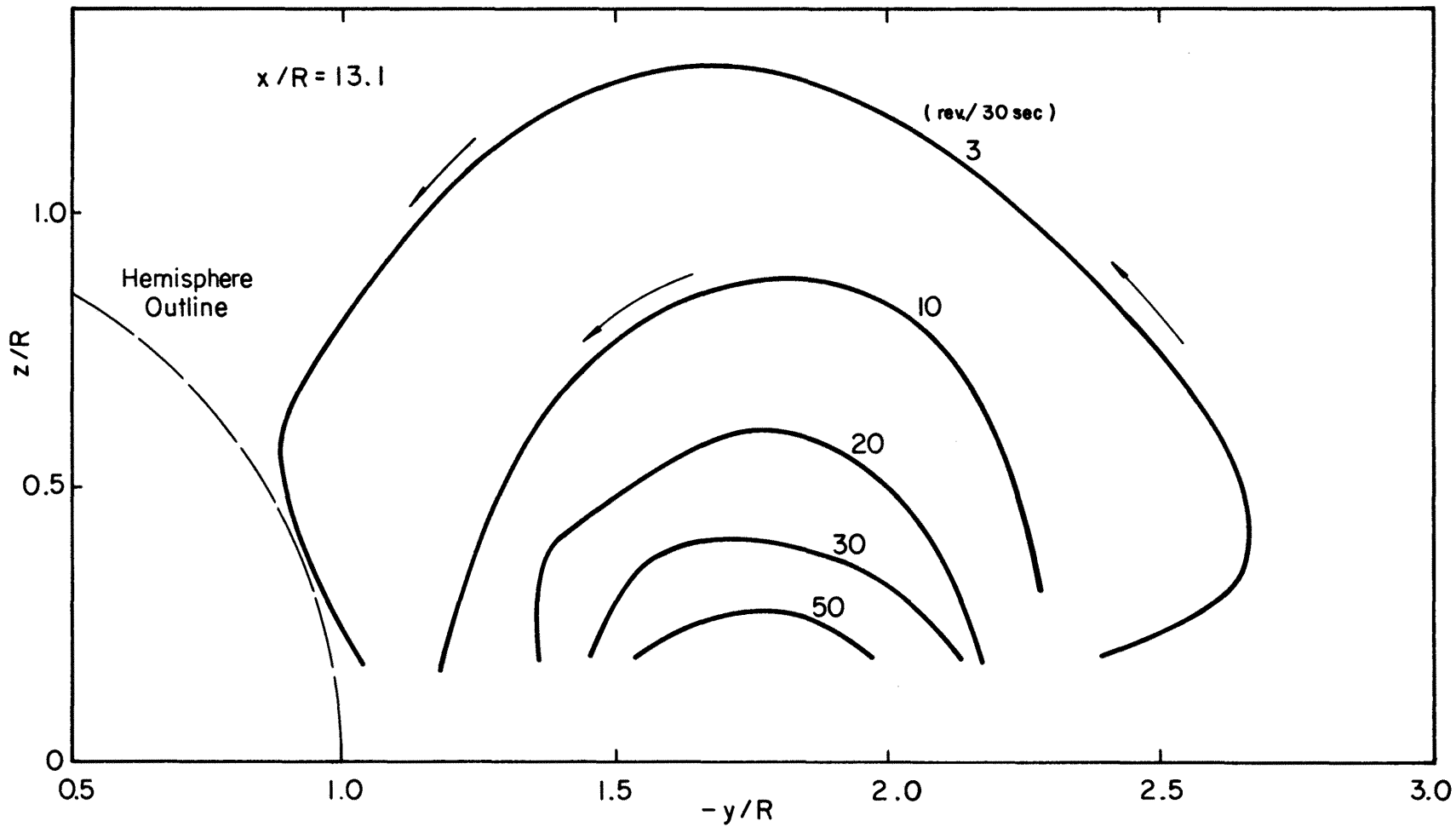
Figure 27b.   x/R = 13.1.
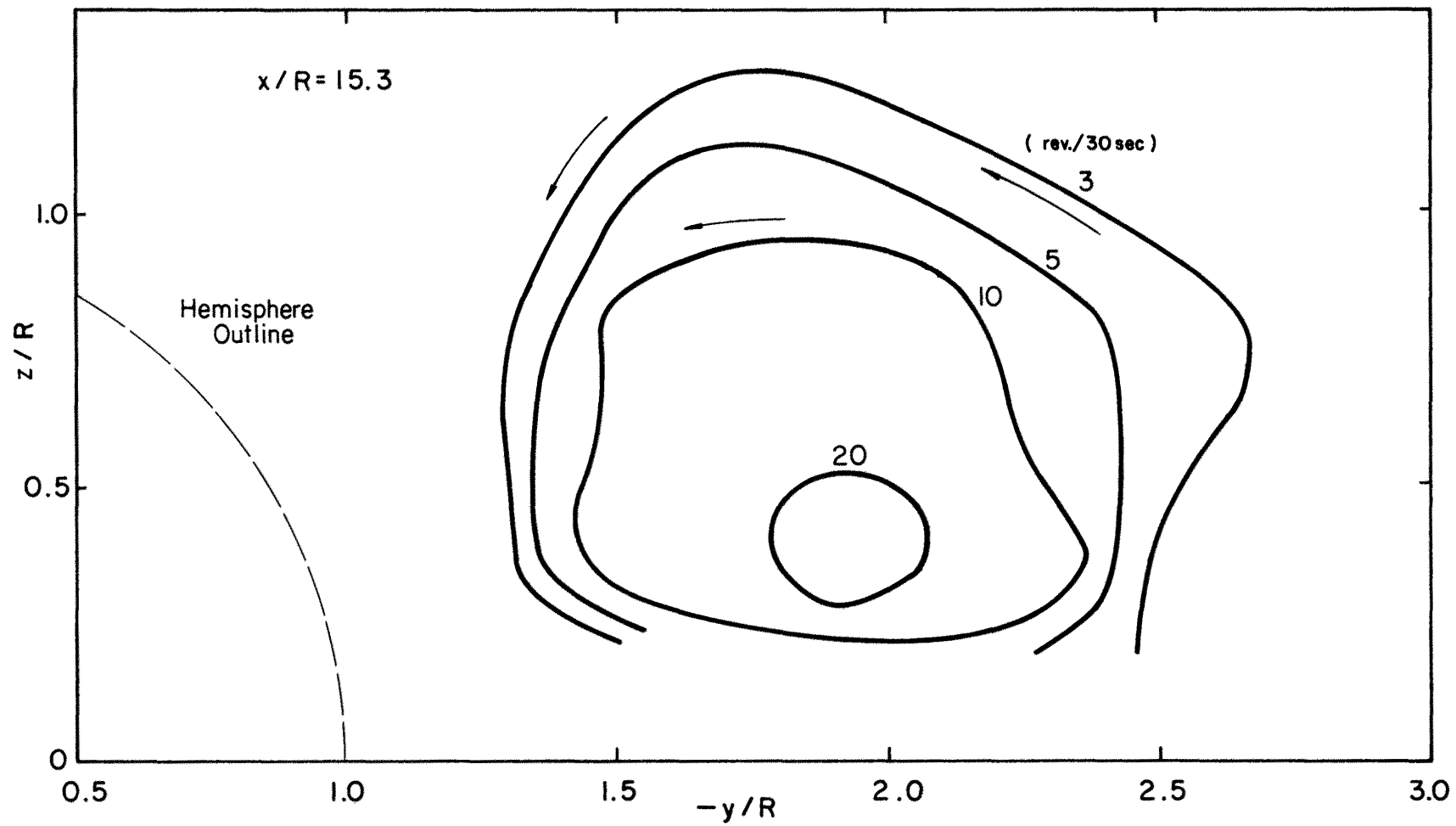
Figure 27c. x/R = 15.3.
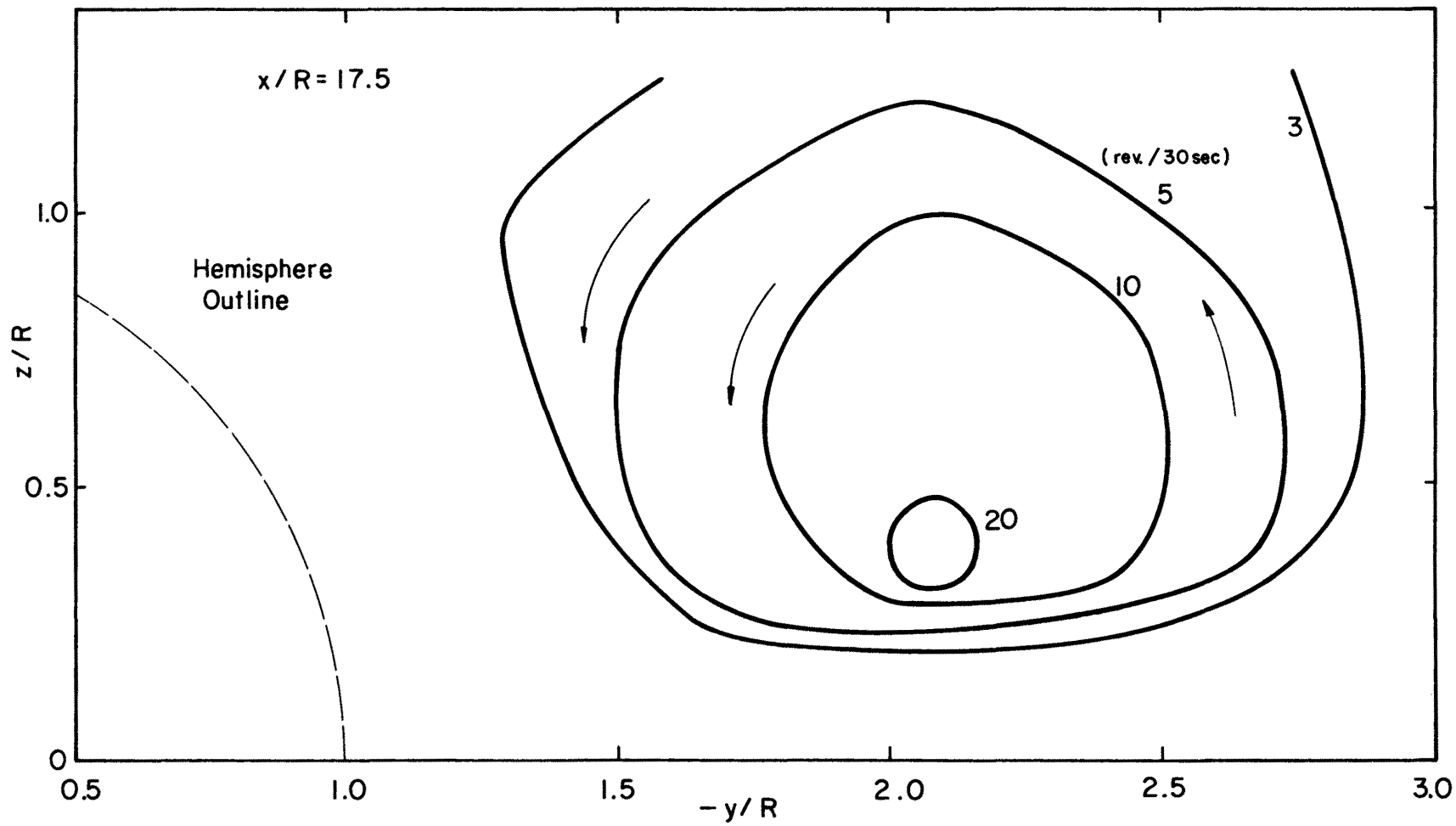
Figure 27d.   x/R = 17.5.
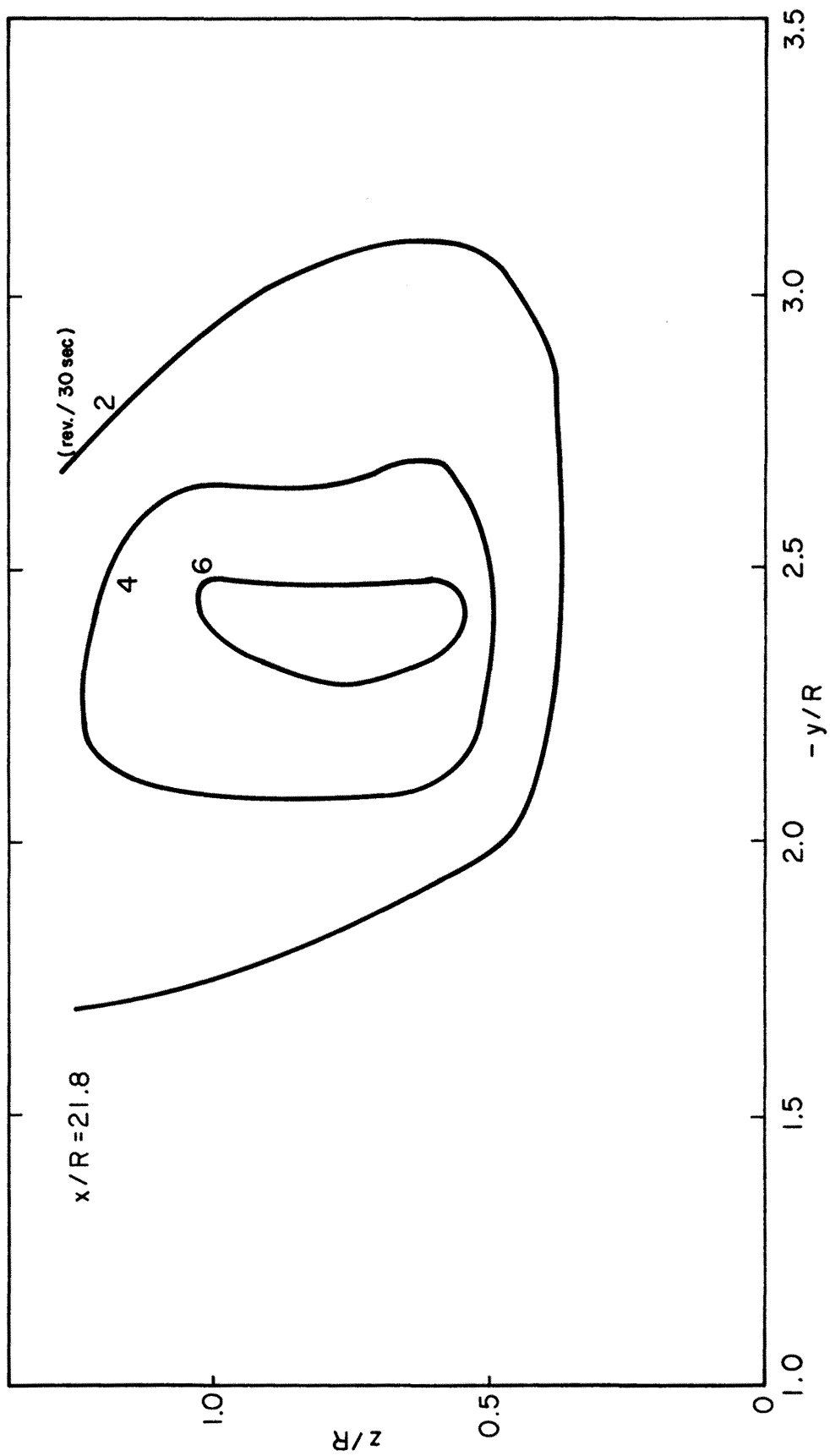
Figure 27e. x/R = 21.8.
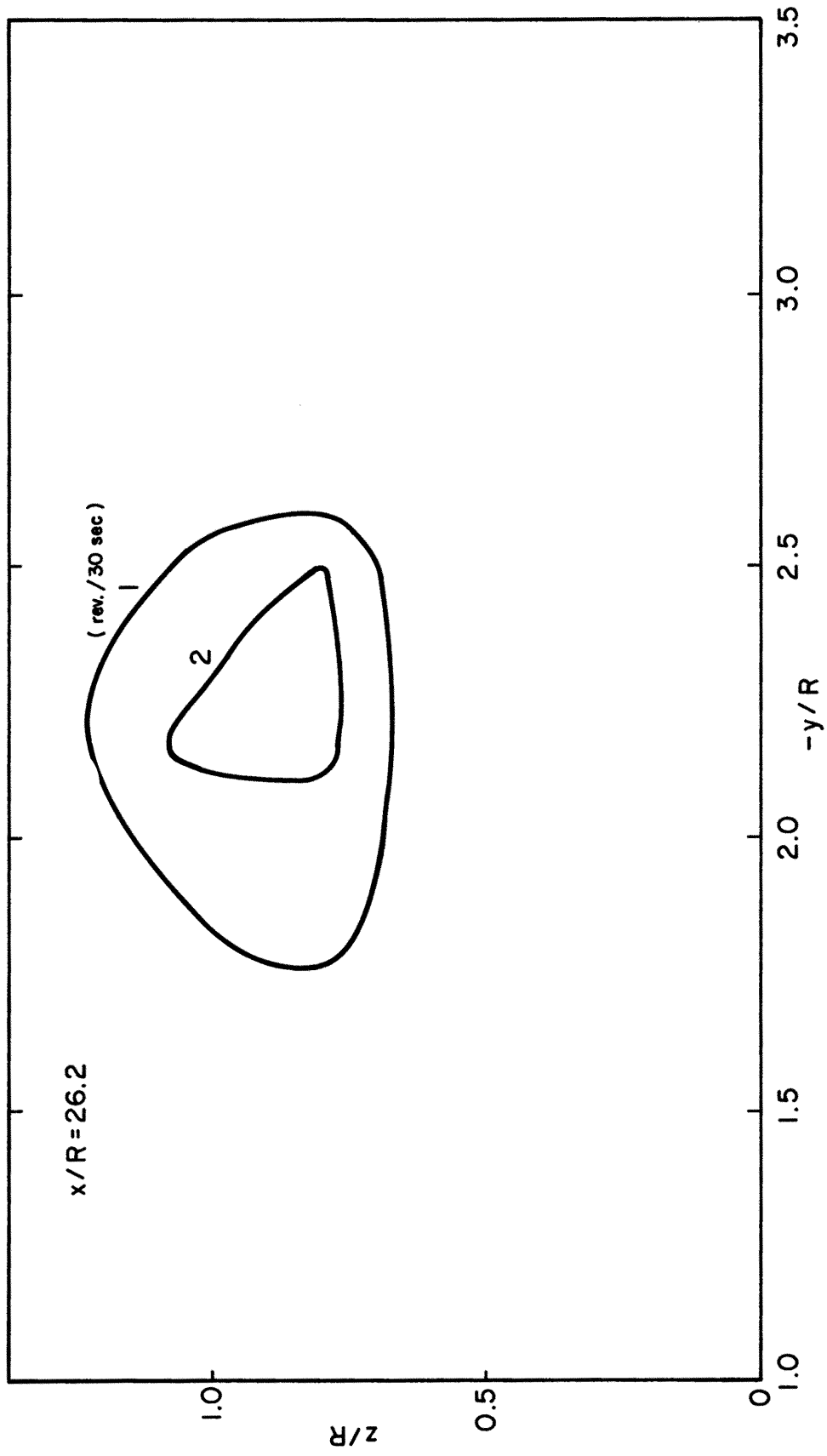
Figure 27f.   x/R = 26.2.
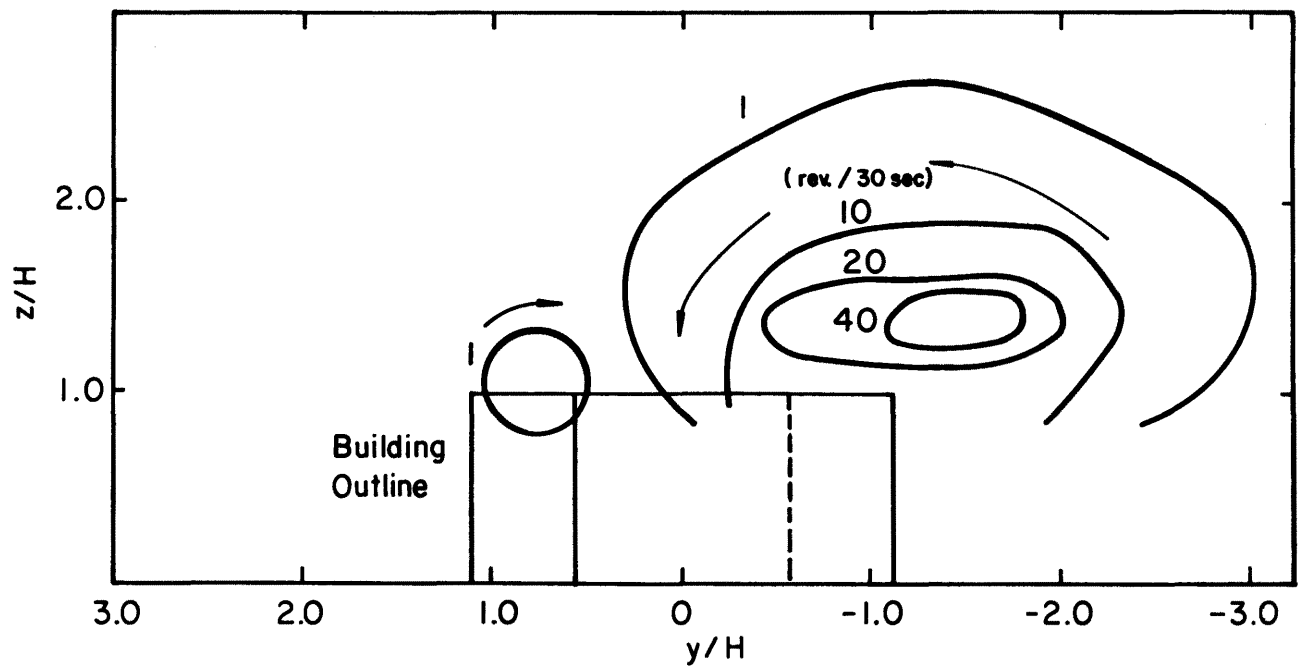
Figure 28. Contours of constant streamwise vorticity in the wake of the block building with the wind at $\alpha = 47$ degrees. $x/H = 12.9$, Test series 10. (Viewed looking downwind.)
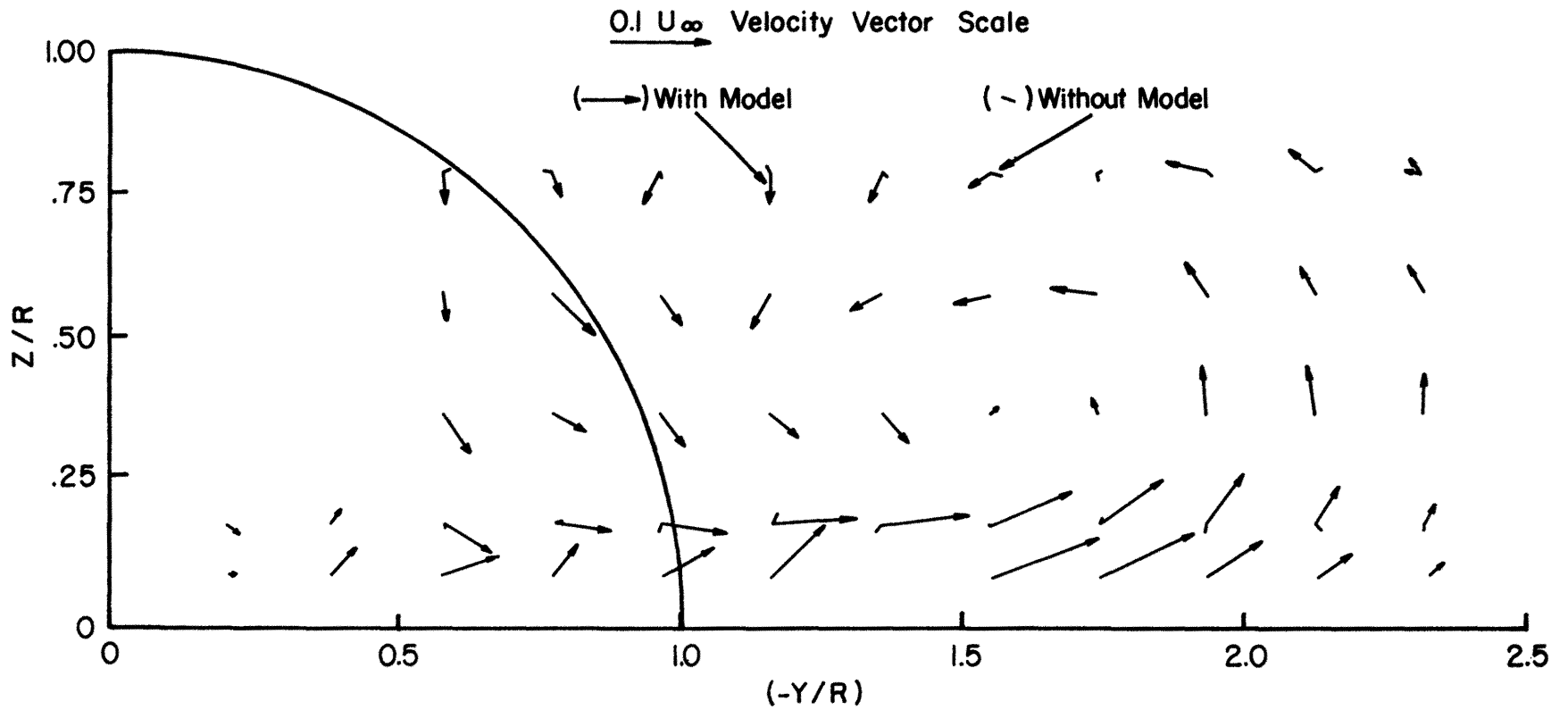
Figure 29a. Cross-flow velocity vector distribution in one-half of the wake as seen looking downwind past the hemisphere. (Small arrows without heads show the cross flow in the absence of the model.) x/R = 8.73, Test series 1.
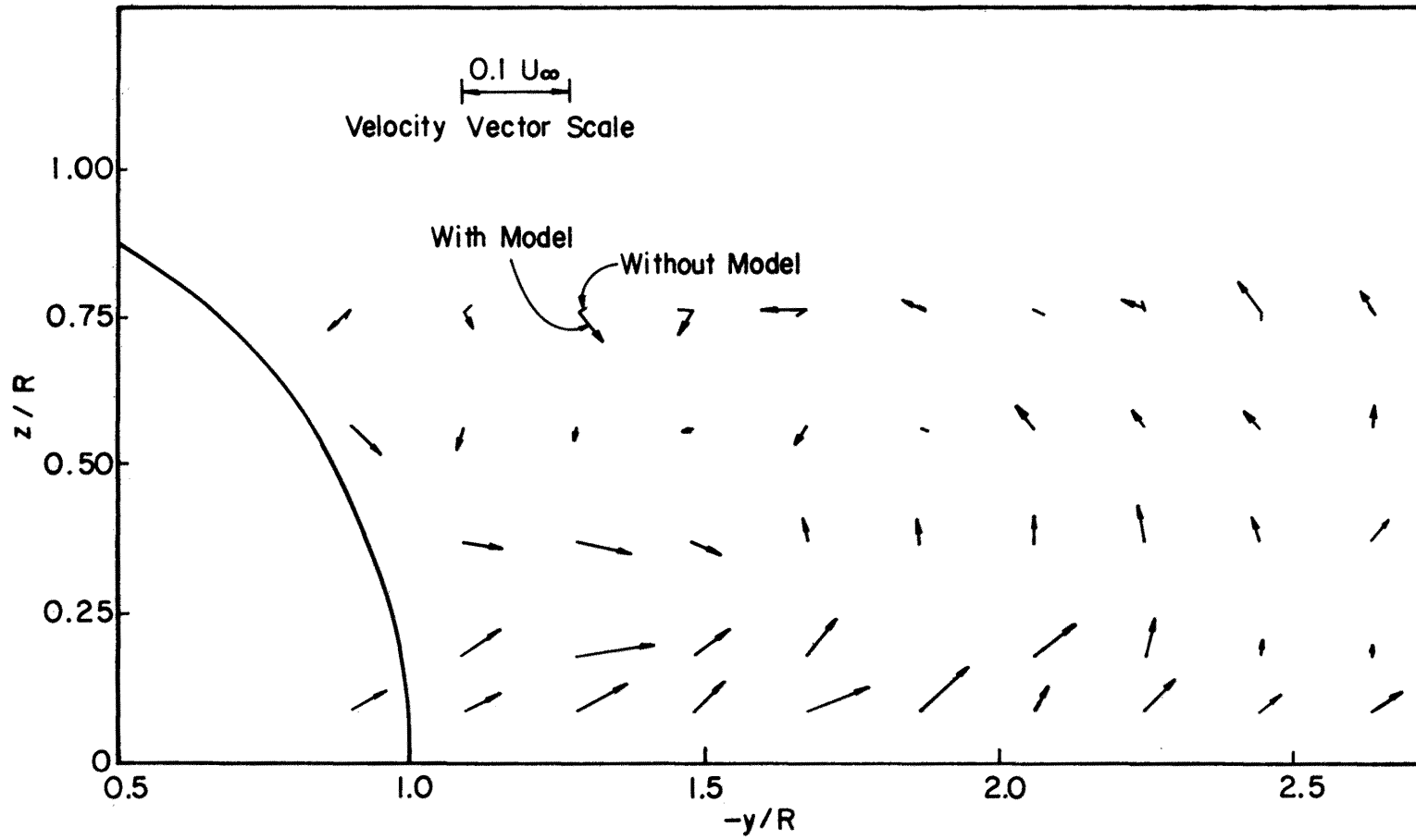
Figure 29b.   x/R = 13.1.
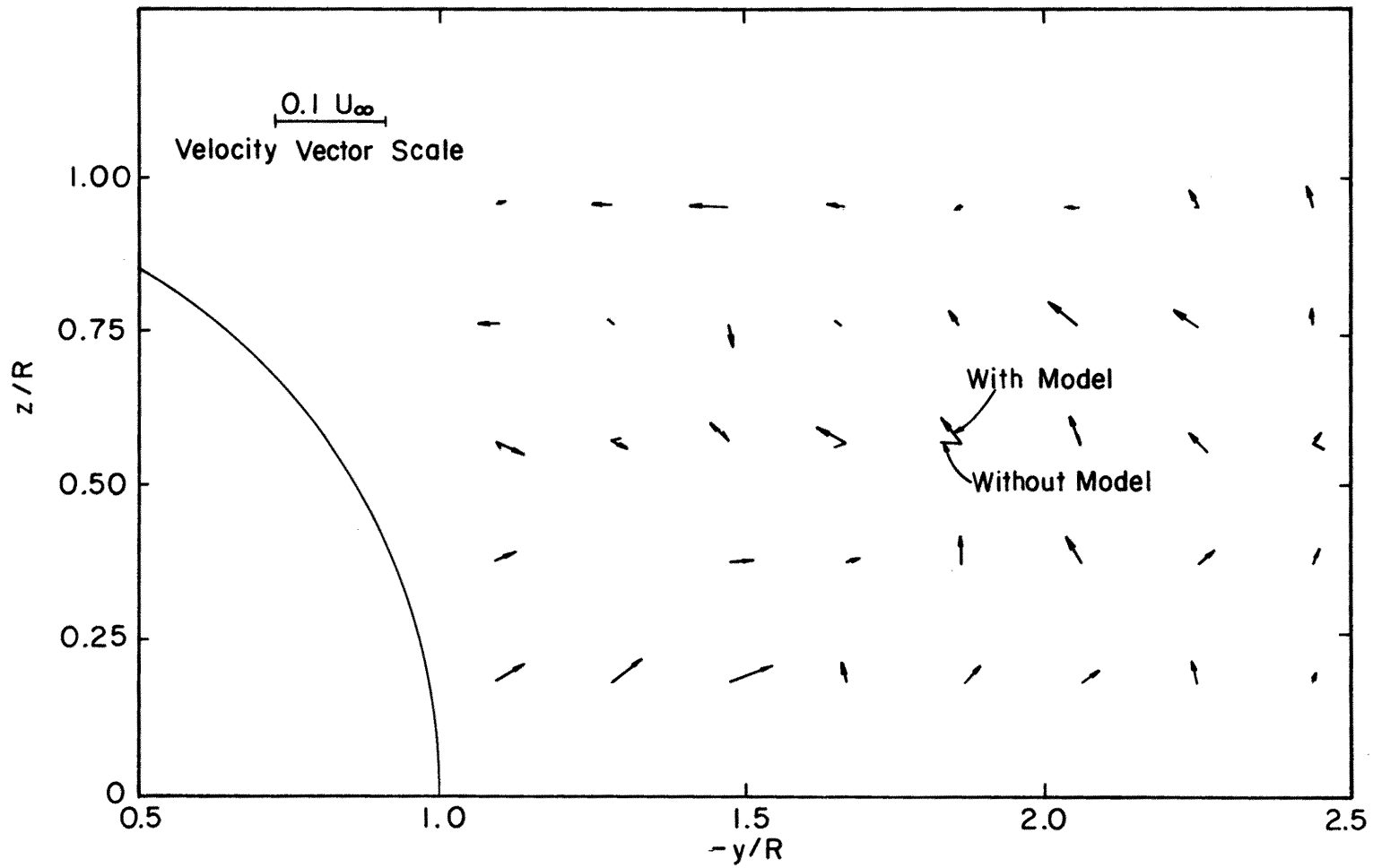
Figure 29c. x/R = 17.5.
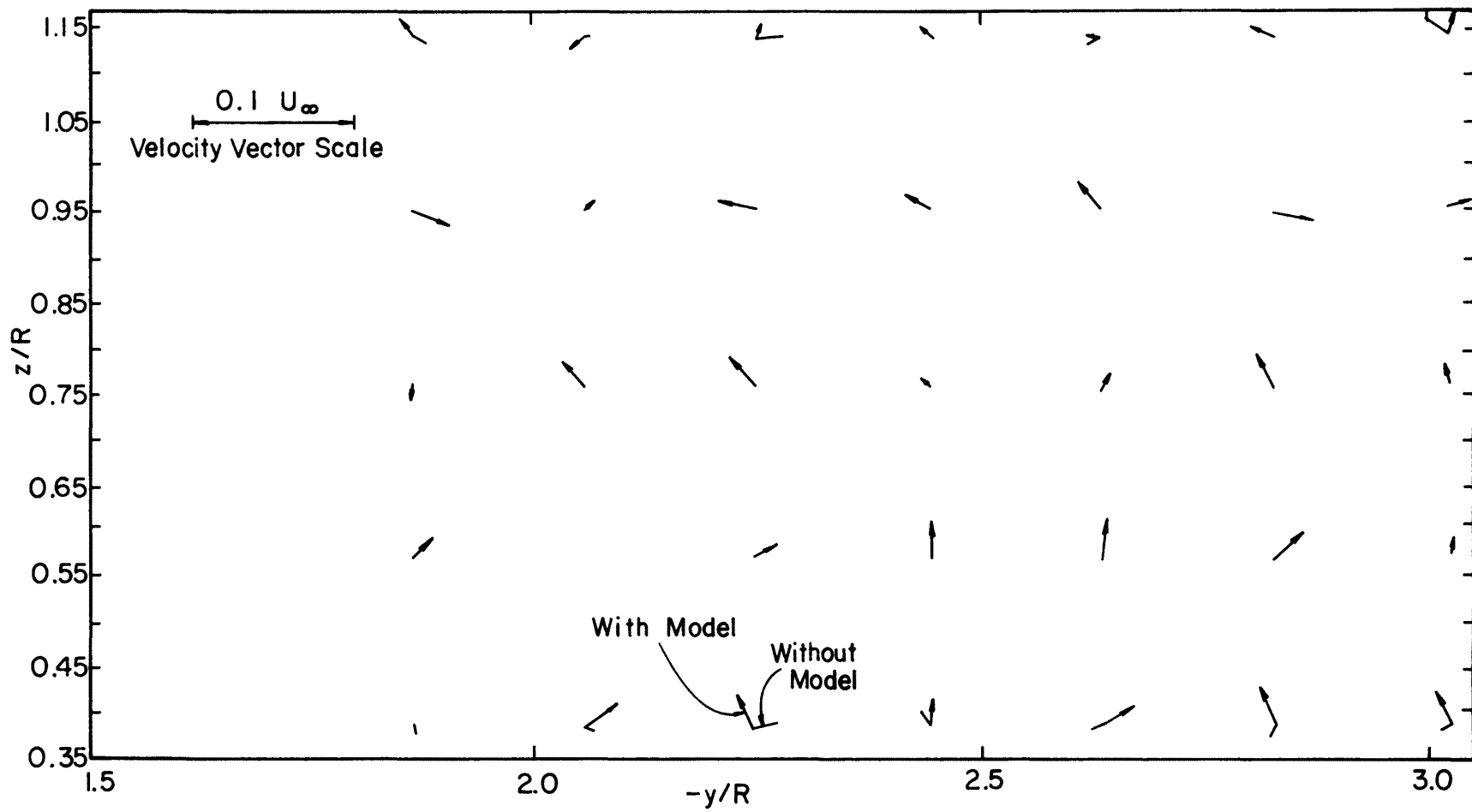
Figure 29d. x/R = 21.8.
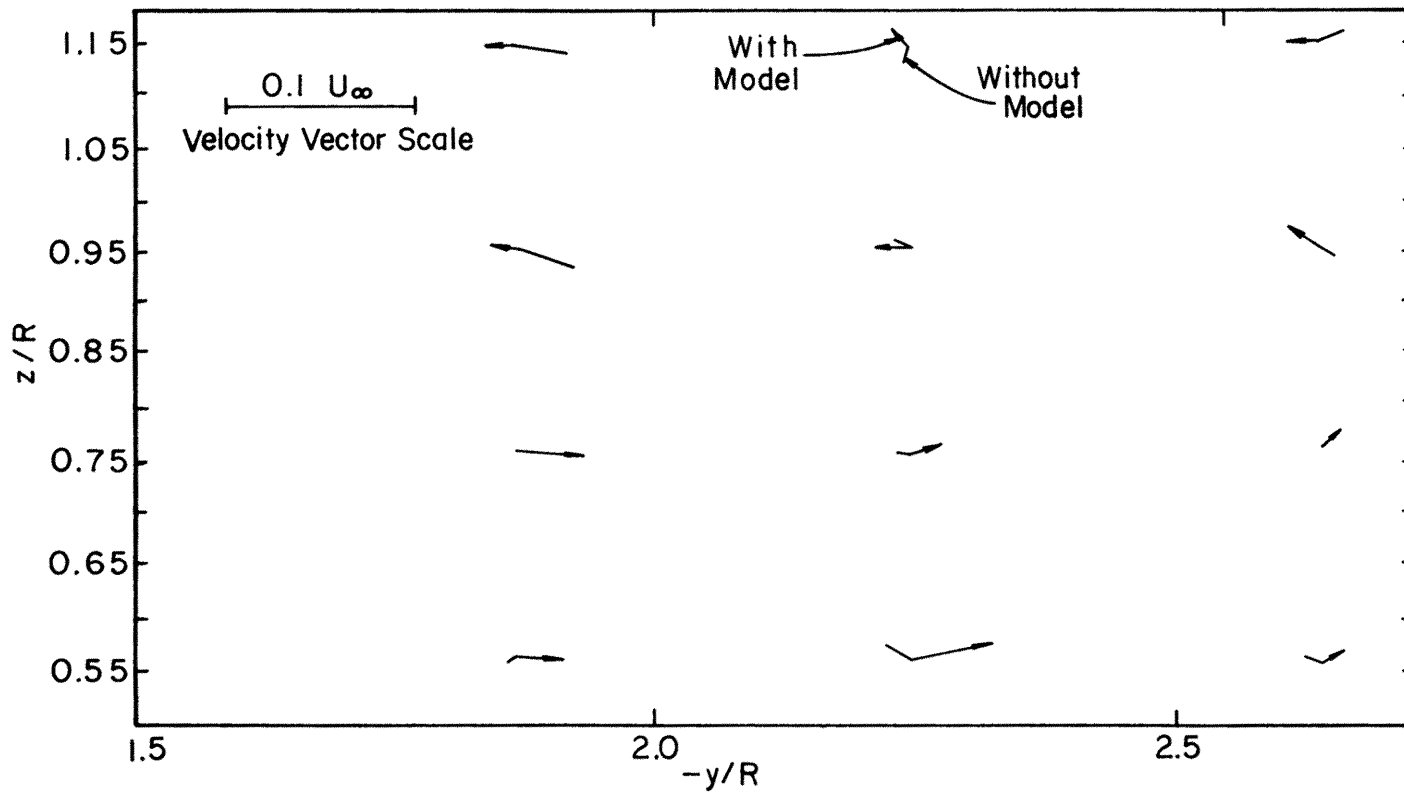
Figure 29e.   x/R = 26.2.
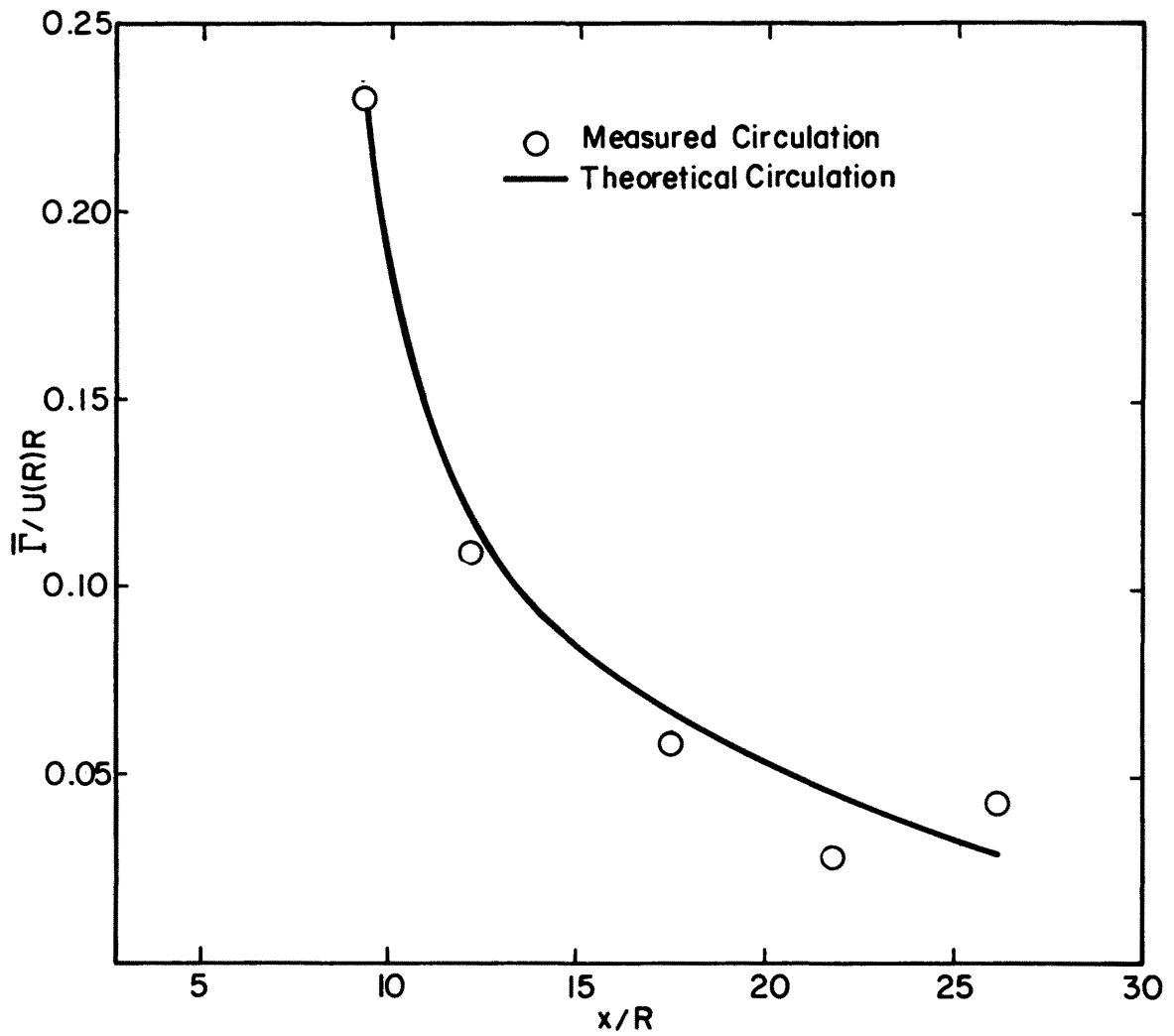
Figure 30. Comparison of the theoretical and actual horseshoe vortex average strengths in the wake of a hemisphere. Test series 1.
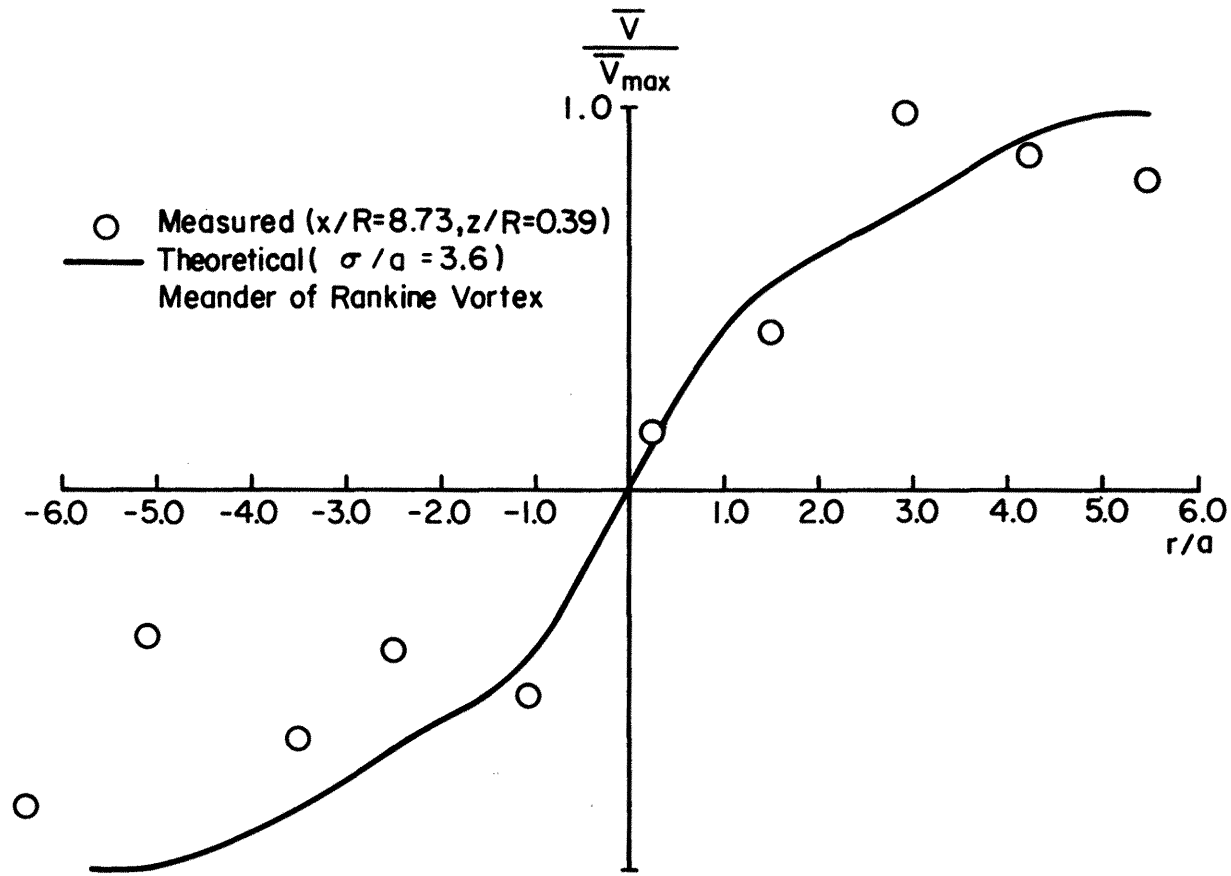
Figure 31. Comparison of the theoretical and actual vertical velocity in a lateral traverse through the vortex core in the wake of a hemisphere. Test series 1.
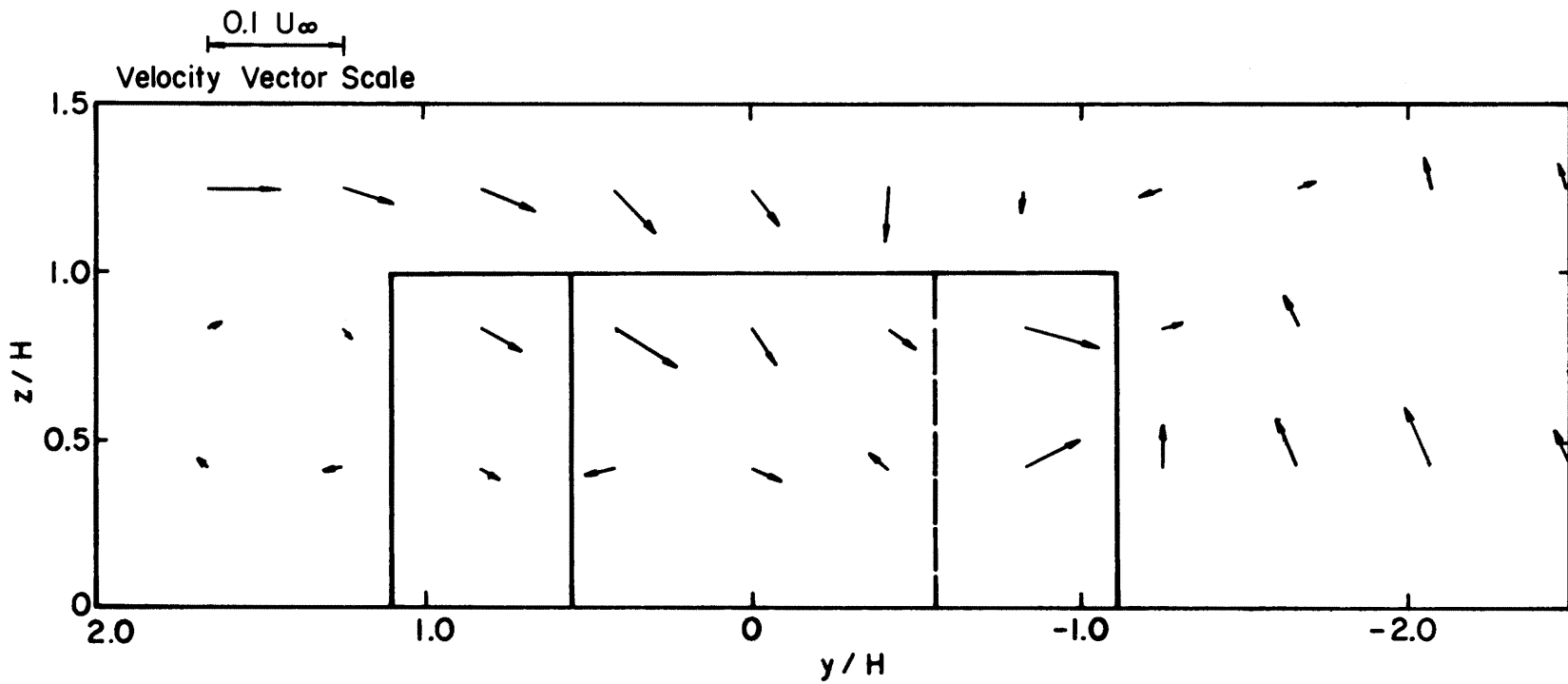
Figure 32. Cross-flow velocity vector distribution as seen looking downwind past the block building with the wind approaching at α = 47 degrees. x/H = 12.9, Test series 10.

Figure 33. Comparison of the theoretical and actual vortex
positions in the wake of a hemisphere. Test
series 1.
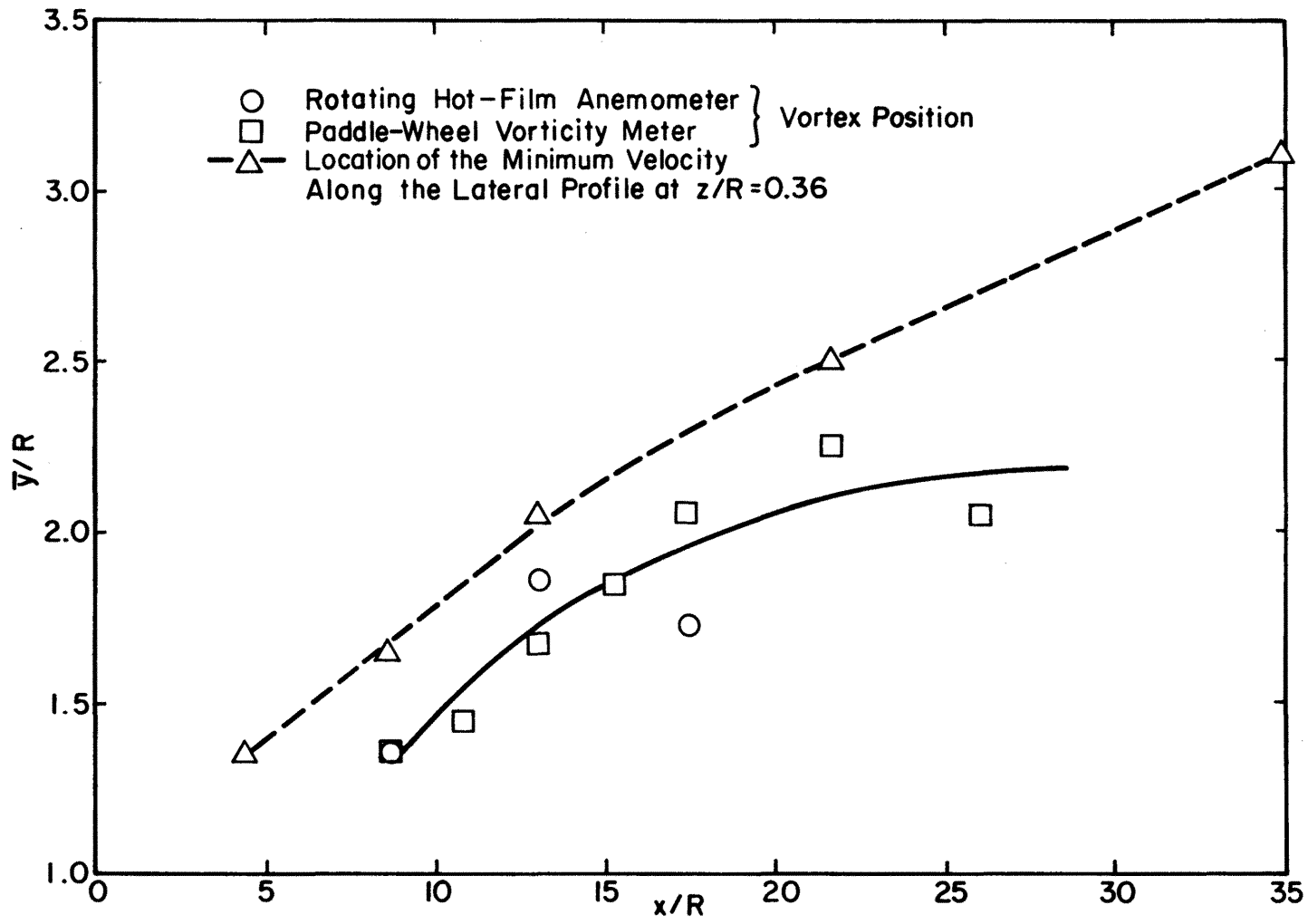
Figure 34. Comparison of the location of the vortex lateral position with the location of the minimum longitudinal velocity in a lateral profile at the height of the vortex. Wake of a hemisphere, Test series 1.
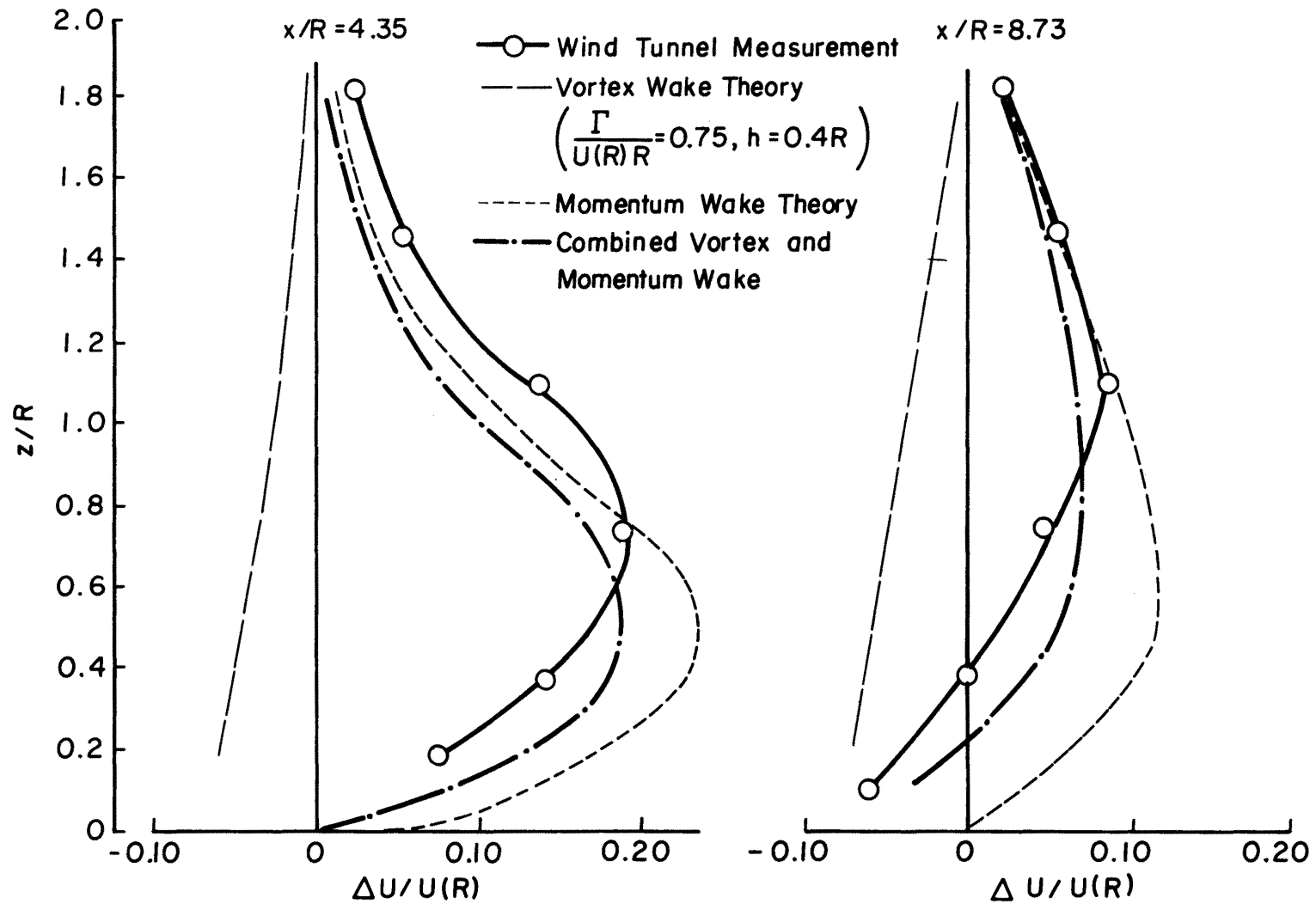
Figure 35. Comparison of the actual vertical profiles of velocity deficit on the hemisphere wake centerline with the theoretical profiles of Hunt. Test series 2.
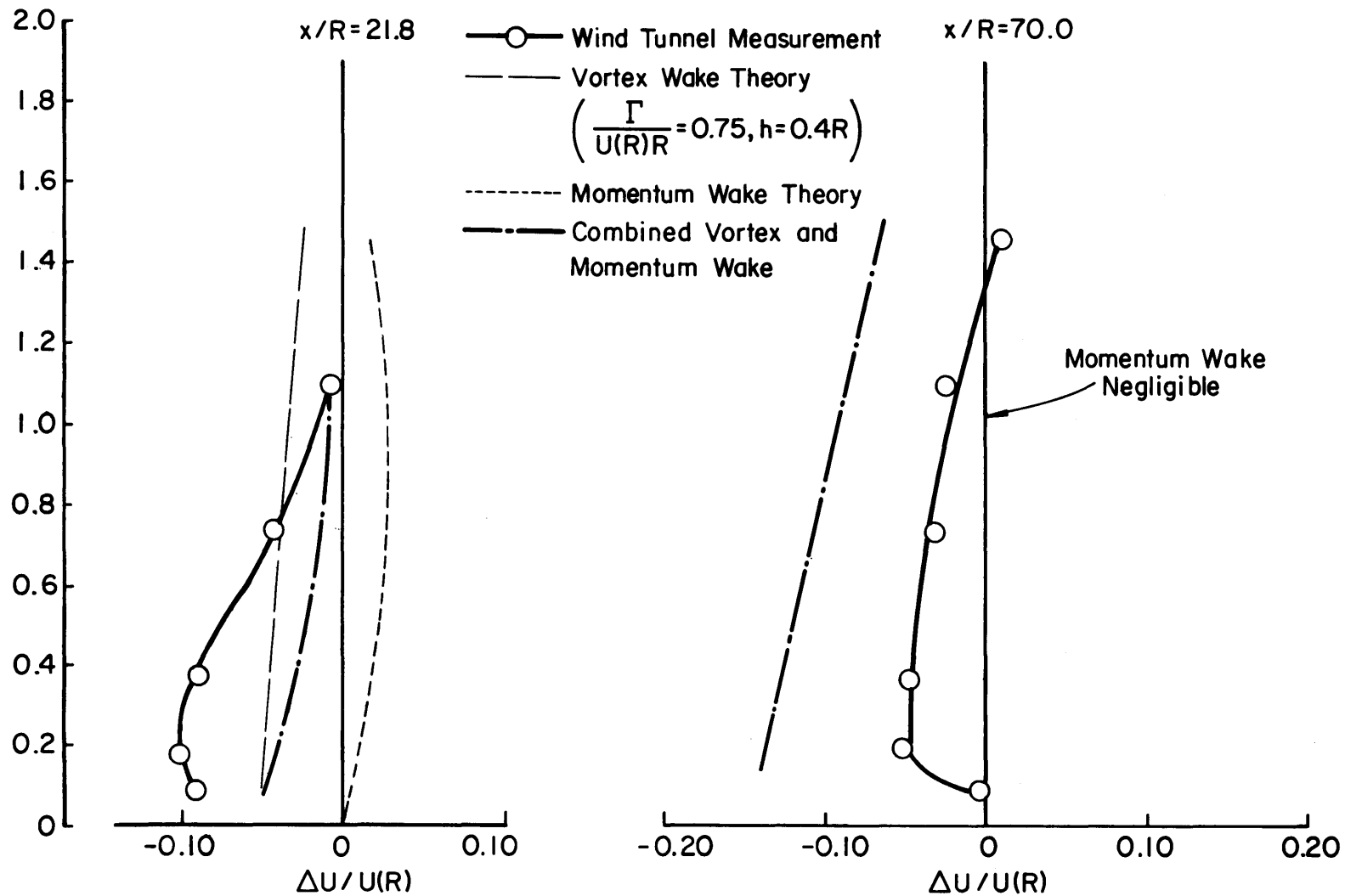
Figure 35. Continued
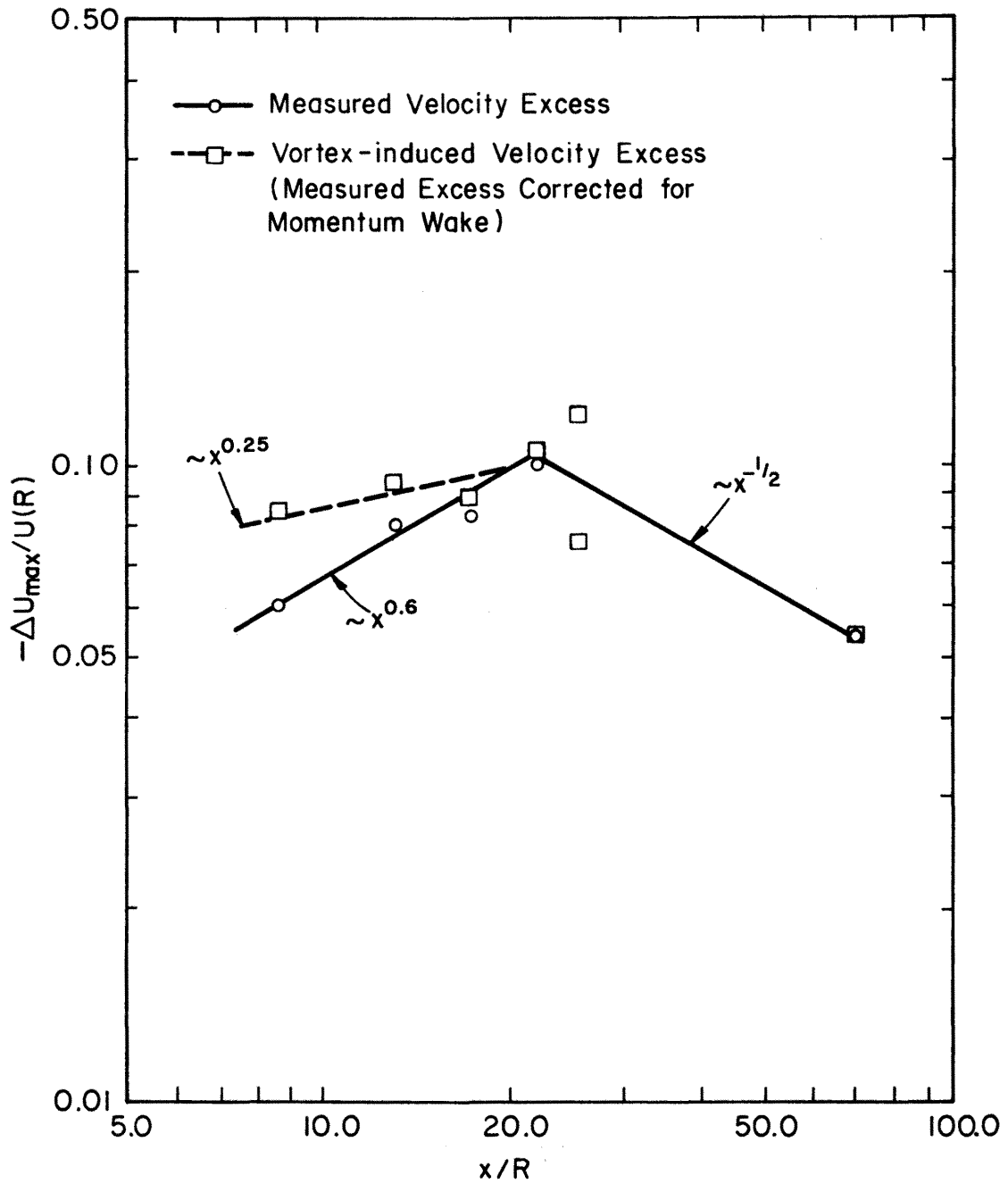
Figure 36. Decay of the maximum vortex-induced velocity
perturbation observed in the hemisphere wake.
Test series 2.
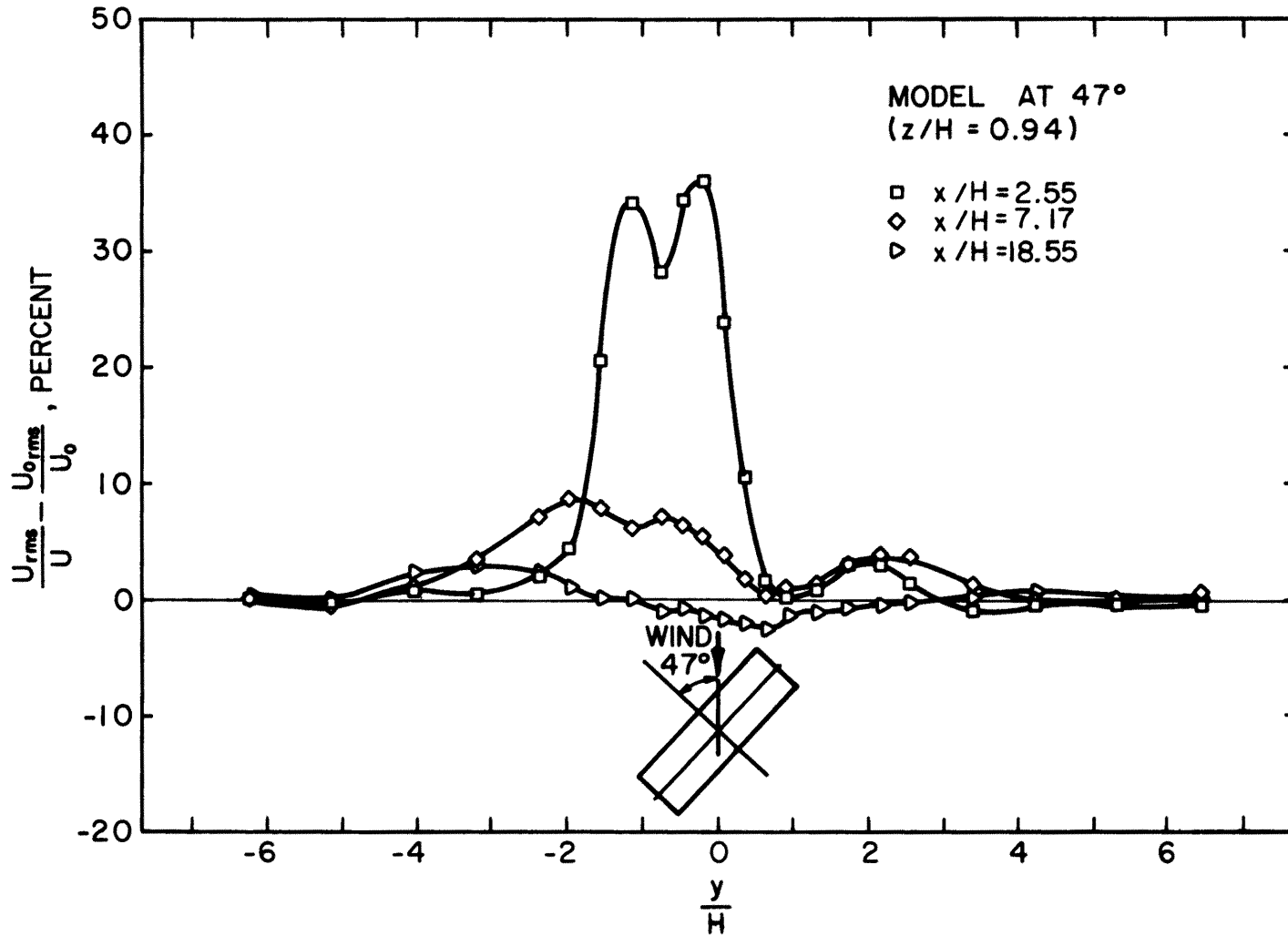
Figure 37. Lateral profiles of turbulence intensity excess in the wake of the building at 47 degrees. Test series 10.
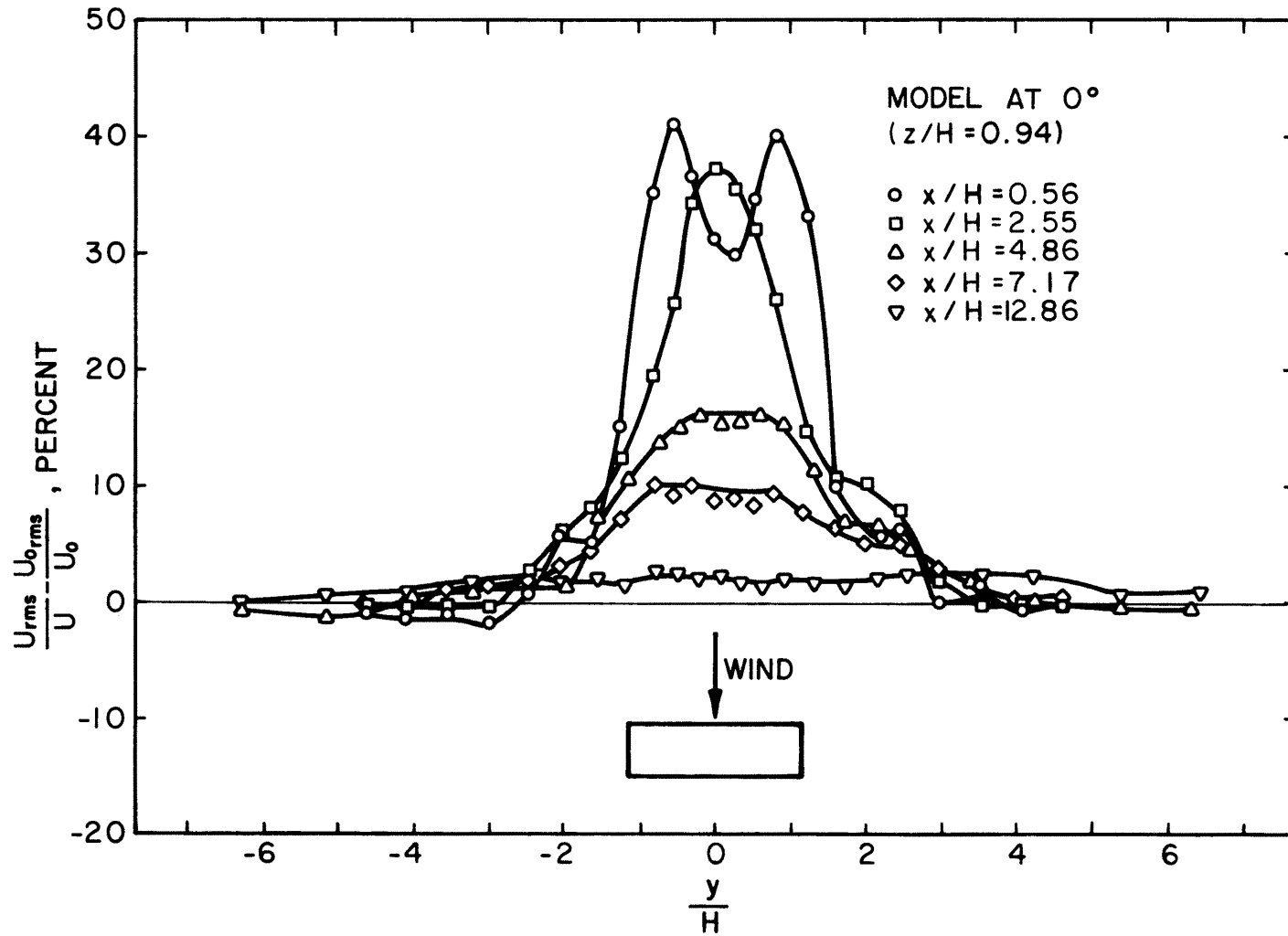
Figure 38. Lateral profiles of turbulence intensity excess in
the wake of the building at 0 degrees. Test series 9.
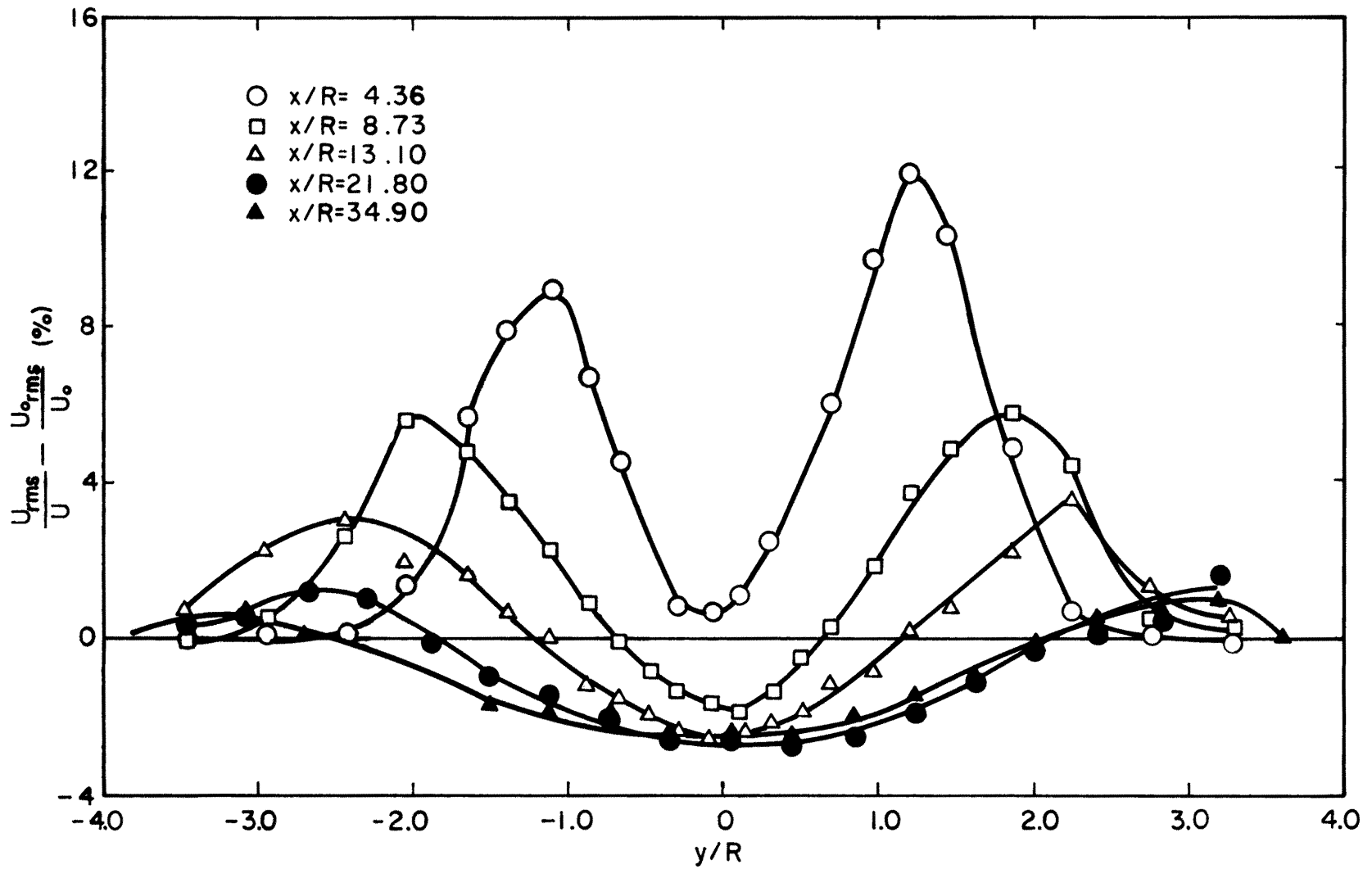
Figure 39. Lateral profiles of turbulence intensity excess in
the wake of a hemisphere. z/R = 0.364, Test series 1.
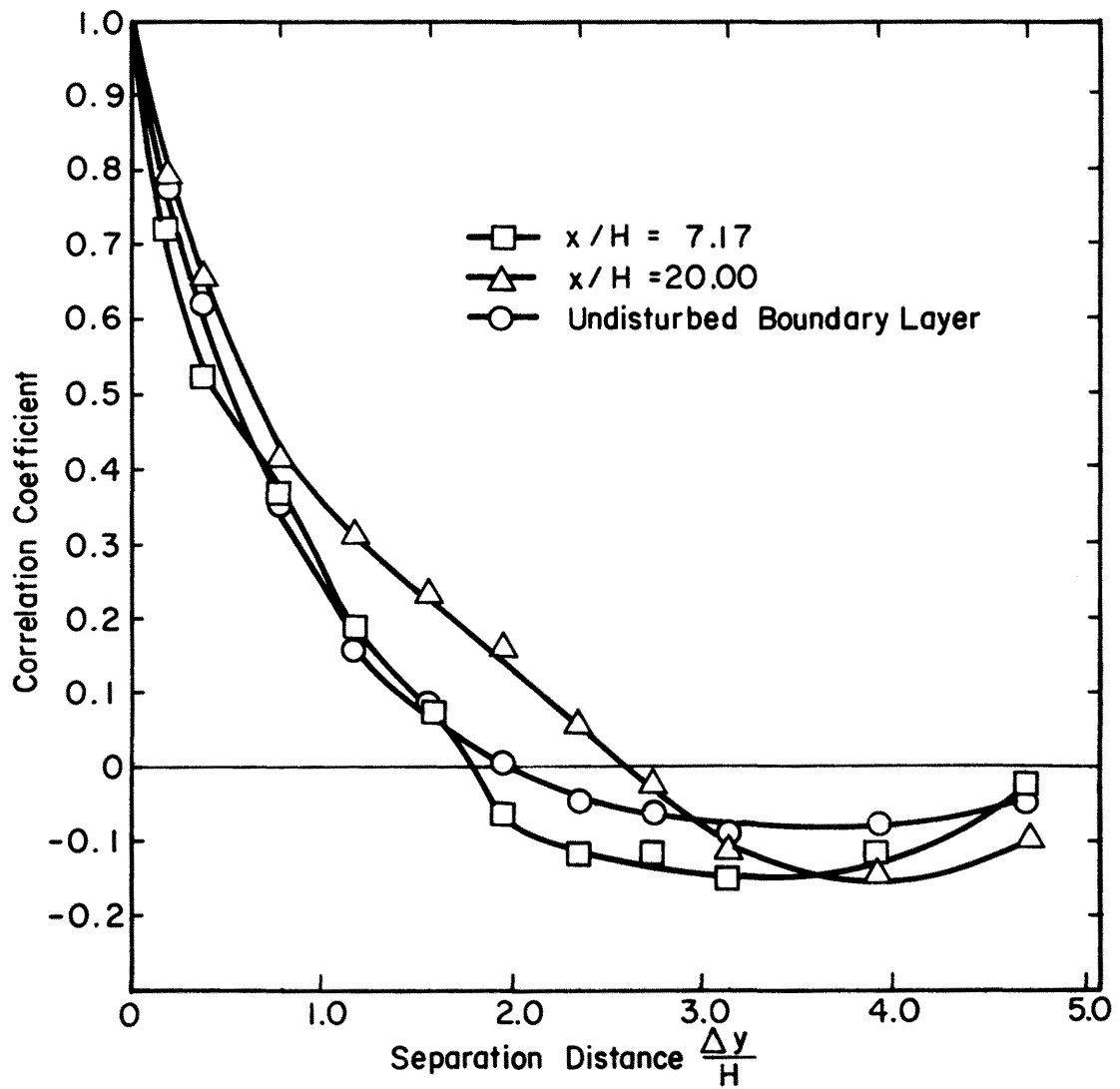
Figure 40. Lateral correlation of longitudinal velocity fluc-
tuations in the wake of the block building with the
wind at α = 47 degrees. Fixed point at y/H = 0.0,
z/H = 0.94. Test series 10.
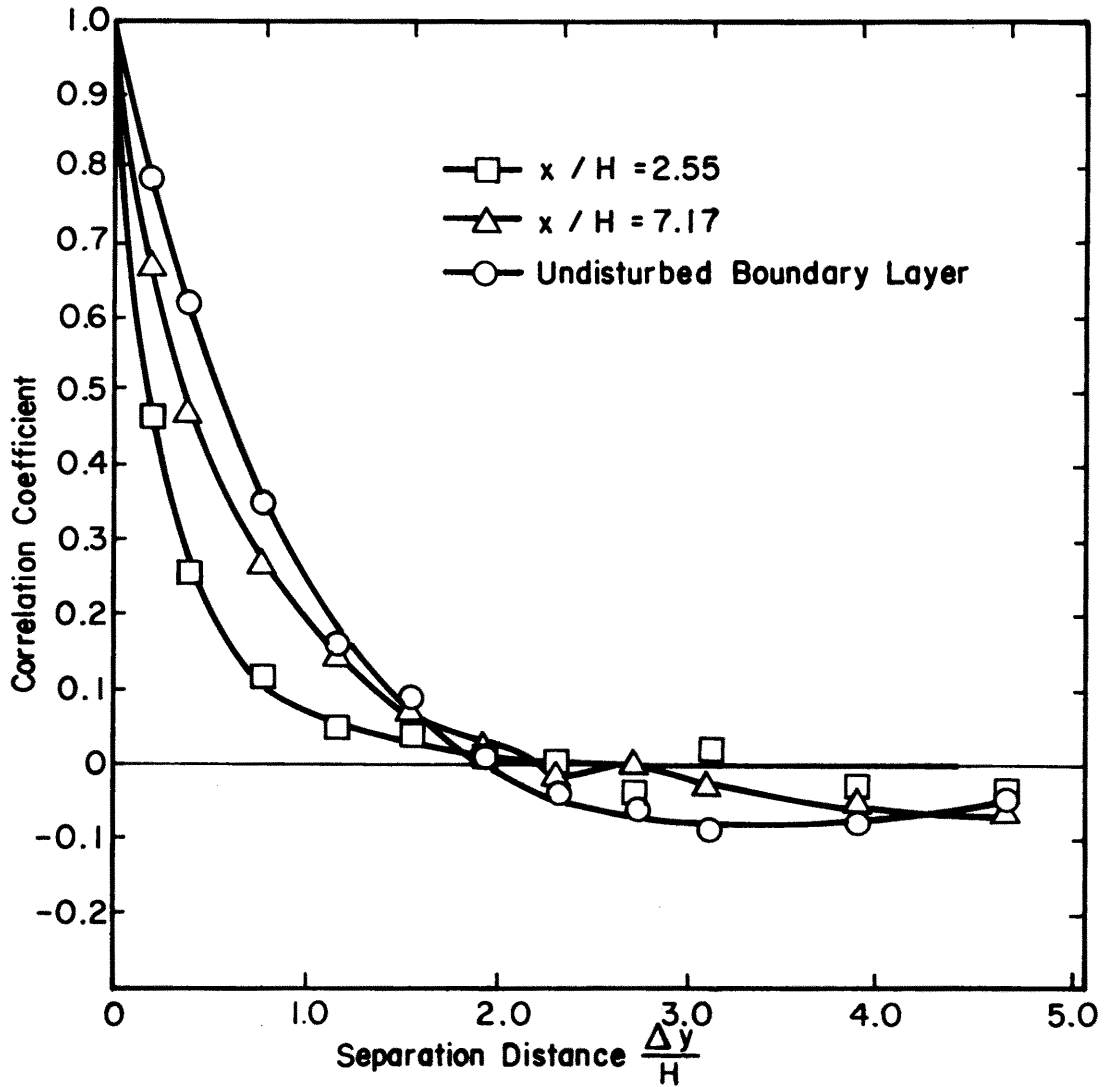
Figure 41. Lateral correlation of longitudinal velocity fluc-
tuations in the wake of the block building with the
wind at α = 0 degrees. Fixed point at y/H = 0.0,
z/H = 0.94. Test series 9.
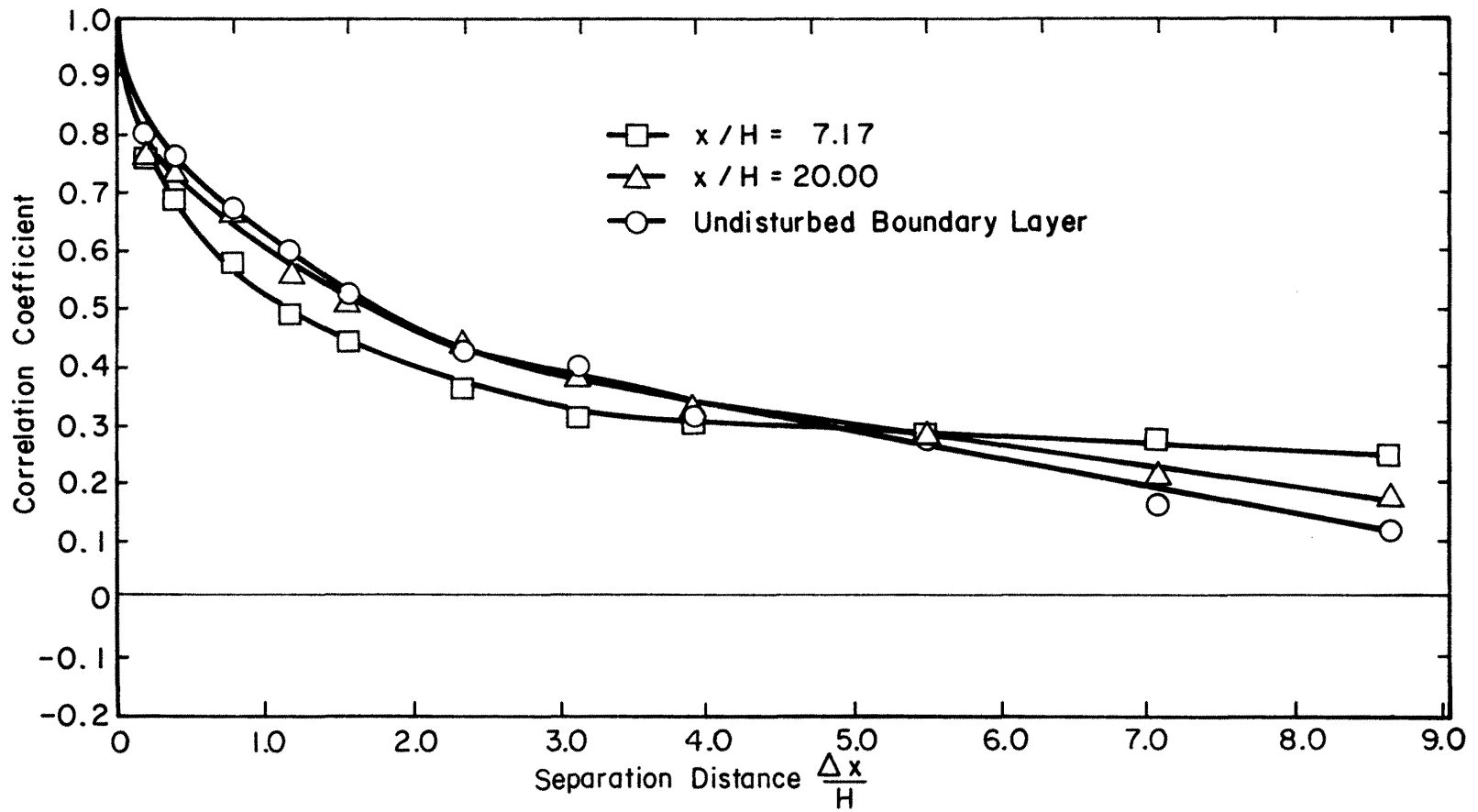
Figure 42. Longitudinal correlation of longitudinal velocity
fluctuations in the wake of the block building with
the wind at α = 47 degrees. The fixed point is
at y/H = 0.0, z/H = 0.94. Test series 10.
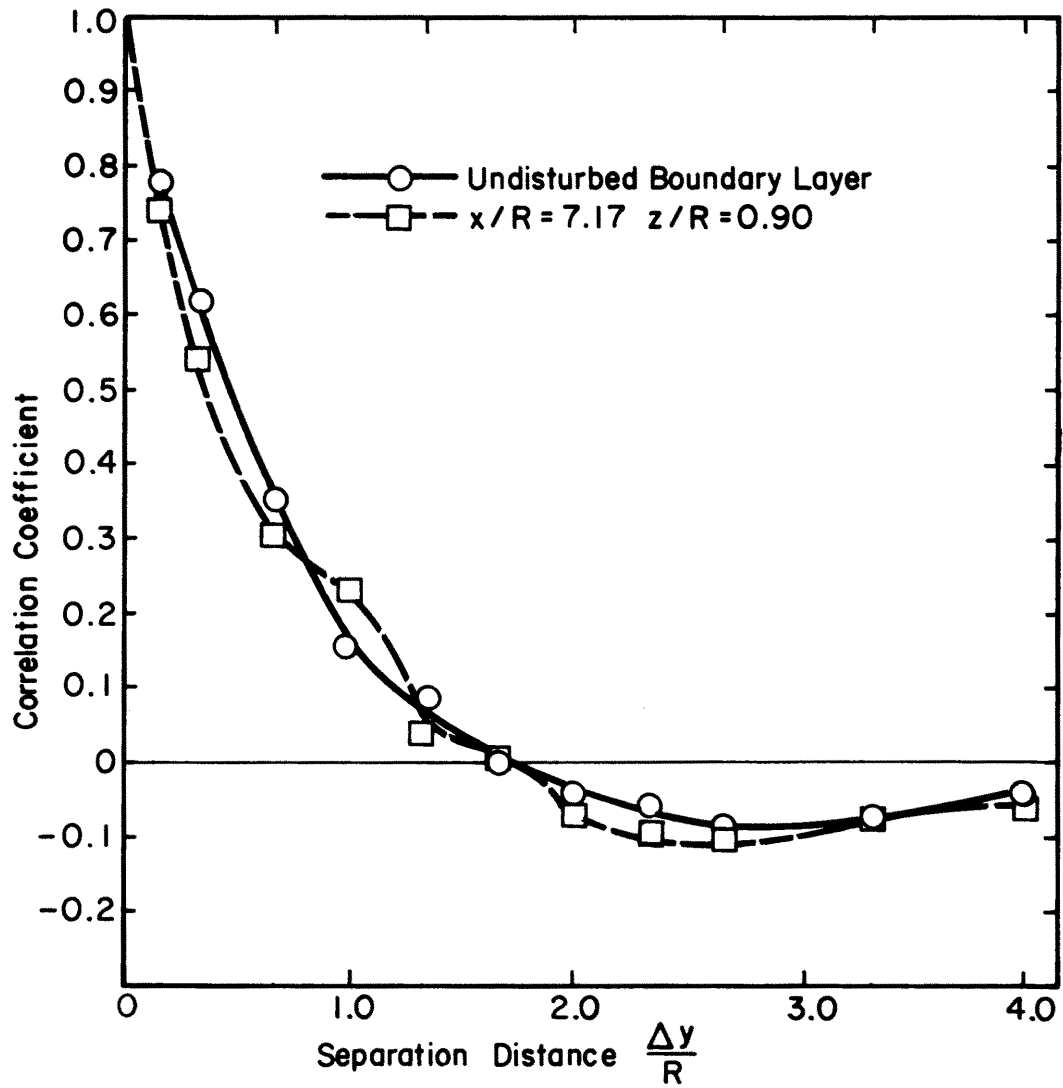
Figure 43. Lateral correlation of longitudinal velocity fluctuations in the wake of a hemisphere. Fixed point at y/R = 0.0, z/R = 0.90. Test series 8.
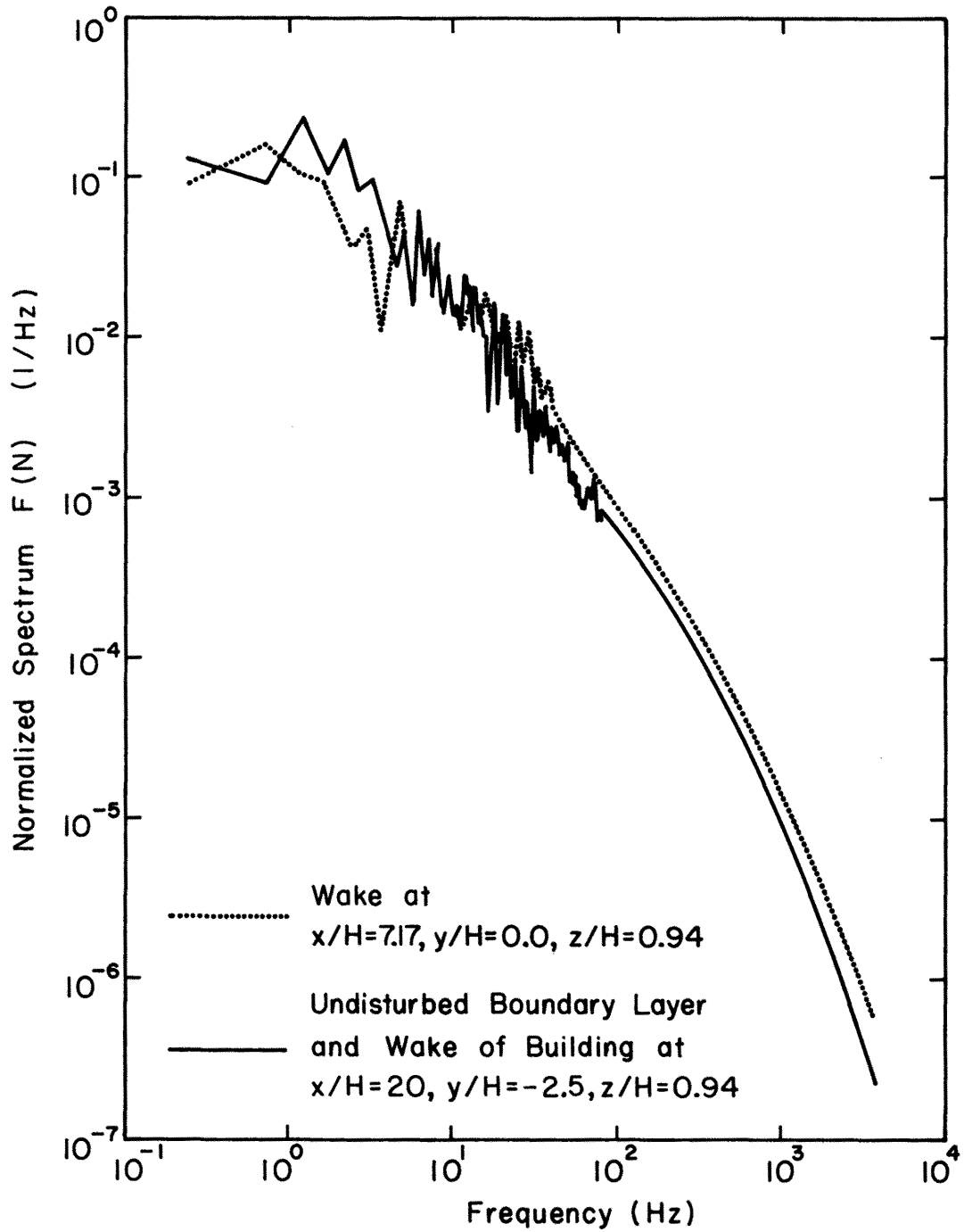
Figure 44. Comparison of normalized one-dimensional turbulent
energy spectra in the wake of the block building
at 47 degrees to the wind and in the undisturbed
boundary-layer approach flow. Test series 10.
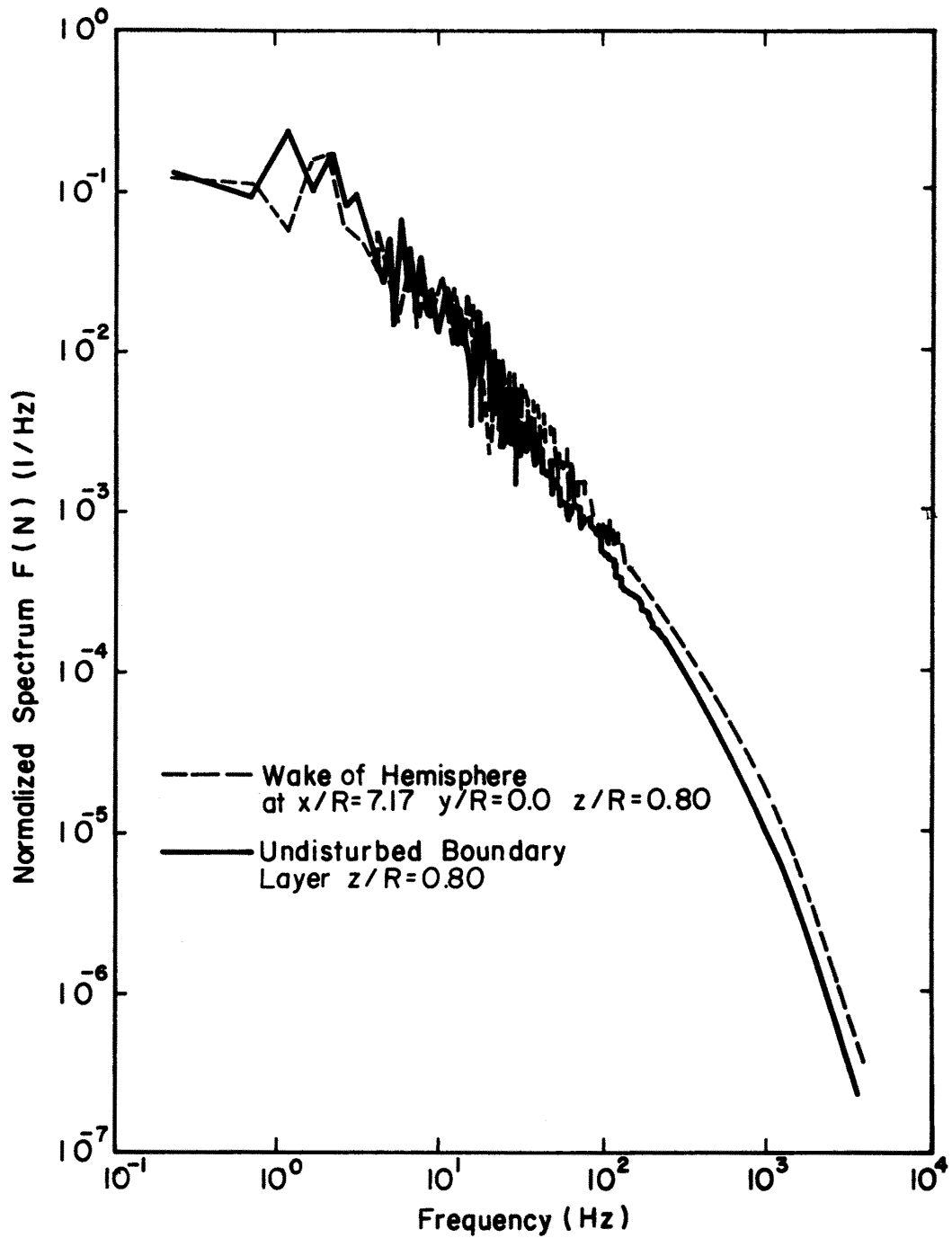
Figure 45. Comparison of the normalized one-dimensional turbulent energy spectra in the wake of a hemisphere and in the undisturbed boundary-layer approach flow. Test series 8.
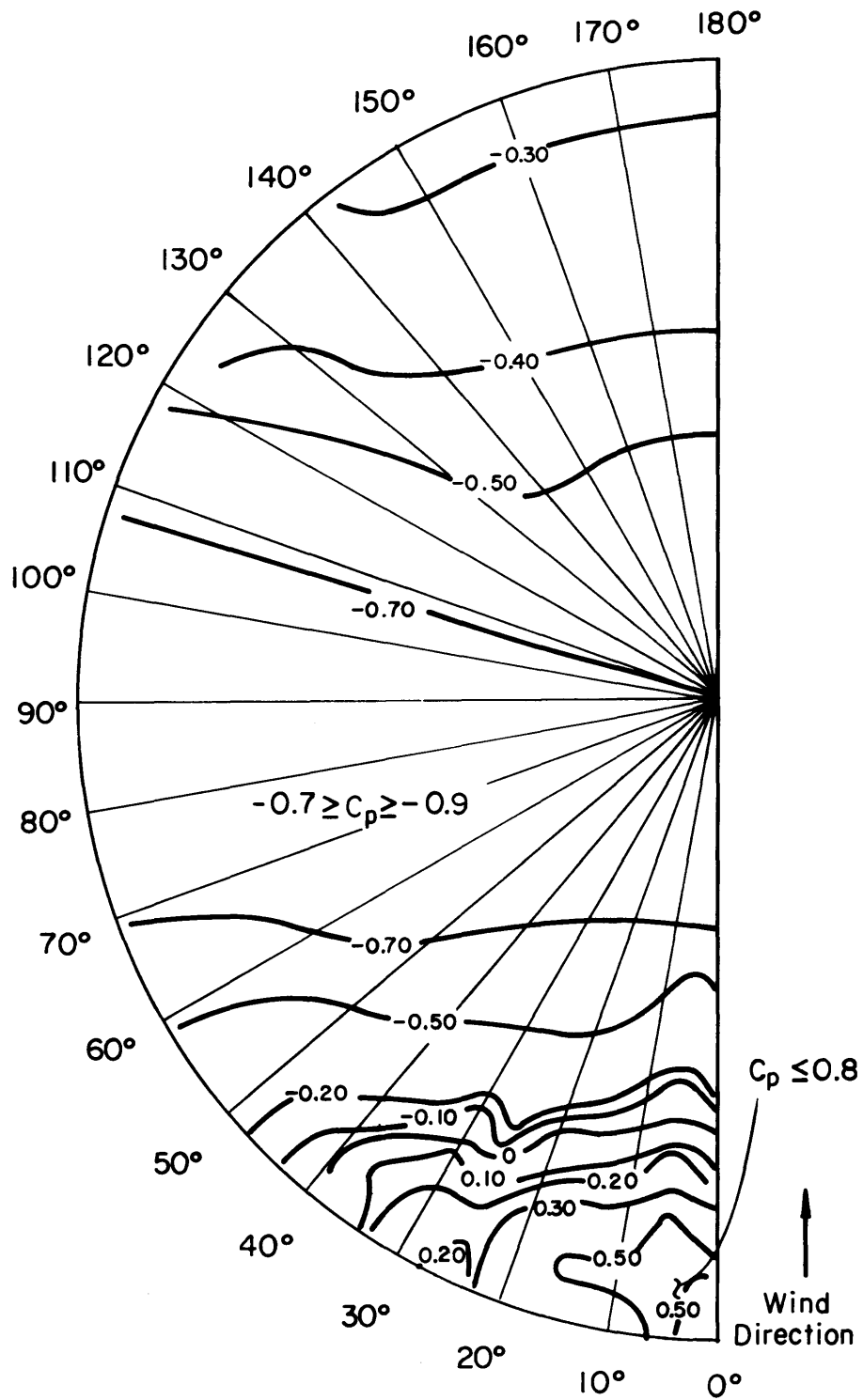
Figure 46. Contours of constant static pressure on a hemisphere
in a shear flow. Test series 4. (From Lin, 1969.)

REPORT DOCUMENTATION PAGE		READ INSTRUCTIONS BEFORE COMPLETING FORM
1. REPORT NUMBER THEMIS Technical Report No. 29	2. GOVT ACCESSION NO.	3. RECIPIENT'S CATALOG NUMBER
4. TITLE (and Subtitle) Vortex-Containing Wakes of Surface Obstacles		5. TYPE OF REPORT & PERIOD COVERED Technical Report
		6. PERFORMING ORG. REPORT NUMBER CER75-76ACH16
7. AUTHOR(s) A. Craig Hansen		8. CONTRACT OR GRANT NUMBER(s) 14-01-0001
9. PERFORMING ORGANIZATION NAME AND ADDRESS Fluid Dynamics and Diffusion Laboratory College of Engineering, Colorado State University Fort Collins, Colorado 80523		10. PROGRAM ELEMENT, PROJECT, TASK AREA & WORK UNIT NUMBERS N00014-68-A-0493-0001
11. CONTROLLING OFFICE NAME AND ADDRESS Office of Naval Research U.S. Department of Defense		12. REPORT DATE December 1975
		13. NUMBER OF PAGES 163
14. MONITORING AGENCY NAME & ADDRESS(If different from Controlling Office)		15. SECURITY CLASS. (of this report) Unclassified
		15a. DECLASSIFICATION/DOWNGRADING SCHEDULE

16. DISTRIBUTION STATEMENT (of this Report)

Distribution of this report is unlimited

17. DISTRIBUTION STATEMENT (of the abstract entered in Block 20, if different from Report)

18. SUPPLEMENTARY NOTES

19. KEY WORDS (Continue on reverse side if necessary and identify by block number)

Wake, Bluff Body, Building, Planetary Boundary Layer, Wind Tunnel, Trailing Vortex-

20. ABSTRACT (Continue on reverse side if necessary and identify by block number)

There are many examples in nature of the occurrence of longitudinal trailing vortices in the lee of surface-mounted obstacles in a turbulent boundary layer. The vortices may be either horseshoe vortices or the well-known roof-corner vortices. This dissertation reports an experimental and theoretical investigation of surface-obstacle wakes which contain organized longitudinal vorticity.

A wind-tunnel study of the wakes behind a hemispherical obstacle and rectangular block building model with two approach wind directions was conducted. The (over)

DD FORM 1473 EDITION OF 1 NOV 65 IS OBSOLETE
1 JAN 73
S/N 0102-014-6601 ;

20. Abstract (continued)

obstacles were surface mounted in a thick, simulated planetary boundary layer. Measurements of mean longitudinal velocity, mean swirl (or cross-flow) velocity and vortex strengths, longitudinal velocity fluctuation intensity, spectra, and two-point space correlations, and the hemisphere surface pressure distribution, at Reynolds numbers between 10^4 and 10^5, were made. In addition, an inviscid model was developed to predict the strength of the horseshoe vortex generated by passage of a shear flow around a hemisphere and to determine the effect of vortex meander on the average strength of the vortex. A theory of combined vortex and momentum wakes developed by J. C. R. Hunt is given preliminary evaluation.

It was found that the vortex-containing wake is quite different from a momentum wake in two important ways. First, the vortex wake is extremely persistent when compared to its momentum wake counterpart. Wake extents of 100 model heights were observed in the vortex-containing wakes, but a momentum wake in the same boundary layer extended only 15 to 20 model heights. Second, the vortex wake contained large regions of mean velocity excess and turbulence intensity deficit. It was found that both the remarkable extent of the wake and its velocity excess character are due to the convective motion induced by the highly persistent vortices.

The theoretical predictions of the horseshoe vortex circulation and the effect of the vortex meander were satisfactory. Meander of the vortex in the turbulent boundary layer resulted in measured (or average) vortex strengths that were only a small fraction of the instantaneous vortex strength. The meander also caused a rapid decay of the average vortex strength while there was very slow decay of the instantaneous vortex strength. Hunt's theory contains the essential feature of the vortex-shear flow interaction to correctly predict the velocity-excess and persistent nature of the wake. Though refinement is needed the theory can be useful in its present state as a research tool.

Defense Documentation Center
Cameron Station
Alexandria, VA 22314   (12 copies)

Technical Library
Naval Ship Research & Dev. Center
Annapolis Laboratory
Annapolis, MD 21402

Professor Bruce Johnson
Engineering Department
Naval Academy
Annapolis, MD 21402

Library
Naval Academy
Annapolis, MD 21402

Professor C. S. Yih
Department of Engineering Mechanics
University of Michigan
Ann Arbor, MI 48108

Professor W. P. Graebel
Department of Engineering Mechanics
University of Michigan
Ann Arbor, MI 48108

Professor T. Francis Ogilvie
Department of Naval Architecture
  and Marine Engineering
University of Michigan
Ann Arbor, MI 48108

Professor W. W. Willmarth
Department of Aerospace Engineering
University of Michigan
Ann Arbor, MI 48108

Professor R. B. Couch
Department of Naval Architecture
  and Marine Engineering
University of Michigan
Ann Arbor, MI 48108

Air Force Office of Scientific
  Research (REM)
1400 Wilson Boulevard
Arlington, VA 22209

Dr. Coda Pan
Shaker Research Corporation
Northway 10 Executive Park
Ballston Lake, NY 12019

Professor S. Corrsin
Department of Mechanics and
  Materials Sciences
The Johns Hopkins University
Charles and 34th Street
Baltimore, MD 21218

Professor L. S. G. Kovasznay
Department of Mechanics and Materials
  Sciences
The Johns Hopkins University
Charles and 34th Street
Baltimore, MD 21218

Professor O. M. Phillips
Department of Earth and Planetary
  Sciences
The Johns Hopkins University
Charles and 34th Street
Baltimore, MD 21218

Professor M. Holt
Department of Mechanical Engineering
University of California
Berkeley, CA 94720

Professor E. V. Laitone
Department of Mechanical Engineering
University of California
Berkeley, CA 94720

Librarian
Department of Naval Architecture
University of California
Berkeley, CA 94720

Professor P. Lieber
Department of Mechanical Engineering
University of California
Berkeley, CA 94720

Professor J. R. Paulling
Department of Naval Architecture
University of California
Berkeley, CA 94720

Professor W. C. Webster
Department of Naval Architecture
University of California
Berkeley, CA 94720

Professor J. V. Wehausen
Department of Naval Architecture
University of California
Berkeley, CA 94720

Professor J. A. Schetz
Department of Aerospace Engineering
Virginia Polytechnic Institute
Blacksburg, VA 24061

Director
Office of Naval Research Branch Office
495 Summer Street
Boston, MA 02210

Commander
Puget Sound Naval Shipyard
Bremerton, WA 98314

Dr. Alfred Ritter
Calspan Corporation
P.O. Box 235
Buffalo, NY 14221

Professor G. Birkhoff
Department of Mathematics
Harvard University
Cambridge, MA 02138

Professor G. F. Carrier
Division of Engineering and
  Applied Physics
Pierce Hall
Harvard University
Cambridge, MA 02138

Commanding Officer
NROTC Naval Administrative Unit
Massachusetts Institute of Technology
Cambridge, MA 02139

Professor M. A. Abkowitz
Department of Ocean Engineering
Massachusetts Institute of Technology
Cambridge, MA 02139

Professor C. C. Mei
Department of Civil Engineering
Massachusetts Institute of Technology
Cambridge, MA 02139

Professor Phillip Mandel
Department of Ocean Engineering
Massachusetts Institute of Technology
Cambridge, MA 02139

Professor E. W. Merrill
Department of Chemical Engineering
Massachusetts Institute of Technology
Cambridge, MA 02139

Professor L. N. Howard
Department of Mathematics
Massachusetts Institute of Technology
Cambridge, MA 02139

Professor R. F. Probstein
Department of Mechanical Engineering
Massachusetts Institute of Technology
Cambridge, MA 02139

Professor E. Mollo-Christensen
Department of Meteorology
Room 54-1722
Massachusetts Institute of Technology
Cambridge, MA 02139

Professor J. Nicholas Newman
Department of Ocean Engineering
Room 5-324A
Massachusetts Institute of Technology
Cambridge, MA 02139

Professor A. R. Kuhlthau, Director
Research Laboratories for the Engineering
  Sciences
Thornton Hall
University of Virginia
Charlottesville, VA 22903

Director
Office of Naval Research Branch Office
536 South Clark Street
Chicago, IL 60605

Library
Naval Weapons Center
China Lake, CA 93555

Institute of Hydrodynamics and Hydraulic
  Engineering
Technical University of Denmark
Building 115   dk-2800
Lyngby/Copenhagen, Denmark

Professor E. Reshotko
Division of Chemical Engineering
  Science
Case Western Reserve University
Cleveland, OH 44106

Professor J. M. Burgers
Institute of Fluid Dynamics and
  Applied Mathematics
University of Maryland
College Park, MD 20740

Professor Pai
Institute for Fluid Dynamics and
  Applied Mathematics
University of Maryland
College Park, MD 20740

NASA Scientific and Technical Information
  Facility
P.O. Box 8757
Baltimore/Washington International Airport
Maryland 21240

Technical Library
Naval Weapons Laboratory
Dahlgren, VA 22418

Computation & Analyses Laboratory
Naval Weapons Laboratory
Dahlgren, VA 22418

Dr. C. S. Wells, Jr.
Advanced Technology Center, Inc.
P.O. Box 6144
Dallas, TX 75222

Dr. R. H. Kraichnan
Dublin, NH 03444

Army Research Office
P.O. Box 12211
Research Triangle Park, NC 27709

Dr. Martin H. Bloom
Polytechnic Institute of New York
Department of Aerospace Engineering
  and Applied Mechanics
Farmingdale, NY 11735

Technical Documents Center
Army Mobility Equipment R&D Center
Fort Belvoir, VA 22060

Professor J. E. Cermak
Department of Civil Engineering
Fluid Mechanics Program
Colorado State University
Fort Collins, CO 80523

Professor O. H. Shemdin
Coastal and Oceanographic Engineering
  Department
University of Florida
Gainesville, FL 32601

Technical Library
Webb Institute of Naval Architecture
Glen Cove, NY 11542

Professor E. V. Lewis
Webb Institute of Naval Architecture
Glen Cove, NY 11542

Dr. M. Poreh
Technion-Israel Institute of Technology
Department of Civil Engineering
Haifa, Israel

Dr. J. P. Breslin
Davidson Laboratory
Stevens Institute of Technology
Castle Point Station
Hoboken, NJ 07030

Mr. C. H. Henry
Stevens Institute of Technology
Davidson Laboratory
Castle Point Station
Hoboken, NJ 07030

Dr..D. Savitsky
Davidson Laboratory
Stevens Institute of Technology
Castle Point Station
Hoboken, NJ 07030

Dr. A. Strumpf
Davidson Laboratory
Stevens Institute of Technology
Castle Point Station
Hoboken, NJ 07030

Dr. J. P. Craven
University of Hawaii
1801 University Avenue
Honolulu, HI 96822

Mr. Norman Nilsen (SP 2022)
Strategic Systems Projects Office
Department of the Navy
Washington, D.C. 20376

Office of Naval Research
Code 438
800 N. Quincy Street
Arlington, VA 22217   (3 copies)

Office of Naval Research
Code 411-7
800 N. Quincy Street
Arlington, VA 22217

Office of Naval Research
Code 411-6
800 N. Quincy Street
Arlington, VA 22217

Office of Naval Research
Code 412-8
800 N. Quincy Street
Arlington, VA 22217

Office of Naval Research
Code 412-3
800 N. Quincy Street
Arlington, VA 22217

Office of Naval Research
Code 473
800 N. Quincy Street
Arlington, VA 22217

Office of Naval Research
Code 200
800 N. Quincy Street
Arlington, VA 22217

Office of Naval Research
Code 481
800 N. Quincy Street
Arlington, VA 22217

Naval Research Laboratory
Code 2627
Washington, D.C. 20375   (6 copies)

Office of Naval Research
Code 1021P (ONRL)
Arlington, VA 22217   (6 copies)

Naval Research Laboratory
Code 6170
Washington, D.C. 20375

Naval Research Laboratory
Code 4000
Washington, D.C. 20375

Naval Research Laboratory
Code 8030
Washington, D.C. 20375

Naval Research Laboratory
Code 8040
Washington, D.C. 20375

Naval Sea Systems Command
Code 03C
Washington, D.C. 20362

Naval Sea Systems Command
Code 0331
Washington, D.C. 20362

Naval Sea Systems Command
Code 0322 (L. Benen)
Washington, D.C. 20362

Naval Sea Systems Command
Code 032 (J. Schuler)
Washington, D.C. 20362

Naval Sea Systems Command
Code 09GS (Library)
Washington, D.C. 20362

Naval Ship Engineering Center
Code 6034
Center Building
Prince George's Center
Hyattsville, MD 20782

Naval Ship Engineering Center
Code 6101E
Center Building
Prince George's Center
Hyattsville, MD 20782

Naval Ship Engineering Center
Code 6110
Center Building
Prince George's Center
Hyattsville, MD 20782

Naval Ship Engineering Center
Code 6114
Center Building
Prince George's Center
Hyattsville, MD 20782

Naval Ship Engineering Center
Code 6136
Center Building
Prince George's Center
Hyattsville, MD 20782

Dr. A. Powell (Code 01)
David Taylor Naval Ship R&D Center
Bethesda, MD 20084

Mr. W. M. Ellsworth (Code 11)
David Taylor Naval Ship R&D Center
Bethesda, MD 20084

Dr. W. E. Cummins (Code 15)
David Taylor Naval Ship R&D Center
Bethesda, MD 29984

Mr. G. H. Gleissner (Code 18)
David Taylor Naval Ship R&D Center
Bethesda, MD 20084

Mr. R. Wermter (Code 152)
David Taylor Naval Ship R&D Center
Bethesda, MD 20084

Dr. W. B. Morgan (Code 154)
David Taylor Naval Ship R&D Center
Bethesda, MD 20084

Library (Code 5641)
David Taylor Naval Ship R&D Center
Bethesda, MD 20084

Dr. P. Pien (Code 1521)
David Taylor Naval Ship R&D Center
Bethesda, MD 20084

Mr. Paul S. Granville (Code 1541)
David Taylor Naval Ship R&D Center
Bethesda, MD 20084

Mr. J. McCarthy (Code 1552)
David Taylor Naval Ship R&D Center
Bethesda, MD 20084

Dr. Nils Salvesen (Code 1552)
David Taylor Naval Ship R&D Center
Bethesda, MD 20084

Ms. Joanna Schot (Code 1843)
David Taylor Naval Ship R&D Center
Bethesda, MD 20084

Naval Air Systems Command
AIR 03
Washington, D.C. 20361

Naval Air Systems Command
AIR 5301
Washington, D.C. 20361

Naval Air Systems Command
AIR 50174
Washington, D.C. 20361

Naval Sea Systems Command
Code 03B
Washington, D.C. 20362

Naval Sea Systems Command
Code 03512 (T. Peirce)
Washington, D.C. 20362

Dr. Steven Crow, President
Poseidon Research
15434 Vista Haven Place
Sherman Oaks, CA 91403

Strategic Systems Projects Office
Department of the Navy
Washington, D.C. 20376

Oceanographer of the Navy
200 Stovall Street
Alexandria, VA 22332

Commander
Naval Oceanographic Office
Washington, D.C. 20373

Dr. A. L. Slafkosky
Scientific Advisor
Commandant of the Marine Corps
(Code AX)
Washington, D.C. 20380

Librarian Station 5-2
Coast Guard Headquarters
NASSIF Building
400 Seventh Street, SW
Washington, D.C. 20591

Office of Research and Development
Maritime Administration
441 G Street, NW
Washington, D.C. 20235

Division of Ship Design
Maritime Administration
441 G Street, NW
Washington, D.C. 20235

National Science Foundation
Engineering Division
1800 G Street, NW
Washington, D.C. 20550

Professor H.-P. Pao
Department of Aerospace & Atmospheric
   Sciences
The Catholic University of America
Washington, D.C. 20017

Dr. G. Kulin
Fluid Mechanics Section
National Bureau of Standards
Washington, D.C. 20234

Science & Technology Division
Library of Congress
Washington, D.C. 20540

Chief of Research and Development
Office of Chief of Staff
Department of the Army
Washington, D.C. 20310

Professor A. Thiruvengadam
Department of Mechanical Engineering
Catholic University of America
Washington, D.C. 20017

Librarian
Naval Surface Weapons Center
White Oak Laboratory
Silver Spring, MD 20910

Mr. J. Enig (Room 3-252)
Naval Surface Weapons Center
White Oak Laboratory
Silver Spring, MD 20910

Dr. A. S. Iberall, President
General Technical Services, Inc.
451 Penn Street
Yeadon, PA 19050

Professor J. Wu
College of Marine Studies
Robinson Hall
University of Delaware
Newark, DE 19711

Professor V. W. Goldschmidt
School of Mechanical Engineering
Purdue University
Lafayette, IN 47907

Professor T. W. Kao
Department of Aerospace & Atmospheric
   Sciences
The Catholic University of America
Washington, D.C. 20017